APPROVED FOR RELEASE: 2007/02/08: CIA-RDP82-00850R000300060001-1

1 [illegible] 1980 [illegible] 1 of 2

APPROVED FOR RELEASE: 2007/02/08: CIA-RDP82-00850R000300060001-1

APPROVED FOR RELEASE: 2007/02/08: CIA-RDP82-00850R000300060001-1

JPRS L/9420

1 December 1980

Translation

BIONICS

FBIS FOREIGN BROADCAST INFORMATION SERVICE

APPROVED FOR RELEASE: 2007/02/08: CIA-RDP82-00850R000300060001-1

APPROVED FOR RELEASE: 2007/02/08: CIA-RDP82-00850R000300060001-1

NOTE

JPRS publications contain information primarily from foreign newspapers, periodicals and books, but also from news agency transmissions and broadcasts. Materials from foreign-language sources are translated; those from English-language sources are transcribed or reprinted, with the original phrasing and other characteristics retained.

Headlines, editorial reports, and material enclosed in brackets [] are supplied by JPRS. Processing indicators such as [Text] or [Excerpt] in the first line of each item, or following the last line of a brief, indicate how the original information was processed. Where no processing indicator is given, the information was summarized or extracted.

Unfamiliar names rendered phonetically or transliterated are enclosed in parentheses. Words or names preceded by a question mark and enclosed in parentheses were not clear in the original but have been supplied as appropriate in context. Other unattributed parenthetical notes within the body of an item originate with the source. Times within items are as given by source.

The contents of this publication in no way represent the policies, views or attitudes of the U.S. Government.

COPYRIGHT LAWS AND REGULATIONS GOVERNING OWNERSHIP OF MATERIALS REPRODUCED HEREIN REQUIRE THAT DISSEMINATION OF THIS PUBLICATION BE RESTRICTED FOR OFFICIAL USE ONLY.

APPROVED FOR RELEASE: 2007/02/08: CIA-RDP82-00850R000300060001-1

APPROVED FOR RELEASE: 2007/02/08: CIA-RDP82-00850R000300060001-1

JPRS L/9420

1 December 1980

BIONICS

Kiev BIONIKA in Russian 1979 signed to press 14 June 79 No 13, pp 2-100

[Translation of the book BIONIKA. RESPUBLIKANSKIY MEZHVEDOMSTVENNYY SBORNIK. OSNOVAN V 1965 g. (Bionics. Republic Interagency Collection. Founded in 1965.) from the Academy of Sciences UkSSR, Institute of Hydromechanics, Editor-in-Chief G.V. Logvinovich, Izdatel'stvo "Naukova Dumka", 1,000 copies, 100 pages]

CONTENTS

APPROVED FOR RELEASE: 2007/02/08: CIA-RDP82-00850R000300060001-1

APPROVED FOR RELEASE: 2007/02/08: CIA-RDP82-00850R000300060001-1

APPROVED FOR RELEASE: 2007/02/08: CIA-RDP82-00850R000300060001-1

APPROVED FOR RELEASE: 2007/02/08: CIA-RDP82-00850R000300060001-1

ANNOTATION

THE COLLECTION IS DEVOTED TO HYDRODYNAMIC PROBLEMS OF BIONICS. INDIVIDUAL PROBLEMS OF GENERAL HYDROMECHANICS ARE CONSIDERED WITH RESPECT TO SWIMMING OF AQUATIC ANIMALS AND SOME HYDRODYNAMIC PROBLEMS OF SWIMMING OF AQUATIC ANIMALS ARE DEVELOPED. THE MORPHOLOGICAL STRUCTURE OF THE SKIN OF MARINE ANIMALS IS DESCRIBED. THE POSSIBILITIES OF USING THE DERIVED INFORMATION FOR TECHNICAL PURPOSES ARE INVESTIGATED.

THE COLLECTION IS INTENDED FOR SCIENTIFIC WORKERS, TEACHERS IN VUZES AND POSTGRADUATE STUDENTS INVOLVED IN PROBLEMS OF BIONICS.

APPROVED FOR RELEASE: 2007/02/08: CIA-RDP82-00850R000300060001-1

APPROVED FOR RELEASE: 2007/02/08: CIA-RDP82-00850R000300060001-1

UDC 591.524.1;591.177

THE HYDRODYNAMICS OF AQUATIC ANIMALS WITH LUNATE CAUDAL FIN

Kiev BIONIKA in Russian No 13, 1979 signed to press 14 Jun 79 pp 3-9

[Article by L. F. Kozlov, Institute of Hydromechanics of the Ukrainian SSR Academy of Sciences, from the collection "Bionika," Izdatel'stvo Naukova Dumka, 1,000 copies, 100 pages]

[Text] The approximate hydrodynamic theory of swimming of aquatic animals with lunate caudal fin is proposed in [3]. The basis of this work is the hypothesis that the oscillatory amplitude of the body of an aquatic animal during swimming motions has a constant value along the entire length of the body. However, analysis of movie films of the swimming of numerous classes of aquatic animals showed that the oscillatory amplitude of the body of the said animals varies approximately according to linear law from the nose to its highest value in the region of the caudal fin. A movie film of a swimming sturgeon is presented in Figure 1 as an example of this type of swimming. The numbers 1-6 in this figure denote the sequential positions of its body during a single period of oscillation of the caudal fin. Such remarkable swimmers as Scombridae, bonito, tuna of the Scombridae family, swordfish of the Xiphiidae family, sailfish, spearfish, marlin of the Istiophoridae family, various species of dolphins of the Delphinidae family and other fast-swimming aquatic animals also belong to these classes of animals.

Let us consider the forces acting on the lunate caudal fin of an aquatic animal. Elongation of this caudal fin is evaluated in the hydrodynamic sense by the formula

$$\lambda = \frac{(2R)^2}{S}, \qquad (1)$$

where λ is elongation, 2R is span and S is the area of the caudal fin.

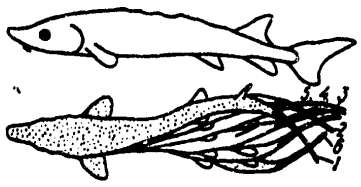

Figure 1. Diagram of Oscillations Made by the Body and Fins of Sturgeon

APPROVED FOR RELEASE: 2007/02/08: CIA-RDP82-00850R000300060001-1

APPROVED FOR RELEASE: 2007/02/08: CIA-RDP82-00850R000300060001-1

To calculate the thrust created by the caudal fin of an aquatic animal (Figure 2), let us use the main propositions of the theory of a high-aspect wing, outlined in [4]. According to the mentioned theory, we have the expressions

$$C_{pi} = (\pi\lambda)^{-1} C_L^2 (1+\delta), \tag{2}$$

$$C_L = \frac{2\pi\lambda\alpha}{\sqrt{\lambda^2+4}+2}. \tag{3}$$

The following additional notations are used here: C_{pi} is the induced drag factor, C_L is the lift coefficient, α is the angle of attack of the caudal fin and $(1+\delta)$ is a factor which takes into account deviation of the geometric shape of the caudal fin in layout from the optimum shape in the sense of least inductive losses. Moreover

$$(1+\delta) = \sum_{n=1}^{\infty} n \frac{A_n^2}{A_1^2} = 1 + 2\frac{A_2^2}{A_1^2} + 3\frac{A_3^2}{A_1^2} + \ldots, \tag{4}$$

where A_n is the still unknown coefficients of expansion of the rate of circulation along the wing span in the form of a trigonometric series with respect to sines. These coefficients are dependent on the geometric characteristics of the wing and the angle of attack and also satisfy an infinite system of algebraic equations

$$\sum_{n=1}^{\infty} \left(a\frac{b}{R}n + \sin\theta\right) A_n \sin n\theta = a\frac{b}{R}\alpha_1 \sin\theta, \tag{5}$$

where $\alpha_1 = \alpha - \alpha_0$ is the angle of attack with respect to zero lift, $b(z)$ is the cross-sectional chord of the caudal fin in the xOy plane, r_0 is the circumferential radius in the auxiliary plane and $a = 2\pi r_0/b$.

In equation (5), α and $a(b/l)$ are known functions of coordinate z and parameter θ bound to it. The unknown values are coefficients A_n. It is recommended that Glauert's well-known method, outlined in [4], be used to solve the system of algebraic equations (5).

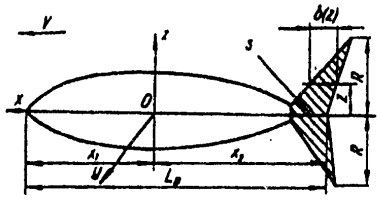

Figure 2. Coordinate System and Main Geometric Characteristics of Aquatic Animal

Since expression (4) is the sum of significantly positive terms, the minimum value of induced drag C_{Di} will be ensured at $\delta = 0$. Consequently, in this case $A_n = 0$

APPROVED FOR RELEASE: 2007/02/08: CIA-RDP82-00850R000300060001-1

APPROVED FOR RELEASE: 2007/02/08: CIA-RDP82-00850R000300060001-1

at $n > 1$. This corresponds to the optimum shape of the caudal fin in the xOz plane.

Let us note the following with regard to determination of the value of δ for the caudal fins of aquatic animals. The main proposition of hydrobionics, which should also be valid for the hydrodynamics of the swimming of aquatic animals, includes the fact that the form of swimming of an aquatic animal should be very close to optimum. Therefore, let us assume the value $\delta = 0$ in further calculations with respect to a caudal fin in the shape of (2). Moreover, even a significant deviation of the geometric shape of the caudal fin of an aquatic animal from the optimum shape of a wing yields slight corrections which can be disregarded in approximate engineering calculations. Thus, for unswept wings which differ significantly from the optimum in the sense of least induced drag, the extent of this correction comprises the following values:

λ,	3	6	8	11
δ,	0.02	0.05	0.06	0.08

The given figures show that this correction comprises approximately 2-3 percent for caudal fins encountered in aquatic animals with lunate fin (λ = 1-3) and it can be disregarded in approximate calculations.

Let us note that interpolation formula (3) for the lift coefficient is in satisfactory agreement with the numerous available experimental data (see Figure 3). For example, for $\lambda = 4$ according to the Fedyayevskiy formula $dC_L/d\alpha = 3.88$ and the experimental value comprises $dC_L/d\alpha = 3.80$. Consequently, the error of the value determined by formula (3) comprises approximately 2 percent in this case. It is interesting to note that the formula for calculating lift used in [3] yields a value of $dC_L/d\alpha = 4.19$ for the given value of λ and the corresponding error comprises more than 10 percent compared to experimental data. There are some advantages of formula (3) in this sense to determine the lift coefficient for high-aspect wings.

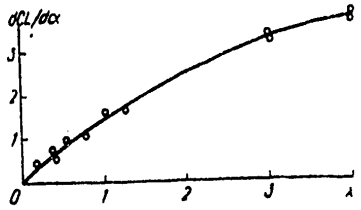

Figure 3. Comparison of Experimental Data of Derivative $dC_L/d\alpha$ to Values Calculated by Formula (3) for Different Wing Aspect Ratios: solid lines--theoretical data; circles--experimental data

It should also be noted that formula (3) is valid only for absolutely rigid hydrodynamic wings, whereas the caudal fins during swimming of aquatic animals are deformed somewhat due to the effect of incident flow. However, the mentioned deformations must be disregarded at the stage of studying the creation of thrust by aquatic animals under consideration.

APPROVED FOR RELEASE: 2007/02/08: CIA-RDP82-00850R000300060001-1

APPROVED FOR RELEASE: 2007/02/08: CIA-RDP82-00850R000300060001-1

Let us subsequently disregard the rotation of the caudal fin with respect to the direction of instantaneous speed, i.e., let us assume that $\phi = 0$ in equation (6). This hypothesis must be made since there is essentially no information about the value of this angle during swimming of various types of aquatic animals. As material is accumulated on the values of angle ϕ for various types of aquatic animals, it will be easy to refine the calculations made in this paper.

Let us turn to calculation of the speeds and forces acting on the caudal fin of an aquatic animal, regarded as a rigid high-aspect wing (Figure 4). It follows from the given layout that the instantaneous thrust coefficient of a caudal fin is determined by the formula

$$C_A = C_L\left(\frac{\partial \eta}{\partial t}\frac{1}{V} + \varphi\right) - C_{Di}, \tag{6}$$

where the additional notations are introduced: $\eta(x, t)$ is deviation of the center line of an aquatic animal from coordinate axis y, t is tim, $\partial\eta/\eta_t = \eta t$ is the transverse velocity of the center line of an aquatic animal, $\eta t/V$ is the slope of the direction of instantaneous speed of the center line to the direction of motion of an aquatic animal, ϕ is the angle of rotation of the caudal fin with respect to the direction of instantaneous speed of the center line and V is the speed of swimming of an aquatic animal.

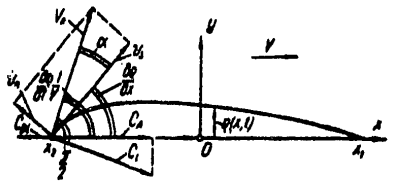

Figure 4. Diagram of Speeds and Forces for Caudal Fin of Aquatic Animal

As theoretical and experimental data are accumulated on the effect of high-aspect wing deformation on the lift coefficient, one can introduce the appropriate corrections to the calculations. It should be assumed that the mentioned corrections do not make any fundamental changes in the derived values of the lift coefficients.

According to the previously postulated problem, let us assume that the oscillatory amplitude of the center line of the body of an aquatic animal increases by linear law as the point under consideration moves from the nose to the tail point x_2. In other words, let us assume that the following formula is applicable to describe the oscillation of the body of an aquatic animal

$$\eta = \eta_0 \frac{x_2 - x}{L_p} \sin\left(\frac{ct}{L} - \frac{x_2 - x}{L}\right). \tag{7}$$

Here η_0 is the oscillatory amplitude of the tail point of the caudal fin, L is the length of the wave travelling along the body of an aquatic animal, n is the number

APPROVED FOR RELEASE: 2007/02/08: CIA-RDP82-00850R000300060001-1

APPROVED FOR RELEASE: 2007/02/08: CIA-RDP82-00850R000300060001-1

of waves added on the length of the body of an aquatic animal, c is the speed of propagation of a wave travelling along the body of an aquatic animal and $L_p = 2\pi L_n = x_2 - x_1$ is the length of the body of an aquatic animal. From the graph given in Figure 4, for the angle of attack we find

$$\alpha = -\frac{v_n}{V} = \frac{1}{V}\left(\frac{\partial \eta}{\partial t} - V\frac{\partial \eta}{\partial x}\right), \tag{9}$$

where v_n is the normal speed component of the tail point of the caudal fin.

Let us calculate the values of the derivatives in formula (8). To do this, let us differentiate the values of (7) with respect to coordinate x and time t. After calculation, we find

$$\frac{\partial \eta}{\partial t} = \frac{\eta_0}{L} c \frac{x_3 - x}{L_p} \cos\left(\frac{ct}{L} - \frac{x_3 - x}{L}\right); \tag{9}$$

$$\frac{\partial \eta}{\partial x} = -\frac{\eta_0}{L} \sin\left(\frac{ct}{L} - \frac{x_3 - x}{L}\right) + \frac{\eta_0}{L}\frac{x_3 - x}{L_p} \cos\left(\frac{ct}{L} - \frac{x_3 - x}{L}\right). \tag{10}$$

Then the normal speed component for the case under consideration has the form

$$v_n = \frac{\eta_0}{L}\frac{x_3 - x}{L_p}(c - V)\cos\left(\frac{ct}{L} - \frac{x_3 - x}{L}\right) + \frac{\eta_0}{L} V \sin\left(\frac{ct}{L} - \frac{x_3 - x}{L}\right). \tag{11}$$

Let us calculate the pulling coefficient. Substituting the values of the lift and induced drag coefficients into equation (6) according to formulas (2) and (3), after simple transformations we find

$$C_A = \frac{2\pi\lambda}{\sqrt{\lambda^2 + 4} + 2}\frac{v_n}{V}\left(\frac{\partial \eta}{\partial t}\frac{1}{V}\right) - \frac{4\pi\lambda}{(\sqrt{\lambda^2 + 4} + 2)^2}\left(\frac{v_n}{V}\right)^2. \tag{12}$$

Let us then calculate the value of the pulling coefficient during period $\tau = 2\pi (L/C)$

$$\{C_A\} = \frac{1}{\tau}\int_0^{\tau} C_A dt. \tag{13}$$

Using the law of averaging (13) permits one to find the expression

$$\{C_A\} = \frac{2\pi\lambda}{\sqrt{\lambda^2 + 4} + 2}\left\{\left(\frac{v_n}{V}\right)\frac{\partial \eta}{\partial t}\frac{1}{V}\right\} - \frac{4\pi\lambda}{(\sqrt{\lambda^2 + 4} + 2)^2}\left\{\left(\frac{v_n}{V}\right)^2\right\}. \tag{14}$$

Let us turn to calculation of the individual terms of the expression.

The calculations made previously in [2] made it possible to find the expressions

APPROVED FOR RELEASE: 2007/02/08: CIA-RDP82-00850R000300060001-1

APPROVED FOR RELEASE: 2007/02/08: CIA-RDP82-00850R000300060001-1

$$\left\{\left(\frac{v_n}{V}\right)^2\right\} = \frac{1}{2}\left(\frac{\eta_0}{L}\right)^2 + \frac{1}{2}\left(\frac{\eta_0}{L}\right)^2 \frac{(x_3 - x)}{L_p}\left(\frac{c}{V} - 1\right)^2. \tag{15}$$

$$\left\{\left(\frac{v_n}{V}\right)\left(\frac{\partial \eta}{\partial t}\right)\frac{1}{V}\right\} = \frac{1}{2}\left(\frac{\eta_0}{L}\right)^2\left(\frac{x_3 - x}{L_p}\right)^2 \frac{c}{V}\left(\frac{c}{V} - 1\right)^2. \tag{16}$$

Substituting them into equation (14), to calculate the pulling coefficient we find the final expression

$$\{C_A\} = \frac{\pi\lambda}{\sqrt{\lambda^2 + 4} + 2}\left(\frac{\eta_0}{L}\right)^2 \frac{c}{V}\left(\frac{c}{V} - 1\right)\left(\frac{x_3 - x_1}{L_p}\right)^3 - \\ - \frac{4\pi\lambda}{(\sqrt{\lambda^2 + 4} + 2)^2}\left[\frac{1}{2}\left(\frac{\eta_0}{L}\right)^2 + \frac{1}{2}\left(\frac{\eta_0}{L}\right)^2 \frac{(x_3 - x_1)}{L_p}\left(\frac{c}{V} - 1\right)^2\right]. \tag{17}$$

Since from expression (1) for the typical area we have

$$S = \frac{(2R)^2}{\lambda},$$

and the reduced mass at the tail point is

$$m_1^* = \rho\pi R^2,$$

then

$$\frac{\rho V^2}{2} S = 2\frac{m_1^* V^2}{\pi\lambda}.$$

Then the mean values of pulling are

$$\{A\} = \{C_A\}\frac{\rho V^2}{2} S = \{C_A\}\frac{2m_1^* V^2}{\pi\lambda}, \tag{18}$$

or, using expression (17), we finally find

$$\{A\} = \frac{2m_1^*}{\sqrt{\lambda^2 + 4} + 2}\left(\frac{\eta_0}{L}\right)^2 V^2\left\{\frac{c}{V}\left(\frac{c}{V} - 1\right)\left(\frac{x_3 - x_1}{L_p}\right)^3 + \right. \\ \left. + \frac{4}{\sqrt{\lambda^2 + 4} + 2}\left[\frac{1}{2} + \frac{(x_3 - x_1)}{L_p}\left(\frac{c}{V} - 1\right)^2\right]\right\}. \tag{19}$$

These expressions can be found by similar calculations.

The mean value for the section force is

$$\{P\} = \frac{m_1^*}{4}\left(\frac{\eta_0}{L}\right)^2 V^2 + \frac{m_1^*}{12}\left(\frac{\eta_0}{L}\right)^2 V^2\left(\frac{c}{V} - 1\right)^2. \tag{20}$$

APPROVED FOR RELEASE: 2007/02/08: CIA-RDP82-00850R000300060001-1

APPROVED FOR RELEASE: 2007/02/08: CIA-RDP82-00850R000300060001-1

The mean value of the kinetic energy coming off the caudal fin to the hydrodynamic wake is equal to

$$\{E\} = \frac{m_1^*}{L}\left(\frac{\eta_0}{L}\right)^2 V^3 + \frac{m_1^*}{4}\left(\frac{\eta_0}{L}\right)\frac{(x_2 - x_1)}{L_p}\left(\frac{c}{V} - 1\right)^2 V^3. \tag{21}$$

The general expression for the hydrodynamic efficiency has the form

$$\{\eta_p\} = \frac{(\{A\} + \{P\})V}{(\{A\} + \{P\})V + \{E\}}. \tag{22}$$

Substituting expressions (19)-(21) into equality (22) after simple transformations for efficiency, we find the final expression

$$\{\eta_p\} = \frac{\frac{2}{V\lambda^2 + 4 + 2}\left\{\frac{c}{V}\left(\frac{c}{V} - 1\right) - \frac{4}{V\lambda^2 + 4 + 2}\left[\frac{1}{2} + \left(\frac{c}{V} - 1\right)^2\right]\right\} + \frac{1}{4} + \frac{1}{12}\left(\frac{c}{V} - 1\right)^2}{\frac{2}{V\lambda^2 + 4 + 2}\left\{\frac{c}{V}\left(\frac{c}{V} - 1\right) - \frac{4}{V\lambda^2 + 4 + 2}\left[\frac{1}{2}\left(\frac{c}{V} - 1\right)^2\right]\right\} + \frac{1}{4} + \frac{1}{3}\left(\frac{c}{V} - 1\right)^2}. \tag{23}$$

The functions of hydrodynamic efficiency $\{\eta_p\}$ and the dimensionless coefficient of thrust for different values of travelling wave velocity c/V are calculated by using formulas (19)-(23). The results of these calculations are presented in Figure 5 for aquatic animals with lunate caudal fin having aspect ratio of $\lambda = 4$.

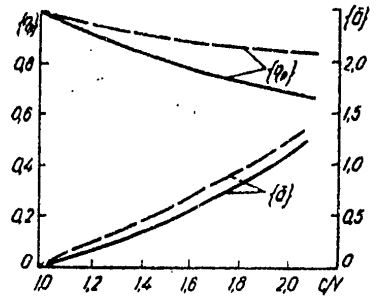

Figure 5. Comparison of Results of Calculating the Pull and Hydrodynamic Efficiency for an Aquatic Animal with Lunate Caudal Fin: solid lines--according to formulas (19)-(23); dashed lines--according to data of G. V. Logvinovich [3]

APPROVED FOR RELEASE: 2007/02/08: CIA-RDP82-00850R000300060001-1

APPROVED FOR RELEASE: 2007/02/08: CIA-RDP82-00850R000300060001-1

It should be noted that one should take into account the effect of the hydrodynamic wake occurring behind the body on the work of the caudal fin as an impeller when calculating the hydrodynamic efficiency of the caudal fin of an aquatic animal by formula (22). This is usually taken into account in shipbuilding by introducing the concept of hull efficiency. This coefficient represents the following relation in the case under consideration

$$\eta_k = i\frac{1-t}{1-\psi}, \tag{24}$$

where ψ is the wake fraction, t is the suction coefficient and i is the coefficient of the effect of velocity field nonuniformity at the location of the caudal fin.

Calculations carried out by the known data of Harwald (see [1]) showed that the following values can be used for aquatic animals: $i \approx 1$ and $1 - t \approx 1 - \psi$, i.e., hull efficiency for fast-swimming aquatic animals is approximately equal to unity. Consequently, the use of formula (24) in the case under consideration to calculate the hydrodynamic efficiency is quite valid. In those cases when η_k differs considerably from unity, the formula for determining the hydrodynamic efficiency has the form

$$\{\eta_p\} = \frac{(\{A\}\eta_k + \{P\})V}{(\{A\}\eta_k + \{P\})V + \{E\}}. \tag{25}$$

We note the problem of swimming of various types of aquatic animals continues to be of great scientific interest and merits serious study both in the theoretical and in the experimental sense.

BIBLIOGRAPHY

1. Voytkunskiy, Ya. I., R. Ya. Pershin and I. A. Titov, "Spravochnik po teorii korablya" [Handbook on Ship Theory], Leningrad, Sudostroyeniye, 1973.

2. Kozlov, L. F. and R. A. Oleynik, "The Hydrodynamics of Aquatic Animals Swimming in Scombroid Fashion," DOKL. AN USSR, SER. A., No 11, 1976.

3. Logvinovich, G. V., "The Hydrodynamics of Swimming of Fishes," BIONIKA, No 7, 1973.

4. Fadyayevskiy, K. K., Ya. I. Voytkunskiy and Yu. I. Faddeyev, "Gidromekhanika" [Hydromechanics], Leningrad, Sudostroyeniye, 1968.

APPROVED FOR RELEASE: 2007/02/08: CIA-RDP82-00850R000300060001-1

APPROVED FOR RELEASE: 2007/02/08: CIA-RDP82-00850R000300060001-1

UDC 591.177

THE HYDRODYNAMIC CHARACTERISTICS OF THE CAUDAL FIN OF THE DOLPHIN

Kiev BIONIKA in Russian No 13, 1979 signed to press 14 Jun 79 pp 9-15

[Article by V. P. Kayan, Institute of Hydromechanics of the Ukrainian SSR Academy of Sciences, from the collection "Bionika," Izdatel'stvo Naukova Dumka, 1,000 copies, 100 pages]

[Text] Investigating the hydrodynamics of swimming of fast-swimming aquatic animals is of great interest on the part of investigators working in the field of hydrobionics. Of special interest are animals which move by means of bending, oscillatory motions of the caudal fin working like a flapping wing (specifically, dolphins).

We previously found the hydrodynamic characteristics of swimming of the aphaline dolphin by the kinematics of bending-oscillatory motions of the entire body [4] by the calculating method based on G. V. Logvinovich's theory [7]. The thrust and ideal hydromechanical efficiency of the dolphin impeller and also the coefficients of the hydrodynamic drag of the dolphin were determined as functions of the Reynolds number and the mean value during oscillation and the sign of variation of speed of swimming [5].

However, since a number of assumptions was introduced into the calculating formulas, it would be interesting to find the same characteristics by a different method for comparison. The results of calculating the propulsive characteristics of the caudal fin of a dolphin working like a flapping wing with known law of its vertical and angular oscillations are presented below. A method based on the hypothesis of stability, i.e., on the assumption that the instantaneous forces occurring on the wing during unsteady flow of a fluid over it, are determined only by the values of the instantaneous angle of attack α_i and speed V_i of the wing, was used for the calculation.

The fundamentals of the theory of an oscillating wing are contained in the papers of A. I. Nekrasov [8] and L. I. Sedov [10]. Experimental investigations on study of the forces and moments occurring on a rigid wing making angular and vertical oscillations in a fluid were carried out at different times by H. Hertel [14], Yu. N. Savchenko [9] and E. P. Grebeshov and O. A. Sagoyam [3]. Unswept [3, 14], elliptical and low-aspect delta wings [9] were tested.

Since the literature contains no data on the hydrodynamic characteristics of the caudal fin of dolphins, some simplifications were made for calculation. The wing

APPROVED FOR RELEASE: 2007/02/08: CIA-RDP82-00850R000300060001-1

APPROVED FOR RELEASE: 2007/02/08: CIA-RDP82-00850R000300060001-1

was regarded as rigid and the natural shape of the caudal fin of the aphaline dolphin was replaced by a swept wing with aspect ratio of $\lambda = l^2/s = 4$ and taper $\eta = b_1/b_2 = 4$, where $l = 0.52$ m is the wing span and $b_2 = 0.059$ m is the end chord of the wing (Figure 1), equal to the caudal fin in area $S = 0.077$ m^2 and by the value of the root chord $b_1 = 0.236$. The mean aerodynamic chord b_{SAKh} of this wing is determined by the known method [1] and is equal to 0.164 meter.

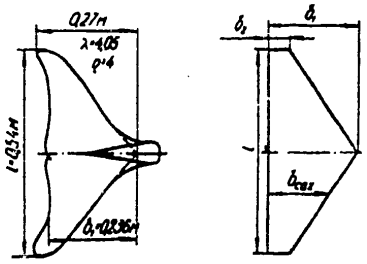

Figure 1. Shape of Caudal Fin of Bottlenosed Dolphin and of Equal Area of Swept Wing

The NACA-0018 symmetrical profile [6], whose aerodynamic characteristics for an unswept wing of $\lambda = 6$ are known and are presented in Figure 2 (C_y is the lift coefficient, C_x is the drag factor, $k = C_y/C_x$ is wing efficiency and α is the angle of attack of the wing), was selected from the catalog as the wing profile. Figure 3 serves as justification for selection of NACA-0018 profile. Profiles 3 and 4 in the forward part almost completely coincide, while they have a slight difference in the tail part.

Variation of the hydrodynamic coefficients of the wing upon transition from unswept at $\lambda = \infty$ to swept at $\lambda = 4$ and $\eta = 4$ is shown in Figure 4. The functions $C_y(\alpha)$ and $C_y(C_x)$, found by wind-tunnel testing for plates in the form of wings of different shape, are shown on the graph. Thus, by introducing the correcting coefficient to functions $C_y(\alpha)$ and $C_x(\alpha)$ presented in Figure 2, we find the coefficients C_x and C_y for a rigid wing of the adopted shape with NACA-0018 profile.

One can then determine the hydrodynamic forces on this wing at each moment of time by the formulas [1]

$$X_i = C_{xi}\frac{\rho V_i^2}{2}S, \tag{1}$$

$$Y_i = C_{yi}\frac{\rho V_i^2}{2}S. \tag{2}$$

The unknown values of α_i and V_i are determined from the trajectories of motion of the caudal fin of the dolphin, found by making motion pictures in a biohydrodynamic channel [12, 13]. The investigations were carried out with six bottlenosed dolphins having length of $L = 2.35$-2.65 meters [5]. The components of the kinematics of motion of the caudal fin of the animal under investigation were recorded with the

APPROVED FOR RELEASE: 2007/02/08: CIA-RDP82-00850R000300060001-1

APPROVED FOR RELEASE: 2007/02/08: CIA-RDP82-00850R000300060001-1

Konvas-avtomat movie camera with RO-ZZM objective having focal length of 50 mm. An electric timer was used to record the time intervals between movie frames [12].

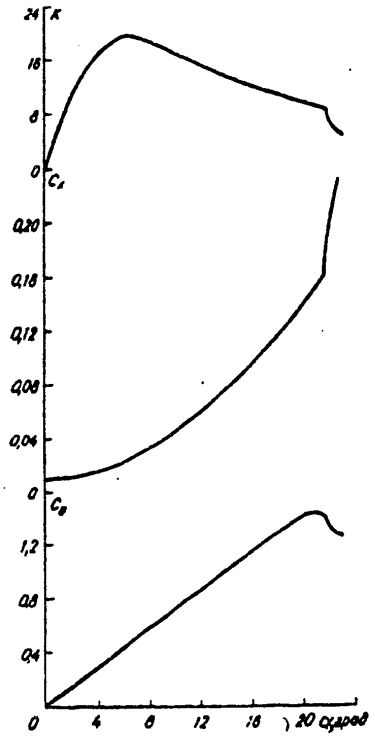

Figure 2. Dependence of Aerodynamic Coefficients and Efficiency on Angle of Attack α

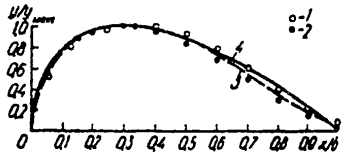

Figure 3. Comparison of Mean Cross-sectional Span Profiles of Caudal Fin of Bottlenosed Dolphin (1) [11], of the White-Finned Porpoise (2) [15] and Their Mean Value (3) to NACA-0018 Profile (4) [6]

Conditions where the dolphin moves in a straight line and where the plane of the caudal fin does not make rotary motions around the root chord, i.e., the caudal fin is projected onto the longitudinal vertical plane XOY only by the root profile which was replaced by a straight-line segment equal to the root chord (Figure 5, a), were selected for subsequent processing.

APPROVED FOR RELEASE: 2007/02/08: CIA-RDP82-00850R000300060001-1

APPROVED FOR RELEASE: 2007/02/08: CIA-RDP82-00850R000300060001-1

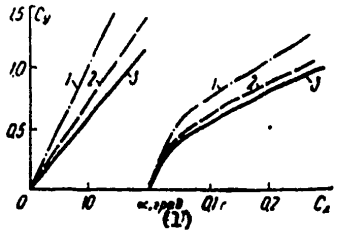

Figure 4. Aerodynamic Characteristics of Plate in the Shape of Unswept and Swept Wing: 1--unswept wing with $\lambda = \infty$; 2--with $\lambda = 6$; 3--swept wing with $\lambda = 4$ and $\eta = 4$

Key:
1. Degree

Let us plot the path travelled by the caudal fin in the longitudinal direction, the number of frames on the movie film and time t in seconds on the x-axis. Let us plot the amplitude of vertical oscillations A_0 of the caudal fin of the dolphin along the y axis. Variation of the swimming speed V_0 of the dolphin is shown in Figure 5, b and of the speed V_y of the caudal fin in the vertical plane during the period of oscillation is shown in Figure 5, c, while curve $V_y(t)$ is the same as function $A_0(t)$, but is shifted in phase by $\pi/2$. The transverse speed of the fin is determined as a function of the amplitude of vertical oscillations:

$$V_y = \frac{\partial A_0}{\partial t} = f(A_0). \tag{3}$$

The instantaneous speed of the center of pressure of the caudal fin is determined by the formula

$$V_i = \sqrt{V_0^2 + V_y^2}. \tag{4}$$

The angle of attack α of a rigid swept wing (here the angle of attack of the root chord) is found as the difference of the angle of downwash γ (i.e., the angle of slope of the instantaneous speed vector to the direction of forward motion of the center of gravity of the dolphin's body) and the angle of motion of the wing β (i.e., the instantaneous angle of inclination of the profile chord to the direction of forward motion of the center of gravity of the dolphin's body). An example of variation of angles γ and β during the period of oscillations of the caudal fin is shown in Figure 5, d.

We find angle γ from the ratio of speeds V_0 and V_y:

$$\operatorname{tg}\gamma = -\frac{V_y}{V_0}, \tag{5}$$

and angle β is found graphically directly from the trajectory of the caudal fin (Figure 5, a). Angle β is also the amplitude of the angular oscillations of the profile around its own pressure center. It follows from comparision of Figure 5, a and 5, d that the phase shearing angle δ of vertical and angular oscillations of

APPROVED FOR RELEASE: 2007/02/08: CIA-RDP82-00850R000300060001-1

APPROVED FOR RELEASE: 2007/02/08: CIA-RDP82-00850R000300060001-1

the profile is equal to $\pi/2$. In the case of variable δ, this corresponds to the maximum efficiency of an impeller of the flapping wing type, all things being equal [3].

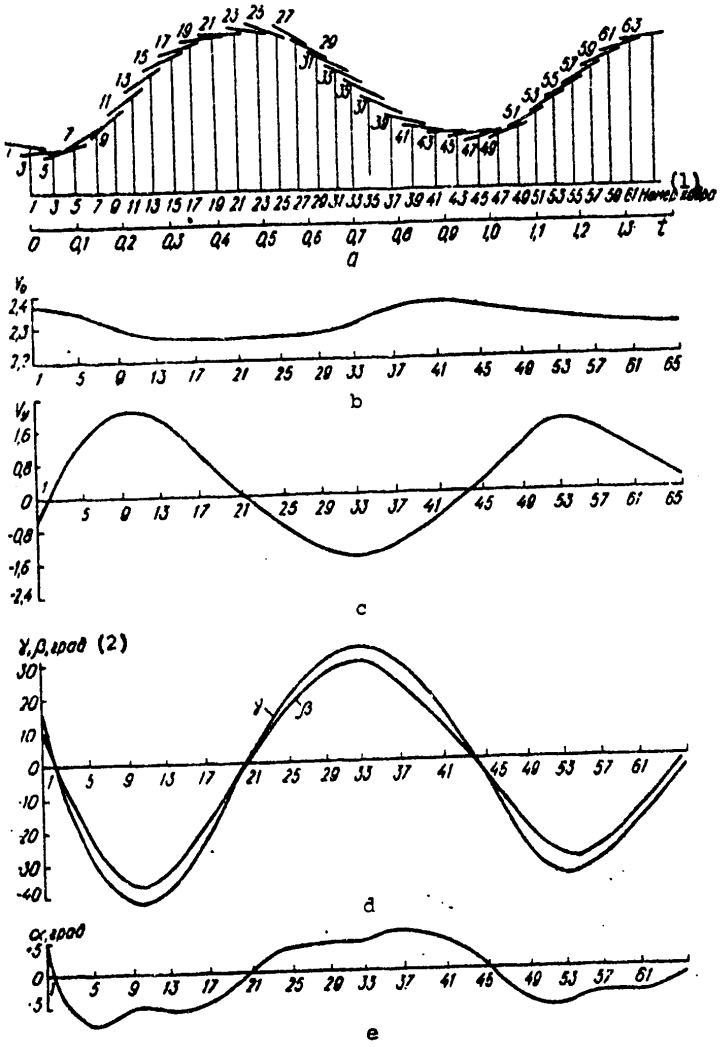

Figure 5. Kinematic Characteristics of Motion of Caudal Fin of Dolphin

Key:
1. Number of frame
2. Degrees

The nature of variation of the angle of attack of profile α during the period of oscillation of the caudal fin, found by the method described above (i.e., $\alpha = \gamma - \beta$), is presented in Figure 5, e. Graph $\alpha(t)$ has a clearly marked maximum in

APPROVED FOR RELEASE: 2007/02/08: CIA-RDP82-00850R000300060001-1

APPROVED FOR RELEASE: 2007/02/08: CIA-RDP82-00850R000300060001-1

the shape of the surface during each half-period of oscillations and at the same time when the values of transverse speed V_y of the caudal fin have the greatest values. The maximum value of angle α which we found from the trajectories of the caudal fins of dolphins usually does not exceed 10° and the mean values are within the range of 4-6°. According to Lang's data [15], obtained by computer calculation for a wing with the profile of the caudal fin of the common dolphin (curve 2 of Figure 3), cavitation on this wing begins at α = 4° and V_i = 11.7 m/s and at α = 6° and V_i = 9.9 m/s (this corresponds in our case to the swimming speed of a dolphin V_0 equal to approximately 9.5 and 8.0 m/s, respectively), while the appearance of cavitation on the caudal fin can be very painful for a dolphin.

Now, if the angle of attack and the instantaneous speed of motion of the wing are known at each moment of time, one can determine the hydrodynamic forces X and Y by formulas (1) and (2). Having projected them onto the horizontal and vertical axes and having integrated during period of oscillations τ, we find the averaged values of the horizontal thrust {T} and of the transverse force {F}:

$$\{T\} = \frac{1}{\tau}\int_0^{\tau} (Y_i \sin\gamma_i - X_i \cos\gamma_i)\, dt; \tag{6}$$

$$\{F\} = \frac{1}{\tau}\int_0^{\tau} (Y_i \cos\gamma_i + X_i \sin\gamma_i)\, dt. \tag{7}$$

For the case shown in Figure 5, the mean horizontal thrust of the caudal fin of the dolphin with length L = 2.4 meters and weighing G = 140 kg is equal to 2.2 kg during the period of oscillations.

Since the forward motion of the dolphin is usually transient, when processing the graphs we determine the mean variation of speed $\{\dot{V}\}$ and force $\{R_i\}$ required to overcome inertial forces during the period of oscillation:

$$\{R_i\} = m_A (1 + k_{11})\{\dot{V}\}, \tag{8}$$

where $m_A = G/g$ is the mass of the dolphin and k_{11} is the coefficient of reduced mass determined by nomograms [2] for the body of a dolphin replaced by an equivalent ellipsoid of rotation (the effect of variation of the body configuration of the dolphin during the period of oscillations of the caudal fin was not taken into account).

We find the value of hydrodynamic drag as the difference of the thrust of the fin {T} and inertial forces {Ri}:

$$\{R\} = \{T\} - \{R_i\}. \tag{9}$$

The values of the hydrodynamic drag coefficients of dolphins are determined by the formula

$$\zeta = \frac{2\{R\}}{\rho V_0^2 \Omega}. \tag{10}$$

APPROVED FOR RELEASE: 2007/02/08: CIA-RDP82-00850R000300060001-1

APPROVED FOR RELEASE: 2007/02/08: CIA-RDP82-00850R000300060001-1

The area of the wetted surface of the dolphin Ω is determined from the results of measurements of its body and fins [5]. The results found previously [5] using Logvinovich's formulas on the kinematics of bending-oscillatory motions of the dolphin body at different accelerations of forward motion are represented in Figure 6 by points 3-7. The points in the additional circles show the values of ζ found by the method described above and calculated by formula (10). The dependence of the drag coefficient of a rigid body equivalent in shape and area to the wetted surface of the dolphin body on Re number during completely turbulent and laminar flow is shown by curves 1 and 2.

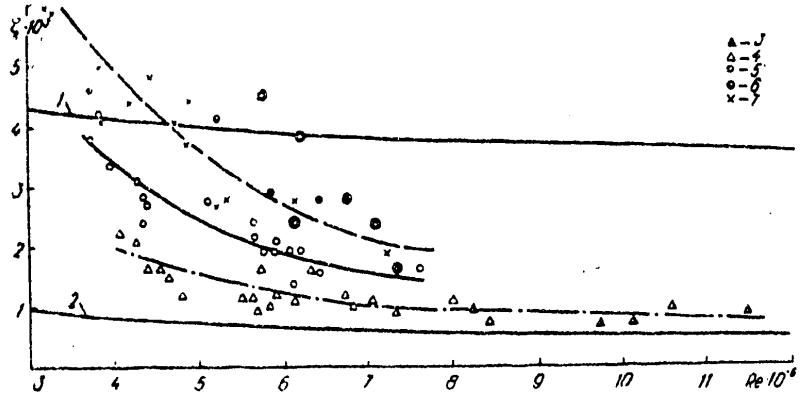

Figure 6. Dependence of Hydrodynamic Drag Coefficient of Dolphin on Re Number and Mean Acceleration of Motion: 1--during turbulent flow; 2--during laminar flow; 3--V = (0.35-0.70) m/s^2; 4--V = = (0.10 30) m/s^2; 5--V = (0-+0.07) m/s^2; 6--V = -(0.08-0.15) m/s^2; 7--motion by inertia with nonworking fin

The hydrodynamic drag coefficients of the dolphin whose fin is assumed to be working in the flapping wing mode, found by using the quasi-steady approach, is approximately double the value of the same coefficients in all cases found in the same swimming modes for the dolphin whose fin creates thrust by bending-oscillatory movements of the entire body (points 3-6).

The values found by the quasi-steady method can be assumed the upper limit of coefficient ζ since the assumptions and simplifications made above exaggerate the values of the aerodynamic coefficients C_x and C_y which are the basis for calculating the hydrodynamic forces on an oscillating wing. Thus, analysis of the movie materials shows that flexing of the trailing edge of the fin increases as the instantaneous speed V_i of the caudal fin of the dolphin increases and thus the angle of attack of the rear part of the fin with significant area decreases. This leads to a decrease of hydrodynamic forces X and Y on a flexible wing compared to a rigid wing and accordingly to a decrease of the thrust {T} of the dolphin fin, all things being equal. Based on the foregoing, one may assume that the effective value of the hydrodynamic drag coefficient of the dolphin during uniform swimming at Re = = $(5-9)\cdot10^6$ is within the range of $(3-1.5)\cdot10^{-3}$, having a tendency to decrease as Re number increases.

APPROVED FOR RELEASE: 2007/02/08: CIA-RDP82-00850R000300060001-1

APPROVED FOR RELEASE: 2007/02/08: CIA-RDP82-00850R000300060001-1

Comparison of the results of calculating the thrust of the dolphin film by two different methods shows their poor agreement and gives the upper and lower bounds of the real values of thrust. However, the real caudal fin of a dolphin has a flexible surface, flexibility along the profile and smoother streamlining. Therefore, more precise data by the method described above can be found after water tunnel tests of models of the real caudal fins of dolphins and more precise determination of stereofilming of the components of trajectory of the caudal fin of the dolphin.

BIBLIOGRAPHY

1. Andriyevskiy, V. V., V. M. Belokonov, A. F. Bochkarev and V. I. Klimov, "Aeromekhanika samoleta" [The Aeromechanics of the Aircraft], Moscow, Mashinostroyeniye, 1977.

2. Voytkunskiy, Ya. I., R. Ya. Pershits and I. A. Titov, "Spravochnik po teorii korablya" [Handbook on Ship Theory], Leningrad, Sudpromgiz, 1960.

3. Grebeshov, E. P. and O. A. Sagoyan, "The Hydrodynamic Characteristics of an Oscillating Wing Performing the Function of the Supporting Element and Impeller," TRUDY TSAGI, No 1725.

4. Kayan, V. P. and V. Ye. Pyatetskiy, "The Kinematics of Swimming of the Bottlenosed Dolphin as a Function of the Mode of Acceleration," BIONIKA, No 11, 1977.

5. Kayan, V. P. and V. Ye. Pyatetskiy, "The Hydrodynamic Characteristics of the Bottlenosed Dolphin in Different Modes of Acceleration,"BIONIKA, No 12, 1978.

6. Kravets, A. S., "Kharakteristiki aviatsionnykh profiley" [Characteristics of Aviation Profiles], Moscow-Leningrad, Oborongiz, 1939.

7. Logvinovich, G. V., "The Hydrodynamics of Swimming of Fishes," BIONIKA, No 7, 1973.

8. Nekrasov, A. I., "Teoriya kryla v nestatsionarnom potoke" [The Theory of the Wing in a Transient Flow], Moscow, Izd-vo AN SSSR, 1947.

9. Savchenko, Yu. N., "Experimental Investigation of the Hydromechanics of a Flapping Wing," author's abstract of candidate dissertation, Kiev, 1970.

10. Sedov, L. I., "Ploskiye zadachi gidrodinamiki i aerodinamiki" [Plane Problems of Hydrodynamics and Aerodynamics], Moscow, Nauka, 1966.

11. Pershin, S. V., "Hydrodynamic Analysis of the Fin Profiles of Dolphins and Whales," BIONIKA, No 9, 1975.

12. Pyatetskiy, V. Ye., V. P. Kayan and A. M. Kravchenko, "Experimental Installations, Apparatus and Methods of Studying the Hydrodynamics of Swimming of Aquatic Animals," BIONIKA, No 7, 1973.

APPROVED FOR RELEASE: 2007/02/08: CIA-RDP82-00850R000300060001-1

APPROVED FOR RELEASE: 2007/02/08: CIA-RDP82-00850R000300060001-1

13. Pyatetskiy, V. Ye., V. P. Kayan, L. F. Kozlov and N. P. Semenov, "A Device for Investigating the Kinematics of Swimming of Dolphins," BIONIKA, No 12, 1978.

14. Hertel, H., "Structure, Form and Movement," New York, Reinhold Publishing Company, 1966.

15. Lang, T. G., "Hydrodynamic Analysis of Dolphin Fin Profiles," NATURE, Vol 209, No 5028, 1966.

APPROVED FOR RELEASE: 2007/02/08: CIA-RDP82-00850R000300060001-1

APPROVED FOR RELEASE: 2007/02/08: CIA-RDP82-00850R000300060001-1

UDC 532.6.04

A THIN PERMEABLE LIFTING SURFACE IN AN INCOMPRESSIBLE FLUID FLOW

Kiev BIONIKA in Russian No 13, 1979 signed to press 14 Jun 79 pp 15-18

[Article by I. I. Yefremov, Institute of Hydromechanics of the Ukrainian SSR Academy of Sciences, from the collection "Bionika," Izdatel'stvo Naukova Dumka, 1,000 copies, 100 pages]

[Text] Solution of the problem of flow over a permeable lifting surface is of interest with regard to investigation of the hydrodynamic characteristics of the wings of some birds. Investigating the effect of air permeability is also important to evaluate the effect of the porosity of the material on the hydrodynamic characteristics of sails. The plane problem on a thin permeable profile was first solved approximately by Kh. A. Rakhmatulin [4]. A precise solution of this problem is given in [6]. The purpose of the given paper is to investigate the effect of the finiteness of aspect ratio on manifestation of the permeability effect.

Let us consider the problem of steady vortex-free flow of an incompressible fluid over a thin permeable wing of finite span. Permeability means that the normal velocity of the fluid particles encountering the wing differs from the normal velocity of the wing points by a value called the permeation rate.

According to Kh. A. Rakhmatulin's model [4], a wing is uniformly permeable at all points and the permeation rate is a function of the pressure drop along the wing. Specifically, the dependence of the permeation rate on pressure drop is taken as linear:

$$v_p = \varkappa \frac{p_- - p_+}{\rho v_\infty}, \qquad (1)$$

where $\varkappa$ is the dimensionless coefficient of permeability, p_- and p_+ are the values of pressure on the lower and upper surfaces of the wing, respectively, and V_∞ is the velocity of undisturbed flow. Assuming that the wing is thin, slightly distorted and presented at a small angle of attack to the incident flow, let us consider the problem in linear postulation.

Let us connect a movable coordinate system to the wing, having combined the origin with the inlet edge of the wing root section. Let us direct the Ox axis along the velocity of incident flow, the Oz axis vertically upwards and the Oy axis in the direction of the span to obtain left-hand coordinate system Oxyz.

APPROVED FOR RELEASE: 2007/02/08: CIA-RDP82-00850R000300060001-1

APPROVED FOR RELEASE: 2007/02/08: CIA-RDP82-00850R000300060001-1

The boundary value problem of flow over a thin permeable wing of finite span is formulated in terms of acceleration potential $\phi(x, y, z)$.

As is known [2, 3], the following relations occur in linear airfoil theory

$$\theta(x, y, z, t) = \frac{p_\infty - p}{\rho} = v_\infty \frac{\partial \varphi}{\partial x} = N\varphi, \tag{2}$$

where $\phi(x, y, z)$ is the potential of disturbed velocities, which is a harmonic function in the flow region. Since θ and ϕ are linked by a linear differential operator, the acceleration potential satisfies the Laplace equation

$$\Delta\theta = 0 \text{ outside S.} \tag{3}$$

Here S is projection of the wing onto plane xOy. If $z = f(x, y)$ is the equation of a lifting surface, the boundary condition of flow over a permeable surface has the form

$$\varphi_z|_{z=0} = v_\infty \frac{\partial f}{\partial x} + \varkappa \frac{\theta_+ - \theta_-}{v_\infty} \text{ for } (x, y) \in S. \tag{4}$$

Hence, it is easy to find the boundary condition for vertical acceleration θ_z. However, since the differentiation operation used in transition from velocity potential to acceleration potential can lead to a loss of terms corresponding to boundary condition $\phi_z = \text{const}$, let us satisfy the flow condition for the value of a vertical rate of disturbed motion. To do this, let us use the recovery operator

$$\varphi = N^{-1}\theta = \frac{1}{v_\infty} \int_{-\infty}^{x} \theta(\tau, y, z)\, d\tau. \tag{5}$$

Then condition (4) is written thusly:

$$\frac{1}{v_\infty} \frac{\partial}{\partial z} \int_{-\infty}^{x} \theta(\tau, y, 0) d\tau = v_\infty \frac{\partial f}{\partial x} + \varkappa \frac{\theta_+ - \theta_-}{v_\infty}. \tag{6}$$

At infinity the acceleration potential should disappear:

$$\theta \to 0 \text{ at } r = \sqrt{x^2 + y^2 + z^2} \to \infty. \tag{7}$$

The pressure is continuous on the outlet edge: $\theta_+ = \theta_-$. The wing is a surface of pressure discontinuity and consequently of acceleration potential as well. Let us solve boundary value problems (3), (6) and (7) in the form of double layer potential with intensity:

$$\theta_+ - \theta_- = v_\infty^2 \gamma(x, y), \tag{8}$$

$$\theta = \frac{v_\infty^2}{4\pi} \iint_S \gamma(\xi, \eta) \frac{z}{[(x-\xi)^2 + (y-\eta)^2 + z^2]^{3/2}} d\xi d\eta. \tag{9}$$

APPROVED FOR RELEASE: 2007/02/08: CIA-RDP82-00850R000300060001-1

APPROVED FOR RELEASE: 2007/02/08: CIA-RDP82-00850R000300060001-1

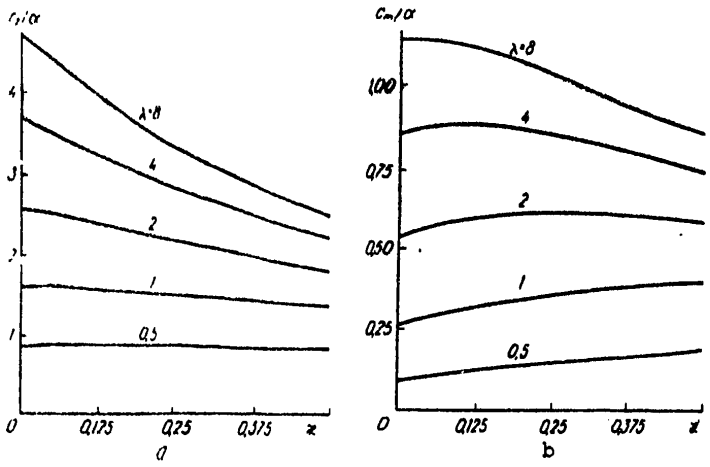

Figure 1. Dependence of Lift Coefficient (a) and Longitudinal Moment (b) of Unswept Finite-Aspect Wing on Degree of Permeability

Having substituted equality (9) into condition (6), we find the integral equation

$$\varkappa\gamma(x, y) + \frac{1}{4\pi}\frac{\partial}{\partial y}\int\limits_S\int \frac{\gamma(\xi, \eta)}{y-\eta}\left[1 + \frac{\sqrt{(x-\xi)^2+(y-\eta)^2}}{x-\xi}\right]d\xi d\eta = -\frac{\partial f}{\partial x}, \quad (x, y) \in S. \tag{10}$$

Equation (10) can also be found by using the vortex scheme of a finite-span wing and by replacing the latter with continuous distribution of U-shaped vortices with peaks at the wing points [5].

Let us consider an unswept wing

$$\varkappa\gamma(x, y) - \frac{1}{4\pi}\int\limits_0^1\int\limits_{-b}^{+b} \frac{\gamma(\xi, \eta)}{(y-\eta)^2}\left[1 + \frac{x-\xi}{\sqrt{(x-\xi)^2+(y-\eta)^2}}\right]d\xi d\eta = -\frac{\partial f}{\partial x}. \tag{11}$$

(The special integral should be understood in the sense of Mangler [5]). Let us use the discrete vortex method for numerical solution of equation (11). To do this, let us divide the half-span of the wing into K parts and let us assume that the intensity of the U-shaped vortices inside each segment is independent of η. Let us satisfy the boundary condition (4) in the middle of the small interval. Let us use the "3/4" method in the direction of the chord [1]. Thus, we find a system of linear algebraic equations

APPROVED FOR RELEASE: 2007/02/08: CIA-RDP82-00850R000300060001-1

APPROVED FOR RELEASE: 2007/02/08: CIA-RDP82-00850R000300060001-1

$$\varkappa\gamma_{i\mu}+\frac{1}{4\pi M}\sum_{j=1}^{M}\sum_{\nu=1}^{K}\gamma_{j\nu}\left\{\frac{1}{y_\mu+\eta_\nu}\left[1+\frac{\sqrt{(x_i-\xi_j)^2+(y_\mu+\eta_\nu)^2}}{x_i-\xi_j}\right]-\right.$$
$$-\frac{1}{y_\mu+\eta_{\nu-1}}\left[1+\frac{\sqrt{(x_i-\xi_j)^2+(y_\mu+\eta_{\nu-1})^2}}{x_i-\xi_j}\right]-$$
$$-\frac{1}{y_\mu-\eta_\nu}\left[1+\frac{\sqrt{(x_i-\xi_j)^2+(y_\mu-\eta_\nu)^2}}{x_i-\xi_j}\right]+\frac{1}{y_\mu-\eta_{\nu-1}}\times \tag{12}$$
$$\left.\times\left[1+\frac{\sqrt{(x_i-\xi_j)^2+(y_\mu-\eta_{\nu-1})^2}}{x_i-\xi_j}\right]\right\}=-\frac{\partial f_i}{\partial x},$$

where

$$x_i=\left(i-\frac{1}{4}\right)\frac{1}{M};\quad \xi_j=\left(j-\frac{3}{4}\right)\frac{1}{M};$$
$$y_\mu=\left(\mu-\frac{1}{2}\right)\frac{b}{K};\quad \eta_\nu=\nu\frac{b}{K}; \tag{13}$$
$$(i,j)=1,2,\ldots,N,\quad (\mu,\nu)=1,2,\ldots,K.$$

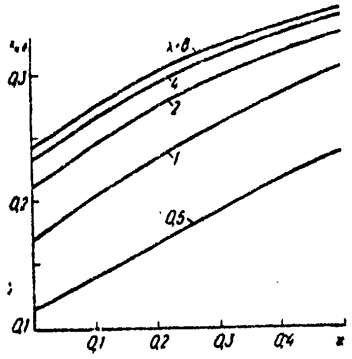

Figure 2. Variation of Position of Pressure Center of Unswept Wing as a Function of Coefficient of Permeability

After solution of system (12), the aerodynamic characteristics of a permeable wing is found by the formulas

$$c_z=\frac{2}{MK}\sum_{j=1}^{M}\sum_{\nu=1}^{K}\gamma_{j\nu},\quad c_m=\frac{2}{MK}\sum_{j=1}^{M}\sum_{\nu=1}^{K}\xi_j\gamma_{j\nu}. \tag{14}$$

The calculations were made* on a BESM-6 computer using FORTRAN algorithmic language.

*The calculations on the computer were made by M. E. Marko.

APPROVED FOR RELEASE: 2007/02/08: CIA-RDP82-00850R000300060001-1

APPROVED FOR RELEASE: 2007/02/08: CIA-RDP82-00850R000300060001-1

The number of wing divisions along the span to K and along the chord M was varied in the calculations as a function of aspect ratio. Thus, K = 12 and M = 5 at $\lambda = 2b = 8$ and K = 5 and M = 12 at $\lambda = 0.5$. The results of calculation of C_z and C_m are presented in Figure 1. Hence, it is obvious that the effect of permeability on the value of the lift coefficient becomes weak as aspect ratio decreases. However, the center of pressure is shifted toward the center of the chord as permeability increases (Figure 2). This shift is especially appreciable at low aspect ratios. The load distribution along the span also becomes more uniform and decreases sharply in value only near the lateral edges. The indicated circumstance for a sale is very undesirable since it leads to an increase of the rolling moment.

BIBLIOGRAPHY

1. Belotserkovskiy, S. M., "Tonkaya nesushchaya poverkhnost' v dozvukovom potoke gaza" [A Thin Lifting Surface in a Subsonic Gas Flow], Moscow, Nauka, 1965.

2. Nekrasov, A. I., "Teoriya kryla v nestatsionarnom potoke" [Theory of a Wing in a Transient Flow], Moscow, Izd-vo AN SSSR, 1947.

3. Panchenkov, A. N., "Teoriya potentsiala uskoreniy" [Theory of Acceleration Potential], Irkutsk, Izd-vo Irkutskogo universiteta, 1970.

4. Rakhmatulin, Kh. A., "Flow Over a Permeable Body," VESTN. MOSK. UN-TA. SER. FIZ.-MAT. I YESTESTV. NAUK, No 2, 1950.

5. Ashley, H. and M. Lindall, "Aerodinamika korpusov i kryl'yev letatel'nykh apparatov" [The Aerodynamics of Aircraft Bodies and Wings], Moscow, Mashinostroyeniye, 1969.

6. Barakat, R., "Incompressible Flow Around Porous Two-Dimensional Sails and Wings," J. MATH. AND PHYSICS, Vol 47, No 3, 1968.

APPROVED FOR RELEASE: 2007/02/08: CIA-RDP82-00850R000300060001-1

APPROVED FOR RELEASE: 2007/02/08: CIA-RDP82-00850R000300060001-1

UDC 591.524;591.177

HYDRODYNAMIC EFFECTS OF A TRAVELLING WAVE

Kiev BIONIKA in Russian No 13, 1979 signed to press 14 Jun 79 pp 19-24

[Article by Yu. N. Savchenko, Institute of Hydromechanics of the Ukrainian SSR Academy of Sciences, from the collection "Bionika," Izdatel'stvo Naukova Dumka, 1,000 copies, 100 pages]

[Text] Interest in study of flows along a travelling surface wave was aroused by the bionic investigations of Essapian and Kramer, who suggested that the "travelling folds" on the skin surface of the dolphin may affect swimming speed [5, 10]. The investigators feel that detailed study of the hydrodynamics of travelling waves would yield data of fundamental importance for hydromechanics.

Bionic observations require scientific explanations and a subsequent number of papers laid the basis for the new trend of investigations in hydromechanics related to travelling waves as a possible mechanism of drag reduction [1, 2, 4, 6].

The hopes of investigators were justified: digital computer calculations and direct experiments in a hydrodynamic laboratory showed that a vortex flow, clearly visible on photographs with prolonged exposure of the travelling wave model (Figure 1, a-b), is formed in the depressions between travelling waves under specific conditions.

A special model of the travelling wave which permits consideration of the flow formed in coordinate system OXY bound to the wave crest and moving at phase velocity V_f in an incident fluid flow at velocity V_∞ was used both in the experiments and in digital computer calculation. The wavy surface boundary $y = a \sin(\omega t + kx)$ in this coordinate system becomes a fixed surface in which each point slides along the tangent toward the incident wave at velocity of $-V_g$. The relative velocity in this case is equal to $V_e = V_\infty - V_g$ and $V_f = V_g$.

An experiment on flow visualization was conducted in a flow channel on a model containing four waves of length $\lambda = 110$ mm and amplitude $2A = 45$ mm on its surface at Reynolds numbers of $R_L = V_e L/\nu = 0.12 \cdot 10^6 - 0.3 \cdot 10^6$ and $R_\lambda = V_e \lambda/\nu = 0.2 \cdot 10^5 - 0.5 \cdot 10^5$.

From comparison of the flow patterns found by digital computer calculation [2] (Figure 1, c) and observed in experiment during water flow over the model, their total agreement is obvious.

The investigations showed that stable periodic flow in the form of vortices between wave crests occurs only in the case when the phase velocity of the waves comprises

APPROVED FOR RELEASE: 2007/02/08: CIA-RDP82-00850R000300060001-1

APPROVED FOR RELEASE: 2007/02/08: CIA-RDP82-00850R000300060001-1

half the incident flow velocity, i.e., $V_f/V_e \approx 1/2$. The value of this ratio apparently corresponds to the minimum tangent stresses in interaction of the resulting vortex flow with solid boundary and external flow.

Experiments to measure the force interaction of a surface with a travelling wave and the flow around it [6] showed that the drag coefficient $C_x = 2R_x/V^2S$ is strongly dependent on the value of the relative phase velocity $\bar{V}_f$ and may become less at $\bar{V}_f \approx 0.6$ than that of an equivalent smooth plate [6]. The drag coefficient C_x is no longer dependent on Reynolds number in this case, which can be explained by formation of a stable periodic flow along the entire surface when the drag coefficient of each of the cells of the travelling wave is no longer dependent on its position in the row.

Unlike a surface with fixed boundary on which negative work is carried out to reduce the energy of the incident flow, a travelling wave on the surface may increase the flow energy, which is observed in the case of formation of a stable secondary vortex flow in the depressions between travelling waves when the directions of the normal velocity components of the boundary and flow coincide.

It is obvious that specific work, determined by energy expenditures to form a vortex flow and to maintain it on the flow surface, must be completed to increase the flow energy. The energy expenditure to create a stable system of secondary vortex flow can be estimated in the following manner.

Let us consider a vortex pinch of radius r and length l rotating at angular rate $\omega \approx V_\omega/2r$ in the depression between travelling waves in the coordinate system XOY bound to the center of the vortex (Figure 2).

The moment of the viscous forces applied on the boundary of the vortex pinch rotating as a single whole from the direction of the surrounding fluid can be estimated by using the known solution of the Navier-Stokes equations for a vortex in an infinite fluid [8]:

$$M = 4\pi\mu\omega lr^2. \tag{1}$$

Taking into account that a specific number of waves $n = L/\lambda$ is added simultaneously on the flow surface of length L and width l, we find for the energy expended per unit time to maintain the entire vortex system

$$N_\Sigma = nM\omega = 4\pi\nu\rho\omega^2 r^3 lL/\lambda. \tag{2}$$

This formula permits one to estimate the value of the viscous losses to dissipation of the vortex system of the secondary flow along the entire surface with travelling waves. The energy expended on formation of vortices is equal to the kinetic energy of the vortices formed per unit time on the flow surface.

According to experimental data, a stable secondary flow is formed at phase velocity of travelling waves of $V_f = V_e/2$. In this case $n_1 = V_e/2\lambda$ vortices whose centers are moved along the surface at velocity $V_e/2$ are formed per unit time. Since the kinetic energy of the forward motion of the fluid included in the formed vortices is equal to $N_0 = l\rho\pi r^2 V_e^3/4\lambda$ upon inleakage to a surface with a travelling wave and

APPROVED FOR RELEASE: 2007/02/08: CIA-RDP82-00850R000300060001-1

APPROVED FOR RELEASE: 2007/02/08: CIA-RDP82-00850R000300060001-1

since $N_s = 1\rho\pi r^2 v_e^3/16\lambda$ on the surface itself and in the wake, the energy expended per unit time to brake the forward motion of the fluid is determined by the formula

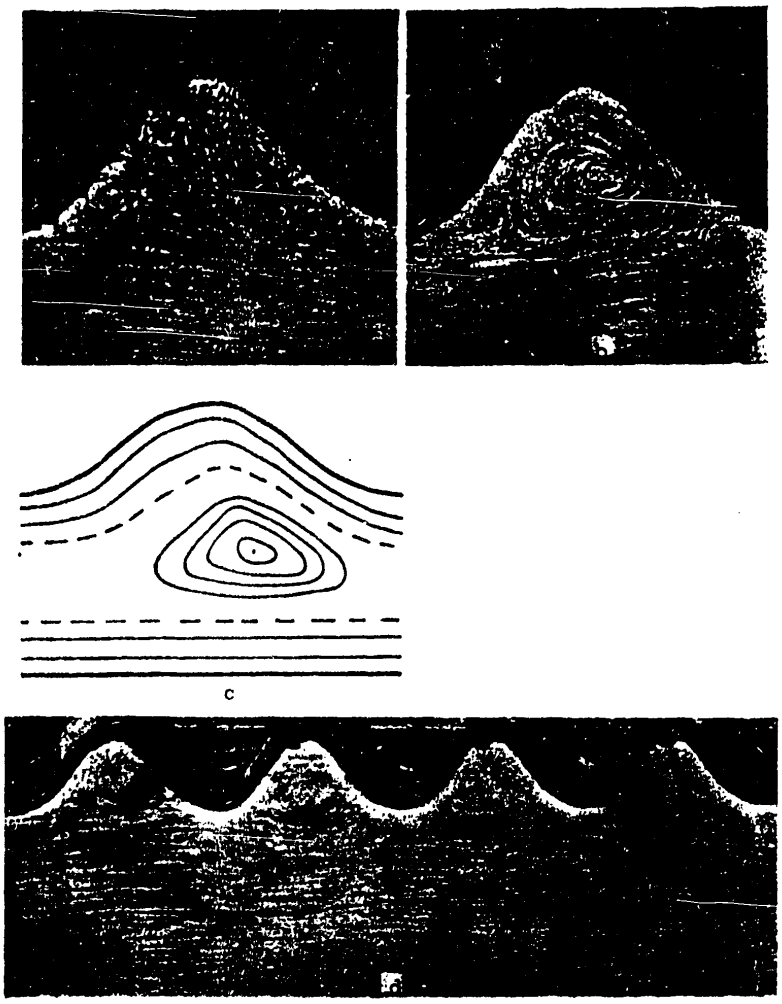

c

Figure 1. Flow Pattern Along Travelling Wave: a--flow in depression between wave crests at $V_f = V_e = 0$; b--at $V_f/V_e = 1/2$; c--digital computer calculation of flow pattern; d--flow along surface of model at $V_f/V_e = 1/2$

$$N_n = N_0 - N_c = \frac{3\rho\pi r^2 V_e^3 l}{16\lambda}. \quad (3)$$

APPROVED FOR RELEASE: 2007/02/08: CIA-RDP82-00850R000300060001-1

APPROVED FOR RELEASE: 2007/02/08: CIA-RDP82-00850R000300060001-1

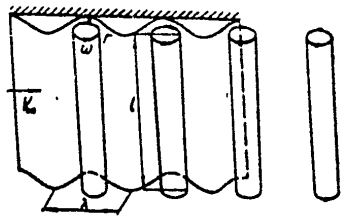

Figure 2. Diagram of Vortex Arrangement Along Surface of Travelling Waves

The kinetic energy of the vortex system during its rotational motion at rate $\omega = V_e/2r$ is found by the formula

$$N_к = \frac{1}{2} J\omega^2 l \frac{V_e}{2\lambda} = \frac{\rho\pi r^4 V_e^3 l}{32\lambda}, \tag{4}$$

where $J = (1/2)\rho\pi r^4$ is the moment of inertia of the circular cross-section of radius r.

Adding expressions (2)-(4), we find the approximate estimate of the energy taken from the incident flow by the vortex system of a travelling wave:

$$N_\Sigma = N_д + N_п + N_к = \frac{\pi}{\lambda}\rho V_e^2 L l \nu \left(1 + \frac{3}{32}\left(\frac{r}{L}\right)^2 \mathrm{Re}_L\right), \tag{5}$$

where $\mathrm{Re}_L = V_e L/\nu$ is Reynolds number along the length of the model L.

Comparing the value of N_Σ to the energy consumption per unit time in a turbulent boundary layer [9]

$$N_{пгс} = \xi \frac{\rho V_e^3}{2} lL = 0{,}0307 (\mathrm{Re}_L)^{-\frac{1}{7}} \frac{\rho V_e^3}{2} lL, \tag{6}$$

we find some coefficient of boundary wave effectiveness

$$\eta = \frac{N_\Sigma}{N_{пгс}} = \frac{\pi}{0{,}0307} \frac{L}{\lambda} \mathrm{Re}_L^{\frac{1}{7}} \left[\mathrm{Re}_L^{-1} + \frac{3}{32}\left(\frac{r}{L}\right)^2\right]. \tag{7}$$

For large Reynolds numbers, expression (7) has a simplified form

$$\eta = 19{,}2 \frac{r^2}{\lambda L} \mathrm{Re}_L^{\frac{1}{7}}. \tag{8}$$

APPROVED FOR RELEASE: 2007/02/08: CIA-RDP82-00850R000300060001-1

APPROVED FOR RELEASE: 2007/02/08: CIA-RDP82-00850R000300060001-1

As can be seen from expressions (7) and (8), the effectiveness of the travelling wave depends on dimensionless parameters r/λ, r/L and Reynolds number. For example, the coefficient of travelling wave effectiveness is $\eta = 0.125$ at $r/\lambda = 0.25$, $r/L = 400$ and $Re_L = 10^7$, which corresponds to energy expenditures one-eighth those in a turbulent boundary layer and is an estimate of the maximum possible advantage of drag.

Since realization of a specific coating containing a device to generate travelling waves is fraught with great difficulties, the mechanism of travelling wave generation in the auto-oscillation mode, which occurs during flow over an elastic shell [4], is of great interest. It is known that transition of laminar flow in a boundary layer to turbulent flow occurs with variation of dynamic stability in the boundary layer, which is characterized by critical Reynolds number of $Re_{kr} = 3.5\ (10^5\text{-}10^6)$. At Reynolds numbers less than critical, the viscous forces in the fluid predominate over the inertial forces and the damping properties of viscosity are sufficient to maintain flow stability. As Reynolds number increases, the ratio of inertial to viscous forces increases proportionally and equilibrium is inevitably violated, leading to the occurrence of auto-oscillations in the boundary layer.

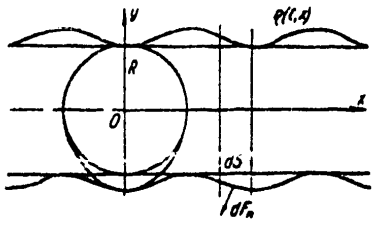

Figure 3. Diagram of Travelling Surface Wave With Amplitude η (t, x) on Cylinder of Radius R

Theoretical analysis and experimental investigations showed that the auto-oscillation process is characterized at near-critical Reynolds numbers by the natural frequency which can be accurately predicted as a function of Reynolds number [4, 9]. Thus, auto-oscillations with phase velocity of $V_f = 0.42\ V_e$ and with wave number of $k = 0.487\ V_e \cdot 10^{-3}/\nu$ occur in a laminar boundary flow at critical point $x_{kr} = (112 \cdot 10^5\ \nu)/V_e$ on a rigid semi-infinite plate.

Upon the onset of the auto-oscillation mode, it becomes possible to select the parameters of an elastic boundary surface such that waves with phase velocities and wave numbers corresponding to auto-oscillations in the boundary layer may appear on it. The drop of the resulting secondary flow can be prevented and it can be maintained on the entire flow surface with corresponding adjustment of the parameters of the elastic surface. In this case periodic flow characterized by wavelength of $\lambda = 2\pi/k = 12.9(\nu/V_e)$ and frequency $\omega = kV_f = 0.42\ V_e k = 204\ V_e$ and $n = \omega/2\pi = 30.4\ V_e$ occurs on the elastic flow surface of the hydrodynamic object.

If the phase velocity of the travelling wave becomes higher than the incident flow velocity, a thrust may occur whose value can be estimated from positions of the theory of swimming of a flexible body [3].

APPROVED FOR RELEASE: 2007/02/08: CIA-RDP82-00850R000300060001-1

APPROVED FOR RELEASE: 2007/02/08: CIA-RDP82-00850R000300060001-1

Let us consider motion of a body with flexible lateral surfaces (Figure 3). In the given case the main cross-section of a body of radius R will not make transverse oscillations, while the transverse variations of shape will be accomplished only due to deformations of the flexible surfaces adjacent to the cylindrical body. The instantaneous inertial force applied to the element of the deformed surface will be:

$$-dF_n = \frac{d}{dt}\left[m^*\left(\frac{\partial \eta}{\partial t} - V\frac{\partial \eta}{\partial x}\right)\right]dSdt, \tag{9}$$

where determines the shape of the body surface, $m^* = \rho\pi R^2$ is the virtual mass of the body cross section and V is velocity. The suction force, due to the constant cross-section of a cylindrical body on a segment with travelling wave R = const, will be equal to zero:

$$dp = \frac{dQ}{dS}\frac{dR}{dS} = 0.$$

Thus, the thrust on the section of a surface with travelling wave will be created only due to hydrodynamic forces of the inertial nature of (9). The mean value during the period will be determined by integration of equation (9) along the length of the active section of surface L and time of period T:

$$F_n = \frac{1}{T}\int_0^T dt \int_0^L \frac{d}{dt}\left[m^*\left(\frac{\partial \eta}{\partial t} - V\frac{\partial \eta}{\partial x}\right)\right]dx. \tag{10}$$

Projecting (10) onto horizontal axis OX, we find the value of the thrust caused by inertial force

$$F_x = \frac{m^*}{T}\int_0^T dt \int_0^L \frac{\partial \eta(x,t)}{\partial x}\frac{d}{dt}\left(\frac{\partial \eta(x,t)}{\partial t} - V(t)\frac{\partial \eta(x,t)}{\partial x}\right)dx. \tag{11}$$

The law of deformation of a flexible surface is given in the form

$$\eta(t,x) = (\eta_0 - \varepsilon x)\sin\left(\frac{V_\phi t}{L_n} - \frac{L-x}{L_n}\right), \tag{12}$$

where $L_p = L/2$ n and V_f is the phase velocity of the waves. Assuming that V = = const, L = const and V_f = const and integrating expression (11), we find

$$F_x = \frac{m^*}{2}\left(\frac{\eta_0}{L}\right)^2 V^2\left\{\left(\frac{V_\phi}{V} - 1\right)\left[\frac{\varepsilon L}{2\eta_0}\left(\frac{V_\phi}{V} - 1\right) - \frac{1}{6}\left(\frac{\varepsilon L}{\eta_0}\right)^2\left(\frac{V_\phi}{V} - 1\right)\right] - \left(\frac{L_n}{\eta_0}\right)^2 \varepsilon^2\right\}, \tag{13}$$

APPROVED FOR RELEASE: 2007/02/08: CIA-RDP82-00850R000300060001-1

APPROVED FOR RELEASE: 2007/02/08: CIA-RDP82-00850R000300060001-1

hence, it follows that the thrust force F_x will also be equal to zero in the case of a travelling wave of constant amplitude ($\varepsilon = 0$).

If phase velocity is introduced in the form $V_f(t) = V_{f0} + bt$, the corresponding increment of thrust force F_x will be determined by the formula $F_{x\Phi} = \frac{\eta_0^2 m^*}{2L_a} 2b\pi\left(n + \frac{V}{V_\Phi}\right)$. with accuracy to second-order value of smallness. In this case the sign of the increment will depend on the sign of the coefficient of the phase velocity increment b[m/s2]. As can be seen from formula (13), an increase of the values of thrust F_x is combined with the increase of the travelling wave amplitude due to parameters η_0 and ε.

BIBLIOGRAPHY

1. Kalugin, V. N. and V. I. Panchuk, "Flow of a Viscous Incompressible Fluid Along a Travelling Wave," BIONIKA, No 4, 1970.

2. Logvinovich, G. V., "Gidrodinamika techenky so svogodnymi granitsami" [The Hydrodynamics of Flows With Free Boundaries], Kiev, Naukova dumka, 1969.

3. Merkulov, V. I., "Flow of a Viscous Fluid Along a Travelling Wave," IZV. SO AN SSSR. SER. TEKH. NAUK, Issue 2, No 8, 1967.

4. Merkulov, V. I., "A Travelling Wave on an Elastic Body Moving in an Ideal Fluid," BIONIKA, no 4, 1970.

5. "Formation of Folds on the Skin Surface of Dolphins," in "Gidrobionika v sudostroyeniye" [Hydrobionics in Shipbuilding], Leningrad, TsNII inform. i tekhn.-ekon. issled., 1970.

6. Savchenko, Yu. N. and V. I. Merkulov, "Experimental Investigation of Fluid Flow Along a Travelling Wave," BIONIKA, No 4, 1970.

7. Savchenko, Yu. N. and V. T. Savchenko, "Estimating the Inertial Forces in Calculation of the Thrust of a Swimming Flexible Body," BIONIKA, No 7, 1973.

8. Slezkin, N. A., "Dinamika vyazkoy i szhimayemoy zhidkosti" [The Dynamics of a Viscous and Compressible Fluid], Moscow, Gostekhizdat, 1955.

9. Taggart, R., "A New Type of Propulsion System," SUDOSTROYENIYE: EKSPRESS-INFORMATSIYA VINITI, No 3, 1964.

10. Schlichting, H., "Teoriya pogranichnogo sloya" [Boundary Layer Theory], Moscow, Nauka, 1969.

11. Essapian, F. S., "Speed-Induced Skin Folds in the Bottle-Nosed Porpoise Tursiops truncatus," BREVIORA MUS. COMP. ZOOL., No 43, 1955.

APPROVED FOR RELEASE: 2007/02/08: CIA-RDP82-00850R000300060001-1

APPROVED FOR RELEASE: 2007/02/08: CIA-RDP82-00850R000300060001-1

UDC 591.524;591.177

THE MONOFLIPPER--A PROMISING WAVE IMPELLER FOR FAST SWIMMING IN THE FASHION OF DOLPHINS

Kiev BIONIKA in Russian No 13, 1979 signed to press 14 Jun 79 pp 24-35

[Article by S. V. Pershin and G. N. Orlov, Leningrad State Institute of Physical Culture imeni P. F. Lesgaft, from the collection "Bionika," Izdatel'stvo Naukova Dumka, 1,000 copies, 100 pages]

[Text] An increase of the propulsive qualities of man when using muscle energy to swim with the simplest individual mass-produced hardware is timely with regard to development of the off-shore shelf of the world ocean. This hardware should include various types of flippers, which have long been widely used in sports and recreation, but which can be improved. Underwater swimming using special equipment as one of the technical aspects of sport of applied significance is also important [6].

Ordinary mass-produced double flippers are well known, by using which the trained athlete increases swimming speed to 15-20 percent in surface or underwater swimming compared to swimming without flippers over the same distance. Some characteristics of these Soviet-produced flippers are presented in the summary [1]. One of the best is regarded as the domestic plant-produced Del'fin rubber flippers with overall length of 0.55 meter, with paddle 0.225 meter wide protruding behind the shoe and with area of working surface of 0.066 m^2. The mass of both flippers is 1.9 kg and the mean thrust developed by them is approximately 21 kg. Each of two flippers is a unique flapping impeller of the swimmer.

The experience of sports competitions showed that the working surface of the flipper should be increased significantly and the paddle should make a longer stroke bending on the wave trajectory to further increase swimming speed by the fastest (freestyle) crawl method with alternation of swimming motions of both feet of the swimmer. Thus, elongated high-speed double flippers manufactured by athletes themselves individually on the basis of mass-produced rubber flippers, but with lightening of them and attachment of thin working paddles of metal or fiberglas laminate, appeared for the first time in our country. As a typical example let us demonstrate [3] the homemade elongated high-speed flippers with paddle of sheet fiberglas laminate having total length of 0.75 meter, paddle width of 0.22 meter and working surface area of 0.092 m^2, which is almost 1.5-fold larger than those of common plant-manufactured rubber flippers. All high-speed heats using the crawl with flippers are now carried out in competitions only using similar elongated high-speed flippers.

APPROVED FOR RELEASE: 2007/02/08: CIA-RDP82-00850R000300060001-1

APPROVED FOR RELEASE: 2007/02/08: CIA-RDP82-00850R000300060001-1

In 1969 athletes also manufactured for the first time in our country and successfully used the monoflipper with large thin titanium paddle for high-speed swimming in the fashion of dolphins, i.e., with simultaneous swimming motions by both feet [11]. The idea of using a monoflipper is that the swimmer makes active forward motions in the vertical plane not only with his extremities but with the entire body in the method of swimming like dolphins and therefore the largest groups of human muscles--the back and stomach--are used efficiently, which permits one to achieve an additional increase in swimming speed. A subsequent sports experiment confirmed the feasibility of using a monoflipper and it is now used extensively in male and female competitions at all swimming distances with record-producing results. As before, the monoflipper is manufactured by the athletes themselves on an individual basis, but using specially treated fiberglas laminate for the working paddle of the flipper, performing laborious production operations manually.

Figure 1. Athlete With Monoflipper in Underwater Swimming in the Fashion of Dolphins in a Pool (Stop-Action Photograph)

The authors of this article, so far as is known, first conducted systematic investigations of swimming by athletes using a monoflipper according to a rather extensive program. Brief data on the method and some preliminary results of hydrodynamic tests are presented below.

In an underwater photograph (Figure 1), the swimmer is recorded with the body in an almost level position and the arms are extended. The main impeller is a large-area monoflipper consisting of a pair of rubber shoes attached to a single sheet paddle of fiberglas laminate. The given material was preferable because it has low density of approximately 1.6 g/cm^3, is easily flexible and is easy to machine. A number of longitudinal bands is visible on the paddle--these are depressions cut manually during manufacture of the monoflipper over part of the thickness of the fiberglas laminate sheet. Athletes state that these longitudinal depressions are supposedly necessary for stability and to prevent transverse yawing of the monoflipper in its extreme positions at the crests of the wave trajectory. However, the longitudinal cuts undoubtedly increase the hydrodynamic drag of the monoflipper.

Study of monoflippers (Figure 2) used by approximately 20 highly qualified athletes shows that the monoflipper paddles are manufactured in different shapes and sizes, being guided mainly by intuition and available experience. The determining factors

APPROVED FOR RELEASE: 2007/02/08: CIA-RDP82-00850R000300060001-1

APPROVED FOR RELEASE: 2007/02/08: CIA-RDP82-00850R000300060001-1

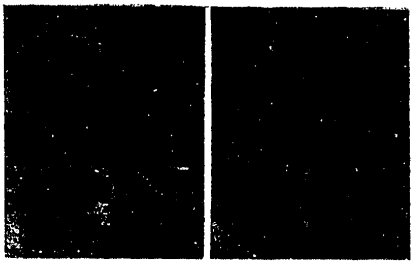

Figure 2. Modern Monoflipper of Fiberglas Laminate With Rubber Shoe (photograph from both sides, the length of the ruler is 0.35 meter)

are assumed to be the sex of the athlete, his height and weight, typical sprint and long distances and the elastic properties of the fiberglas laminate sheet, but it is not yet possible to take all these factors into account completely. The usual shape of the monoflipper paddle, besides that indicated in Figure 1, is trapezoidal, close to a semi-ellipse and so on. The dimensions of the monoflipper vary in the range of total length together with shoes of 0.65-0.90 meter, span of 0.65-0.87 meter and area (on one side) of 0.30-0.45 m^2, which far exceeds that of two elongated high-speed flippers. The total weight of the monoflipper does not exceed 2 kg and swimmers feel every 0.2-0.3 kg of excess weight over a distance. It is assumed that the highly qualified athlete develops an average thrust on the order of 30 kg or more when swimming over short distances with a monoflipper. This permits one to achieve an average swimming speed (when diving) up to 2.75 m/s, which is close to the maximum value for man according to physiological indicators.

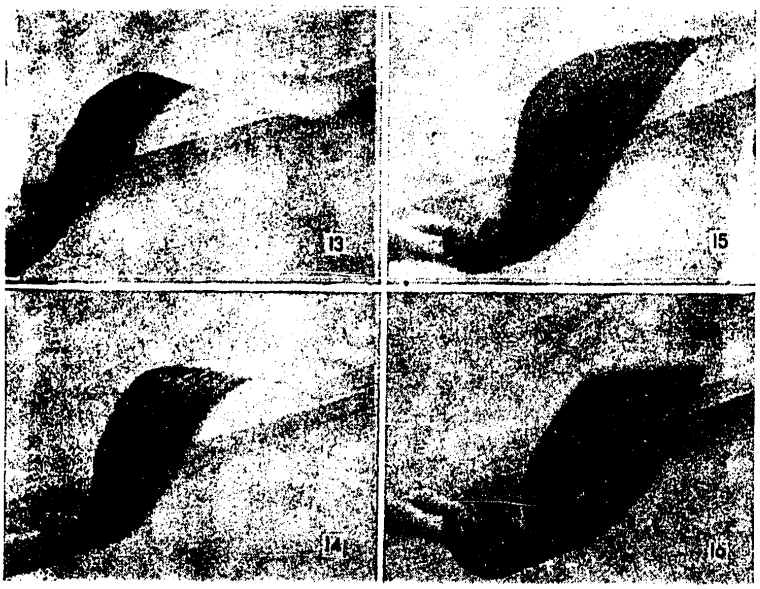

Figure 3. Wave Bending of Monoflipper of Swimming Athlete (sequential frames No. 13-16 of underwater motion picture of tracking camera with speed of 24 frames per second)

APPROVED FOR RELEASE: 2007/02/08: CIA-RDP82-00850R000300060001-1

APPROVED FOR RELEASE: 2007/02/08: CIA-RDP82-00850R000300060001-1

Let us present data of underwater photography of a diver by a tracking camera (Figures 3 and 4) for the physical characteristics of the work of a monoflipper. It follows from analysis of Figure 3 that a monoflipper, including its working paddle of sheet fiberglas laminate, bends significantly during longitudinal forward motion of the swimmer and transverse oscillatory movements with the trunk and legs. The monoflipper is seemingly inscribed into the wave trajectory, being the result of application of both types of motions. On the other hand, it is obvious from the motion-picture frames of Figure 4 that the solid vortex shroud is separated continuously in time and over the entire span of the monoflipper during intermediate stages of thrusts by the monoflipper from the rear edge of its paddle. Hence, it follows that a monoflipper is distinguished hydrodynamically from V. V. Golubev's well-known idealized scheme of a flapping wing with inverted two-row checkerboard pattern of the concentrated vortices in the wake [2].

A general idea of the motions of an underwater swimmer using a monoflipper during several cycles can be gained by the cyclogram (Figure 5). It was taken by a movie camera rigidly attached to the vertical wall of a swimming pool and the swimmer covered a distance parallel to the wall (along the second track of the pool) at a distance of approximately 5 meters from the line of sight of the movie camera. The film was made with the lights turned off and the typical points of the swimmer's body were noted by blinking electric lamps. The movie camera in a waterproof box was supplied with a shutter--a rotating disc with cutouts, which permitted one to make the filming process continuous with known time periods. A single frame of a swimming athlete was taken with pulsed light flash.

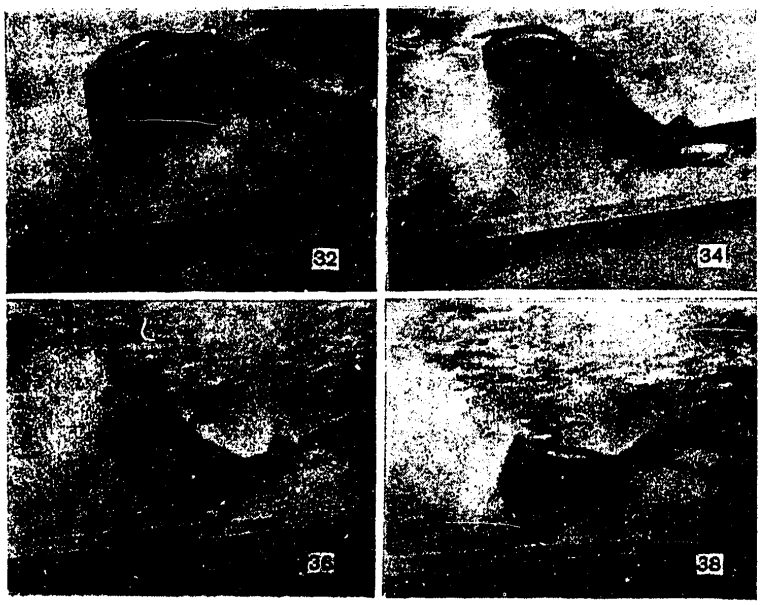

Figure 4. Separation of Vortex Shroud From Edge of Monoflipper (visualization of air bubbles from the athlete's aqualung and was photographed with angle of approach by the tracking camera (selected frames 32, 34, 36, 38))

APPROVED FOR RELEASE: 2007/02/08: CIA-RDP82-00850R000300060001-1

APPROVED FOR RELEASE: 2007/02/08: CIA-RDP82-00850R000300060001-1

Analysis of the cyclogram shows that while the swimmer's wrist follows an almost straight line (Figure 5, a), the point near the center of gravity of the body describes a curvilinear trajectory (Figure 5, b) approaching a sine wave of comparatively low amplitude and the outlet edge of the monoflipper paddle describes a high-amplitude curvilinear trajectory (Figure 5, c) and differs appreciably from a sine wave. As can be seen, when swimming with a monoflipper in the fashion of dolphins, the swimmer makes periodic bending oscillations continuously with the entire body in the vertical plane with a phase shift of the trajectories of the indicated points. Thus, a deformed elastic travelling wave with increasing amplitude, which is periodic, but not harmonic, moves backward along the swimmer's body and the monoflipper during their forward motion. This complex inverse travelling wave of the swimmer's body is generated on his wrist and terminates on the outlet edge of the monoflipper paddle and its passage is easily visualized when observing from the side of the pool.

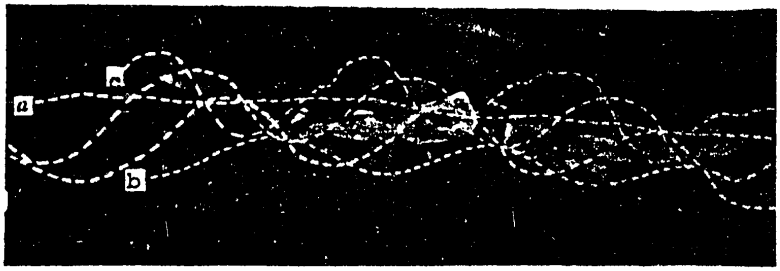

Figure 5. Cyclogram of Trajectories of Typical Points of the Body of an Athlete Using a Monoflipper Underwater in a Pool: a--wrist; b--point near center of gravity of body; c--outlet edge of monoflipper (taken with a fixed movie camera having shutter and photoflash)

We note that the given cyclogram permits one to carry out numerical processing in the length scale--by known anthropometric data of a swimmer recorded in the frame (or by a ruler) and in time scale by the known characteristic of the movie camera with shutter and with dashed lines of the photographed trajectories. The processed cyclogram provides important quantitative information (see below for this).

The wave trajectories of two points in swimming by an athlete using a monoflipper are of greatest interest, namely the center of gravity of the body and the middle of the terminal edge of the monoflipper paddle (Figure 6). Both trajectories are superimposed on a single sheet of paper by superposition of a number of sequential movie frames on 16-millimeter film, magnified 25 times using a projector tube, and the projections of the frames are combined by frames. The points given above, corresponding to each frame, are denoted by identical numbers. The position of the swimmer whose silhouette is shown in Figure 6 when the body is level and the end of the monoflipper paddle occupies the lowest position is taken as the zero frame. Care was taken to see that no less than 1.5 waves of the body and monoflipper were placed within the figure, which is required for further proecessing of the data. The latter is also important due to the fact that the linear scale in the movie frames varies to approximately ± 2 percent of the average value when an athlete is swimming in front of a fixed camera, which can be taken into account specifically by reading the center of gravity of the body backward along the trajectory.

APPROVED FOR RELEASE: 2007/02/08: CIA-RDP82-00850R000300060001-1

APPROVED FOR RELEASE: 2007/02/08: CIA-RDP82-00850R000300060001-1

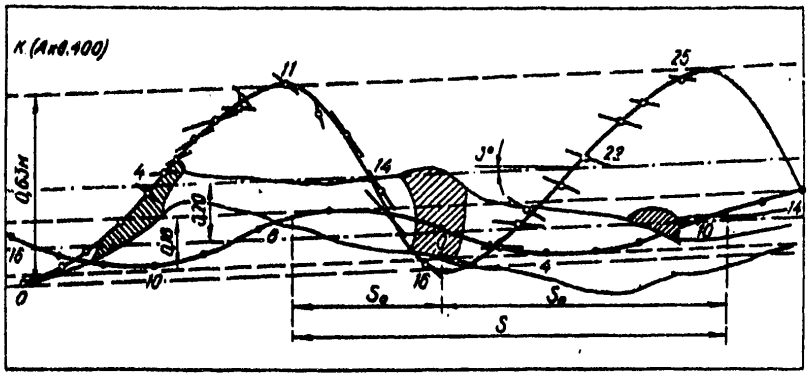

Figure 6. Scale Movie Film of Wave Trajectories of Two Points--Center of Gravity of the Body and Middle of Terminal Edge of Athlete's Monoflipper (the numbering of the points on both trajectories corresponds to the simultaneous position of these points on the movie frames taken by fixed camera at speed of 24 frames per second)

Typical data for an international class master of sport in a record-breaking heat in a swimming pool at a distance of 400 meters using an aqualung are presented in Figure 6. The athlete held a small compressed air tank in front of him in his extended hands and swam at a depth of 1.22 meter of the center of gravity of the body under the surface of the water. The longitudinal axis of motion was sometimes inclined to $\pm$ 3°. Forward motion of the swimmer during a single cycle, corresponding to the rise and fall of the monoflipper, or his action was s = 1.51 meters. The wave trajectory of the center of body grativy is almost symmetrical with sweep of 0.18 meter and with mean curvature of approximately 1/4. The wave trajectory of the center of the terminal edge of the monoflipper paddle is clearly asymmetrical and its sweep is A = 0.63 meter, the mean curvature is close to unity or the wave front has a slope at an angle of approximately 45°. In the given case the axes of both waves are parallel to each other, but do not coincide. They lag by 0.20 meter, which increases the swimmer's hydrodynamic drag. The noncoincidence of the axes of both trajectories can be explained by the different upward and downward flexibility of the human legs when swimming due to the known structure of the knee and ankle joints.

It is interesting to note that a time of T_p = 0.46 second or 0.69 period was expended to raise the monoflipper (upward thrust) and a time of T_0 = 0.21 second or 0.31 period of a cycle was expended to lower the monoflipper (downward thrust) when an athlete was moving during a single swimming cycle with period of T = 0.67 second, i.e., at frequency of n = 1/T = 1.49. In this case the swimmer moved a distance of s_p = 1.00 meter, equal to approximately 2/3 of action, during the rise of the monoflipper, while s_0 = 0.51 meter, i.e., 1/3 of the action during lowering of the monoflipper. Thus, the opinion widely held among athletes that the upward thrust with the monoflipper is seemingly passive and has no great significance in the swimming cycle is refuted.

APPROVED FOR RELEASE: 2007/02/08: CIA-RDP82-00850R000300060001-1

APPROVED FOR RELEASE: 2007/02/08: CIA-RDP82-00850R000300060001-1

The nonuniform thrust by the monoflipper during the cycle should be emphasized. The transverse or vertical components of the speed of the end of the paddle are significantly different with an average of $W_p = A/T_p = 1.37$ m/s during raising and $W_o = A/T_o = 3.00$ m/s during lowering. Nevertheless, the mean longitudinal or horizontal components of speed of the forward motion of the swimmer during the indicated parts of the period are sufficiently close: $V_p = s_p/T_p = 2.18$ m/s during raising of the monoflipper and $V_o = s_o/T_o = 2.43$ m/s when it is lowered.

The average forward speed of swimming in the considered cycle is $V = s/T = 2.25$ m/s. The Strouhal number, expressed by the maximum sweep A of oscillatory motion of the monoflipper, is equal to

$$Sh_A = \frac{nA}{V} = 0{,}41. \tag{1}$$

The value of the Strouhal number is typical: it corresponds to the maximum high value of that for aerohydrobionts with slow flight and swimming and with relatively large sweep of oscillatory motions with the wings and fins in some species of insects, birds, fishes and dolphins. This indicates features of similarity between seemingly such diverse phenomena as follows from the universal criterial function $Sh_A(Re)$ in [9], compiled from experimental data over a wide range of values of Reynolds number $Re = 10^3$-10^6.

Using Golubev's formula [2], for the aerodynamic efficiency of a flapping wing in the given case of swimming by a qualified athlete using a monoflipper, we find

$$\eta = \frac{0{,}17 + Sh}{(5Sh - 0{,}4)\,Sh} \simeq 0{,}50. \tag{2}$$

A value of $\eta = 0.78$, for example, for $Sh_A = 0.32$, is possible in other cases of swimming. The progressive travelling wave along the swimmer's body, which has a useful hydrodynamic effect on formation of the flow impinging on the monoflipper, is not taken into account in formula (2) for a flapping wing. The value of $\eta = 0.50$ is probably low.

Let us explain the nature and parameters of the travelling wave on the fragments of Figure 7, which is a series of point drawings from magnified movie frames in scales of distance x along the horizontal and time t along the vertical, i.e., in coordinates x(t), for the other case of underwater swimming by an athlete using a monoflipper. Selective frames 0, 4, 8 and 10 with initial spacing every 4 frames and then every 2 frames (at writing speed of 24 frames per second) are shown in Figure 7. Forward-sloping line $c_0c_4c_8c_{10}$ is drawn through the center of body gravity in these frames. It indicates the sequential motion of the swimmer from left to right from the initial vertical c_0c_0'. The line $m_4m_8m_{10}$ is drawn with reverse slope through the highest points of the instantaneous positions of the monoflipper paddle in these frames. It shows the passage through the extreme value by the highest point of the travelling wave along the swimmer's body and the monoflipper from right to left, which is obvious when the line is compared to the corresponding positions of local verticals m_4m_4' and m_8m_8'. The auxiliary line m_4m_8'' is parallel to line c_4c_8, while line m_8m_{10}'' is parallel to line c_8c_{10}.

APPROVED FOR RELEASE: 2007/02/08: CIA-RDP82-00850R000300060001-1

APPROVED FOR RELEASE: 2007/02/08: CIA-RDP82-00850R000300060001-1

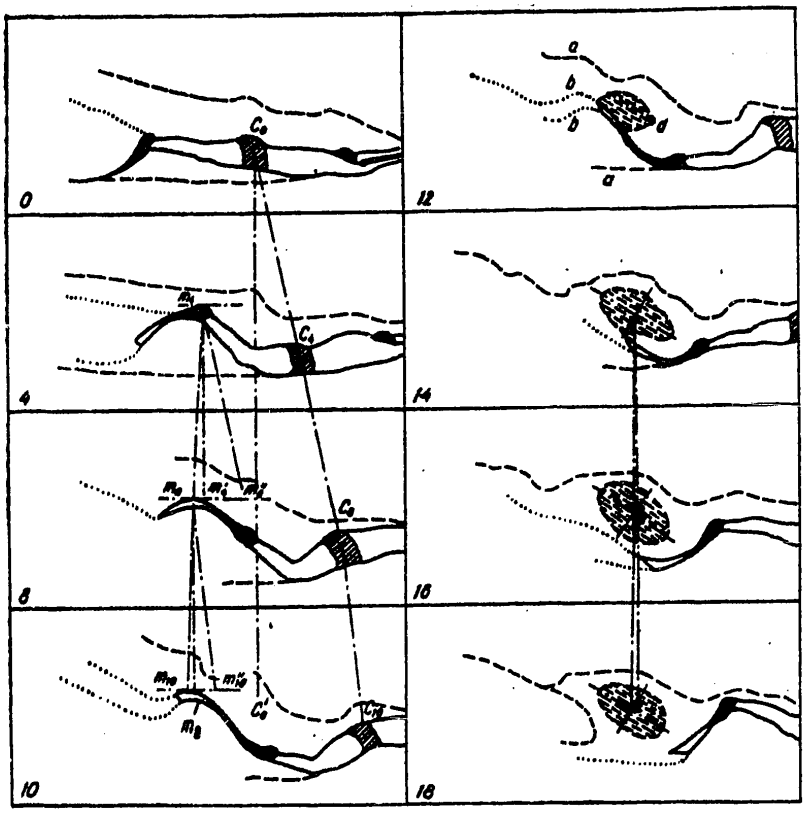

Figure 7. Fragments of Processing of Movie Frames by a Fixed Camera in Length-Time Coordinates in Underwater Swimming of an Athlete Using a Monoflipper

It is obvious that the ratio $(m_8'' - m_4')/(t_8 - t_4) = V$ is the value of the local swimming speed of the athlete from left to right, while the ratio $(m_8'' - m_8)/(t_8 - t_4) = C$ is the value of the local propagation speed of the travelling wave along the swimmer's body and the monoflipper in the opposite direction, i.e., from right to left. According to absolute value, $|C| > |V|$, or $|C/V| > 1$. One can also follow further in similar fashion from frame to frame and one can also superimpose the line of propagation of the extreme value with the highest point of the travelling wave and so on if possible.

The space-time data of the movie film of the type of Figure 6 can be used to determine the parameters of the travelling wave, bearing in mind that it contains no fewer than three pairs of corresponding points with the lowest and highest positions of two wave trajectories--for the center of body gravity and the center of the terminal edge of the monoflipper paddle. This permits one to easily construct the reduced graph x(t) on which straight lines of minimum and maximum propagation of both wave trajectories can be drawn through each pair of indicated points and

APPROVED FOR RELEASE: 2007/02/08: CIA-RDP82-00850R000300060001-1

APPROVED FOR RELEASE: 2007/02/08: CIA-RDP82-00850R000300060001-1

the length of the travelling wave χ and velocity C can be determined. In the considered case $\chi = 2.10$ meters, $C \approx 3.0$ m/s and therefore $C/V = 1.33$ or $V/C = 0.75$. With an athlete's height of $H = 1.82$ meters, the total length of his body together with arms and part of the monoflipper extended is equal to $L = 2.82$ meters. A value of $L:\chi = 1.34$ of the travelling wave is contained on this length.

Returning to Figure 7, we note the remarkable fact that the flow boundaries were visualized under conditions of an athlete swimming a heat in a pool. Here a is the visible outer boundaries of the region of water disturbances caused by the swimming of an athlete using a monoflipper, b is the boundaries of the water jets flowing from the terminal edge of the monoflipper paddle and d is some individual region of elliptical shape in the vertical plane. It is obvious that the upper external curvilinear boundary should be the bends and protruding parts of the athlete's body and the monoflipper, it lags quite far behind them and the region of water disturbances is very wide. This indicates interrupted flow over the athlete's body and primarily flow over the poorly streamlined cylindrical compressed air tank located in front of the athlete. The water jets leave the monoflipper paddle along the tangent, by which the Zhukovskiy-Chaplygin postulate is satisfied. With regard to region d, its boundaries are clearly distinguished on the movie frames, but its nature remains unclear. It is possible that this is one of the concentrated vortices, but the problem requires additional special investigation.

The foregoing provides the basis to use G. V. Logvinovich's formulas [4, 5] on the hydrodynamics of a deformed body and to use the "penetrated layer" concept to calculate the swimming of an athlete using a monoflipper. Since the existing monoflippers have aspect ratio of $\lambda = l^2/F = 0.9\text{-}1.7$, where l is the width of the monoflipper along the outlet edge and F is the lifting area of the monoflipper (on one side), the calculating formulas, according to [4], will be the following (in our notations).

The mean value of the active thrust is

$$P = \frac{\pi^3}{16}\rho l^2\left(\frac{A}{\chi}\right)^2\left[\left(\frac{C}{V}\right)^2 - 1\right]V^2. \tag{3}$$

The hydrodynamic efficiency is

$$\eta = \frac{1}{2}\left(1 + \frac{V}{C}\right). \tag{4}$$

As can be seen, the relative parameters of the travelling wave A/χ and C/V which characterize its steepness and propagation speed and also the width l of the monoflipper along the outlet edge are of main significance in the given theory for thrust. All these parameters are squared in the formula of [3], i.e., the dependence on them is strong. This requires sufficiently accurate management of the kinematic experiment, which is not always achievable in the case of hydrobionts.

Substituting the calculated values given above into formulas (3) and (4), we find $P = 38.8$ kg and $\eta = 0.87$ in the considered case. Taking the known prerequisites

APPROVED FOR RELEASE: 2007/02/08: CIA-RDP82-00850R000300060001-1

APPROVED FOR RELEASE: 2007/02/08: CIA-RDP82-00850R000300060001-1

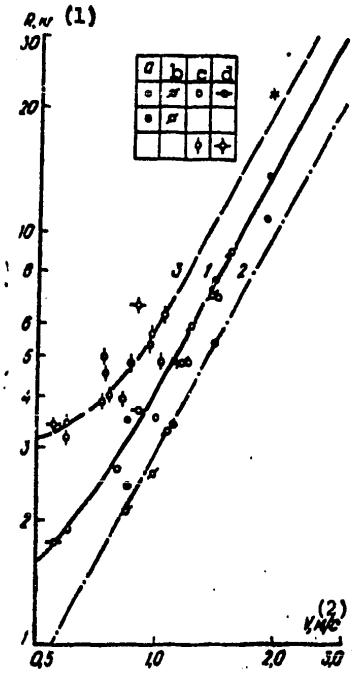

Figure 8. Dependence of Drag on Speed of Towing and Swimming of Trained Athletes Without Flippers (Males, Mean Values for Groups of 3 to 10 Persons): 1--towing of athletes in level position with extended arms by winch, average height of 1.75-1.80 meters and weight of approximately 80 kg; 2--the same, with average height of 1.70 meters and weight of 65 kg; 3--active swimming of athletes in free style and breast stroke on surface of water opposite the current in a physiological swimming pool, height of 1.80 meters and weight of 75 kg (according to "c"), or ordinary swimming in a pool, average height of athletes of 1.75 meters and weight of 78 kg (according to "d")

Key:
1. Kilograms
2. M/s

and assumptions of this theory into account, we assume that both values are somewhat exxagerated. To determine the mean thrust over the entire swimming distance of 400 meters, we took the absolute value of the mean speed of the heat of V = = 1.94 m/s in calculation according to (3), according to the accurately recorded result of 3 minutes 26.2 seconds (unlike the relative values of A/χ and C/V found for a single typical cycle. It is of interest to compare the derived value of thrust P to the total drag of the athlete R, assuming that on the average P = R.

We processed the experimental data available in the literature (Figure 8) to determine the latter. The primary source of these experiments was underwater towing

APPROVED FOR RELEASE: 2007/02/08: CIA-RDP82-00850R000300060001-1

APPROVED FOR RELEASE: 2007/02/08: CIA-RDP82-00850R000300060001-1

of 9-10 athletes without flippers in the pool of the L'vov Institute of Physical Culture [7] (Figure 8, a), towing of an athlete in the Swedish Experimental Pool [14] (Figure 8, b), systematic testing of the swimming physiology of man by Swedish sports organizations [13] (Figure 8, c) and systematic tests of the swimming energy of 10 athletes at New York University [15] (Figure 8, d).

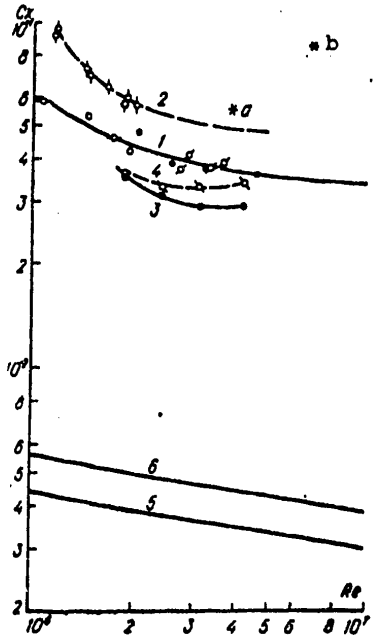

Figure 9. Dependence of Hydrodynamic Drag Coefficient of Body on Reynolds Number of Towing and Swimming of Trained Athletes (males and females, average values): 1--towing of males with a winch; 2--active swimming of males--height was 1.75-1.80 meters and weight was approximately 80 kg in both cases; the notations of the points are according to Figure 1; 3--towing of females with a winch, height of 1.64 meter and weight of 58 kg; 4--towing of female mannequins of the same dimensions; 5--smooth plate with turbulent boundary layer; 6--body of rotation with aspect ratio of L/D = 5 in a completely turbulent mode; a--calculation by energy metabolism; b--calculation by hydrodynamics of deformed body

We note satisfactory agreement between the experimental data of different sources, since the straight segments of all three curves of the graph are located on a logarithmic grid at a slope of 1.8, as should be for drag as a function of speed in the turbulent mode. It is obvious that the hydrodynamic drag of athletes during active swimming is 1.4-fold greater than that during passive towing of the body at the same speed. This is easily explainable by the additional drag of the athlete due to oscillatory motions of the body and extremities with large sweep of the oscillations.

APPROVED FOR RELEASE: 2007/02/08: CIA-RDP82-00850R000300060001-1

APPROVED FOR RELEASE: 2007/02/08: CIA-RDP82-00850R000300060001-1

The total hydrodynamic drag of an athlete with height of H = 1.80 m and weight of G = 82 kg, calculated for enhanced speed of V = 1.94 m/s by the energy method from our functional relation [8], is noted by the asterisk in Figure 8. The calculating formula is

$$R = \frac{Q}{V} = \frac{\eta q G}{V}, \tag{5}$$

where q = f(T) is the maximum specific power takeoff of the athelete, dependent on the length of the swimming period. In our case T = 3'2" = 206 seconds, to which a value of q = 0.0078 hp/kg = 0.585 kg·m/kg corresponds according to the graph of Figure 5 of [8]. Substitution of all the known values in (5) yields a value of R = 21.6 kg, which is very close to the certain extrapolation of straight line 3 in Figure 8. This again confirms the validity of the results of calculating drag by the energy method.

Finally, we determined the dimensionless hydrodynamic drag coefficients of an athlete's body as a function of Reynolds number Re. The calculations were made on two assumptions.

In the case of towing and active swimming of the athlete without flippers, as usual,

$$C_x = \frac{2R}{S\rho V^2}. \tag{6}$$

Here $\rho = 102$ kg·s^2/m^4 is water density and S = f(H, G) is the wetted surface of the athlete's body, which was determined by his height H and weight G by the Dubois graph well known in sports practice and in the field of medicine.

It was assumed in the case of underwater swimming of an athlete using an aqualung that his total drag consists of three parts: body drag according to (6), additional frictional drag of the monoflipper and the additional drag of the shape of the aqualung with attachment, i.e.,

$$R = C_x S\rho \frac{V^2}{2} + 2_n C_f F\rho \frac{V^2}{2} + kC_x S\rho \frac{V^2}{2},$$

since

$$C_x = \frac{2R}{S\rho V^2 (1 + 2_n C_f F/S + k)}. \tag{7}$$

Here C_f is the dimensionless frictional drag coefficient of a smooth plate, n > 1 is the coefficient of increasing the drag for a monoflipper with area F (on one side) with longitudinal notches and k is the additional drag of the shape of the aqualung with attachments. We assumed that n = 2 (arbitrarily) and k = 0.15 in the calculations according to the experimental data in [12]. The results of calculating the drag coefficients are presented in Figure 9.

Analysis of the experimental results shows that the drag coefficient of the athlete's body is an order higher than that for a technically smooth plate with

APPROVED FOR RELEASE: 2007/02/08: CIA-RDP82-00850R000300060001-1

APPROVED FOR RELEASE: 2007/02/08: CIA-RDP82-00850R000300060001-1

turbulent boundary layer or eight or more times higher than that of a body of rotation with turbulent mode of equivalent dimensions at identical Reynolds numbers. This indicates separation flow over the athlete's body. The hydrodynamic drag coefficient of the female body is appreciably lower than that of the male body and is somewhat less than that of a mannequin. The calculated points "a" and "b" agree more or less satisfactorily with experimental data on the drag of athletes' bodies.

Some agreement of calculating the thrust of the athlete using a monoflipper according to the hydrodynamics of a deformed body to experiments on the swimming resistance of athletes in a pool with the separation flow over them noted above, which increases the athletes' drag by almost an order of magnitude compared to a body of rotation of similar streamlined shape, should be emphasized. This permits one to state that similar calculation of drag yields considerably exaggerated values of drag in cases of hydrobionts of streamlined shape such as fishes or dolphins, which we also partially confirmed previously [10]. Not only the assumption of the constant maximum oscillation amplitude over the entire length of the body, which did not occur in reality, but also the fact that these oscillations are not small and the bodies themselves are far from thin, as is used in the given theory, may be of significance.

It should be noted that man is a poorly swimming hydrobiont, but the monoflipper is a promising wave impeller for rapid swimming in the fashion of solphins. Investigations of the monoflipper must be continued and swimming with it must be improved, which is of important interest in the field of hydrobionics.

BIBLIOGRAPHY

1. Alekseyev, V. M., Yu. S. Ivanov and A. M. Tikhonov, "The Characteristics of Flippers," SPORTSMEN-PODVODNIK, No 22, 1970.

2. Golubev, V. V., "Papers on Flapping Wing Theory," in TRUDY PO AERODINAMIKE, Moscow-Leningrad, Gostekhizdat, 1957.

3. Zagozin, V. A., A. T. Salmin and B. A. Samokhin, "High-Speed Flippers," SPORTSMEN-PODVODNIK, No 33, 1973.

4. Logvinovich, G. V., "The Hydrodynamics of a Thin Flexible Body (Analysis of the Hydrodynamics of Fishes)," BIONIKA, No 4, 1970.

5. Logvinovich, G. V., "The Hydrodynamics of Swimming of Fishes," BIONIKA, No 7, 1973.

6. Mazurov, I. V., "Podgotovka podvodnogo plovtsa" [Training the Underwater Swimmer], Moscow, Izd-vo DOSAAF, 1972.

7. Onopriyenko, B. I., "The Effect of Anthropometric Data on the Hydrodynamic Efficiency of Swimmers," BIOLOGIYA MORYA, No 16, 1969.

8. Pershin, S. V., "The Functional Dependence of the Maximum Specific Efficiency of Aquatic Animals on the Length of the Swimming Period," SB. TR. VYSSH. BOYEN-MOR. INZH. UCHILISHCHA, No 60, 1965.

APPROVED FOR RELEASE: 2007/02/08: CIA-RDP82-00850R000300060001-1

APPROVED FOR RELEASE: 2007/02/08: CIA-RDP82-00850R000300060001-1

9. Pershin, S. V., "Hydrobionic Functions of Transient Harmonic Motion of Fishes and Dolphins as Submerged Bodies of Variable Shape," in "Problemy bioniki" [Problems of Bionics], Moscow, Nauka, 1973.

10. Pershin, S. V., "Some Results of Hydrodynamic Investigations of a Wave Impeller," BIONIKA, No 8, 1974.

11. Porotov, B. S., "Developing a New Style of Swimming," SPORTSMEN-PODVODNIK, No 28, 1971.

12. Taggard, R., "The Propulsive Capabilities of Man," in "Podvodnaya laboratoriya 'Silab-2'" [The Sealab-2 Underwater Laboratory], Leningrad, Sudostroyeniye, 1968.

13. Holmer, J., "Physiology of Swimming Man," ACTA PHYSIOL. SCAND., Suppl. 407, 1974.

14. Pengelly, A. E., "The Hydrodynamics of Swimming," NEW SCIENCE, Vol 19, No 358, 1963.

15. Prampero, P. E., D. R. Pendergast, D. W. Wilson and D. W. Rennie, "Energetics of Swimming in Man," J. APPL. PHYSIOL., Vol 37, No 1, 1974.

APPROVED FOR RELEASE: 2007/02/08: CIA-RDP82-00850R000300060001-1

APPROVED FOR RELEASE: 2007/02/08: CIA-RDP82-00850R000300060001-1

UDC 599.53

REGULATED HYDROELASTIC EFFECT IN THE FINS OF THE LARGEST AND FASTEST DOLPHIN, THE KILLER WHALE

Kiev BIONIKA in Russian No 13, 1979 signed to press 14 Jun 79 pp 35-43

[Article by S. V. Pershin, A. S. Sokolov and A. G. Tomilin, Zoological Institute of the USSR Academy of Sciences, Leningrad, from the collection "Bionika," Izdatel'stvo Naukova Dumka, 1,000 copies, 100 pages]

[Text] The regulated hydroelastic effect in the fins of Cetaceans (dolphins and whales) has been outlined in papers [2-6], including reports at international conferences of scientists in 1969 and 1973. This effect has been recorded officially as a scientific discovery in the USSR under the name "The phenomenon of self-regulation of the elasticity of Cetacean fins" [7]. A schematic model has been investigated for subsequent technical use of the phenomenon [8]. A number of inventions has been made on the basis of the discovery, specifically [1, 9-11].

The indicated papers of the authors also aroused interest among foreign scientists. Requests for these papers have come from the United States, Canada, England and Belgium to the Zoological Institute of the USSR Academy of Sciences. The morphological and anatomical characteristics of dolphin fins, which we first discovered, were repeated and confirmed in other species (see, for example, [16]). However, inadequate attention has been devoted in some papers to study of the functional bases of these characteristics, which are the main subject of our investigations from aspects of hydrobionics and possible applications.

Let us recall briefly that the phenomenon of self-regulation of the fin elasticity of Cetaceans occurs by reflex when the swimming mode is changed. It is caused by the effect of the organs of the circulatory system, the first discovered widely branching complex arterial-venous vessels, the capillary system and anastomoses of various types and also by the structure of the integumental tissues of the fins, including the covering of tendenous strands.

Unlike all other organs of various species of animals, every more or less large sanguiferous vessel is complex in Cetacean fins. It consists of a single central thick-walled artery which is immediately surrounded by a crown of several (up to 20) thin-walled veins in which blood flows in opposite directions (Figure 1).

As the mode of Cetacean motion changes, for example, from increased to decreased swimming speed, its energetics and general metabolism change accordingly and therefor the intensity of blood circulation in the swimming organs--the fins--also

APPROVED FOR RELEASE: 2007/02/08: CIA-RDP82-00850R000300060001-1

APPROVED FOR RELEASE: 2007/02/08: CIA-RDP82-00850R000300060001-1

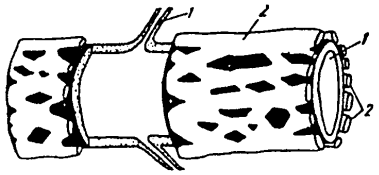

Figure 1. Diagram of Complex Sanguiferous Vessel of Dolphin: 1--central thick-walled artery (with higher blood pressure); 2--surrounding thin-walled veins (with lower blood pressure)

inevitably changes. When the lumen of the artery of a complex vessel expands or contracts, an opposite effect automatically occurs on the surrounding veins since the pressure in the arterial blood is an order of magnitude higher than that in the veins, while the complex vessels are located among the dense tissue of the hypodermis of the fins. As a result the fin becomes more or less elastic, to which the solid covering of the fins of the tendonous strands, which comprises the outer flexible, but practically nonelastic membrane, also contributes (Figure 2).

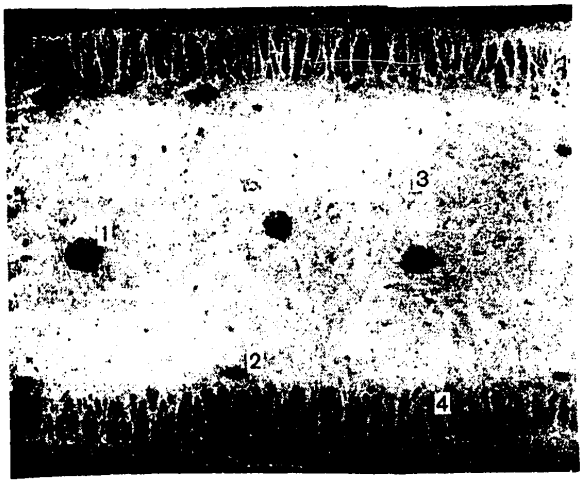

Figure 2. Microphoto (X4) of Transverse Section of Dorsal Fin of Piebald Dolphin Lagenorhynchus obliquidens: 1--large complex arterial-venous vessel in mid-plane of fin; 2--fibers of reticular hypodermis with small sanguiferous vessels; 4--layer of tendenous strands of thin covering

The hydrodynamic and hemodynamic conditionality of the considered effect and the functional bases of the diverse morphology for all three types of fins--caudal, dorsal and pectoral fins of several species of dolphins and whales--is shown in detail in [5]. As examples, let us present here new materials on the complex sanguiferous vessels in the fins of fast-swimming Pacific Ocean dolphins. The dolphin

APPROVED FOR RELEASE: 2007/02/08: CIA-RDP82-00850R000300060001-1

APPROVED FOR RELEASE: 2007/02/08: CIA-RDP82-00850R000300060001-1

Stenella attenuata (Figure 3) is distinguished by the fact that it easily jumps from the water into the air with rotation of the body around its own axis up to two and one-half turns. The arteries of the general network of the complex vessels are visible in Figure 4 in the caudal fin of the dolphin with laminated shape of the body of species Lagenorhynchus obliquidens.

Figure 3. Arteries of Separate Complex Vessels in Mid-Plane of Dorsal Fin of Dolphin Embryo of Stenella attenuata (photograph from X-ray, lead injection)

The different arrangement and structure of the network of complex vessels in the dorsal and caudal fins of dolphins and the presence of a single common regulation assembly in the caudal fin are noteworthy, which is determined by their different functional designation, as we also noted previously [2-4]. These facts were investigated on a schematic model [8] and were used in the inventions mentioned above [1, 9-11].

The possibility of clearly showing the effect of the regulated hydroelastic effect in the dorsal fin of the killer whale is of special interest. The latter is the largest and fastest dolphin and its dorsal fin is distinguished by very large absolute and relative dimensions. We recall that there are no rigid bony formations of any kind in the dorsal fin of dolphins.

The killer whale Orcinus orca is the most widely distributed species from the Arctic to the Antarctic. The body length reaches 10 meters with an average of approximately 6 meters and the total weight of the killer whale reaches 8 tons. As a result of the sharply marked half-dimorphism, the female is almost one-third smaller than males (it does not exceed 7 meters in length). The swimming speed of the killer whale in the sea is up to 13.4 m/s for short periods and approximately 9 m/s for longer periods (for tens of minutes) [12]. The Reynolds number of the killer whale is equal to $(3\text{-}7)\cdot 10^7$, i.e., very high.

APPROVED FOR RELEASE: 2007/02/08: CIA-RDP82-00850R000300060001-1

APPROVED FOR RELEASE: 2007/02/08: CIA-RDP82-00850R000300060001-1

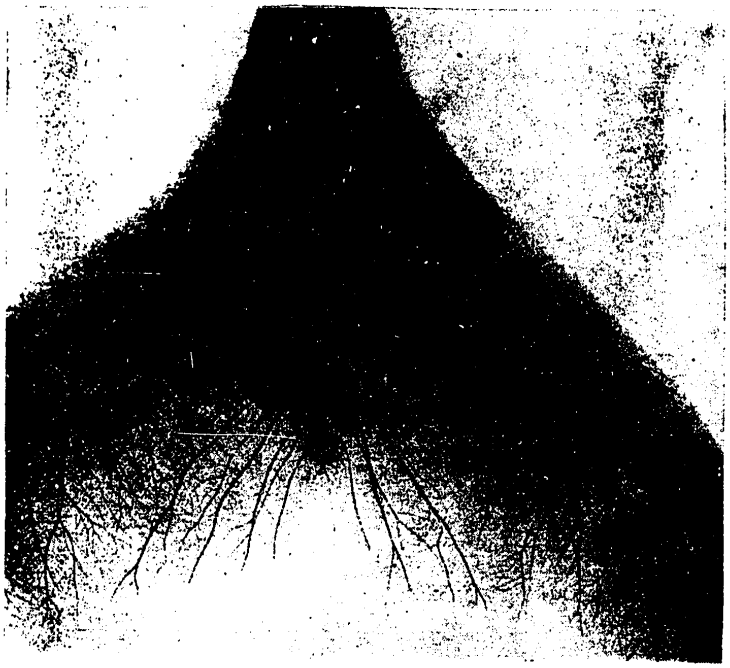

Figure 4. General Network of Arteries of Complex Vessels in Two Planes With Single Common Regulating Assembly of Caudal Fin of Dolphin Lagenorhynchus obliquidens (X-ray photograph, lead injection

The killer whale is distinguished in body shape by relatively small head without a clearly marked beak and by specially large pectoral and dorsal fins. The dorsal fins are oval in shape and wide, i.e., they are low aspect ratio. The length of the chord of the pectoral fin may reach up to 0.7-0.8 the value of the span in the greatest cross-section. On the other hand, the dorsal fin of the killer whale approaches a triangular shape, is high, but narrow and has comparatively high aspect ratio. Its height is greater in males than in females and reaches 1.7 meters. Killer whales swimming near a free surface in the sea are detected from a distance by the protruding dorsal fin of the males.

As the killer whale grows, the fins change in shape (Figure 5) and size. As the killer whale grows and increases in size, the fins increase not only in absolute dimensions, but also in relative value. Using the data of [14, 15, 17] and also of [18], we constructed a graph (Figure 6) which permits one to make specific conclusions.

It is obvious that the fins in newborn killer whales up to 2.5 meters long have the same dimensions, as do those of adult dolphins of the same length of other fast-swimming species, for example, of genus Stenella. The span of the caudal fin comprises 22-25 percent and the height of the dorsal fin comprises 8-10 percent of the

APPROVED FOR RELEASE: 2007/02/08: CIA-RDP82-00850R000300060001-1

APPROVED FOR RELEASE: 2007/02/08: CIA-RDP82-00850R000300060001-1

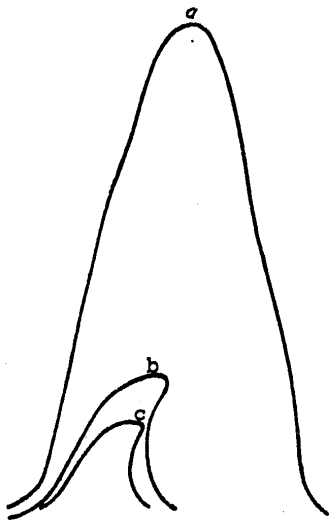

Figure 5. Shape and Dimensions of Dorsal Fin of Killer Whale of Different Sex and Age (1/8 scale): a--adult male 6.45 meters long; b--young male; c--newborn female

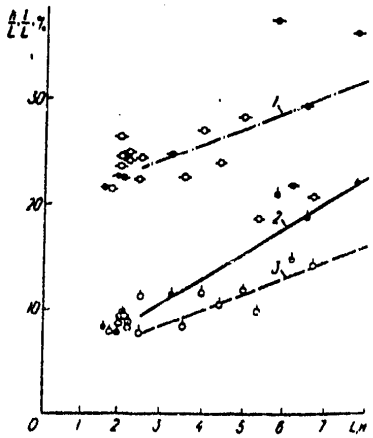

Figure 6. Graph of Relationship of Relative Dimensions of Fins to Total Body Length of Killer Whale Orcinus orca: 1--span of caudal fin lobes (l/L)(L) (males and females); 2 and 3--height of dorsal fin (h/L)(L) of male and female, respectively (compare other species of genus Stenella at L < 2.5 meters)

APPROVED FOR RELEASE: 2007/02/08: CIA-RDP82-00850R000300060001-1

APPROVED FOR RELEASE: 2007/02/08: CIA-RDP82-00850R000300060001-1

body length. However, with subsequent growth of the killer whale to three or more times in body length, the relative span of the caudal fin sometimes increases to 30 percent or more, while the relative height of the dorsal fin reaches 22 percent of body length in males (see Figure 6). Although there are few numerical data and their deviation on the graph is large, one can still state that the relative span of of the caudal fin increases identically with age in males and females, while the relative height of the dorsal fin differs more and more in them. Thus, the geometric similarity of corresponding fins is disrupted in the ontogenesis of the killer whale and consequently there is no dynamic similarity. This can be explained by the necessary increase of swimming speeds as the killer whale grows, determined by its leading biological position among marine mammals and as a hunter in the ocean.

Killer whales began to be maintained in oceanariums quite recently. They tolerate confinement relatively easily and can be easily trained, including being trained to retrieve heavy objects from a depth up to 500 meters in the sea. They must be studied in more detail, but each specimen of killer whale is expensive. Let us use some observations and photographs below which were specially made by one of the authors upon a visit to the Sea World Oceanarium at San Diego, California.

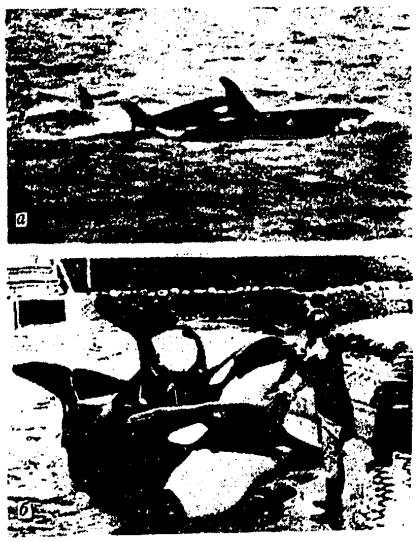

Figure 7. Killer Whale Orcinus orca During Free Swimming at Sea (a) and On Shore in the Oceanarium Together With Trainer (b)

Killer whales at sea and in the oceanarium are shown in Figure 7 and the impressive size of the dolphins (length of approximately 6 meters) and shape of their fins are easily visible. The fact that the dorsal fins of killer whales freely swimming at sea are completely erect, that is, elastic, while these fins in killer whales in the oceanarium are bent somewhat and are obviously less elastic, is noteworthy. The trainer of the killer whales in the oceanarium reported that the dorsal fins of his students are usually not completely erect the greater part of the time, but are more

APPROVED FOR RELEASE: 2007/02/08: CIA-RDP82-00850R000300060001-1

APPROVED FOR RELEASE: 2007/02/08: CIA-RDP82-00850R000300060001-1

or less bent and folded. We point out that the greater or lesser elasticity of the fins of these dolphins is determined by the degree of the main functional designation as vertical course stabilizer in free swimming performed by them. To do this, let us use photographs taken of several specimens of killer whales in the same oceanarium.

In the case when the killer whale swims in a deep bay and swims sufficiently fast, his vertical dorsal fin is completely erect and elastic even in the surface position, which makes it convenient for his trainer sitting on the dolphin's back to hold on (Figure 8, a). If the killer whale is swimming in shallow water of the oceanarium and by necessity at low speed, the dorsal fin is somewhat bent and less elastic (Figure 8, b).

Photographs of killer whales resting in the oceanarium in shallow water (Figure 9, a and b) are interesting. In these cases their dorsal fin clearly does not function as a stabilizer and is either half-bent or even touches the upper part of the body.

Figure 8. Trained Killer Whale in Surface Swimming: a--he is carrying his trainer in a shallow bay (the dorsal fin is erect); b--in the shallow water of the oceanarium (the dorsal fin is somewhat bent)

Finally, let us directly compare the two extreme states of killer whales to each other. Jumping of a dolphin from the water into air, even vertically, is a case of a stress state of his organs when all the animal's energy capabilities are mobilized and therefore the fins are completely erect and elastic and their shape and relative dimensions are easily visible (Figure 10, a). On the other hand, a rear view of a killer whale lying in shallow water in the oceanarium shows that whereas his body,

APPROVED FOR RELEASE: 2007/02/08: CIA-RDP82-00850R000300060001-1

APPROVED FOR RELEASE: 2007/02/08: CIA-RDP82-00850R000300060001-1

caudal stem and caudal fin are erect underwater and ready for action at any moment of time, the dorsal fin in the air is bent, i.e., it is relaxed and less elastic (Figure 10, b).

A photograph of a large killer whale washed up on shore and still alive in [13] is also indicative. The front part of the dolphin is resting on sand while the caudal part is submerged in water, and whereas the caudal fin still flaps in the water (the waves and spray are visible), the dorsal fin of this killer whale is semirelaxed and inelastic.

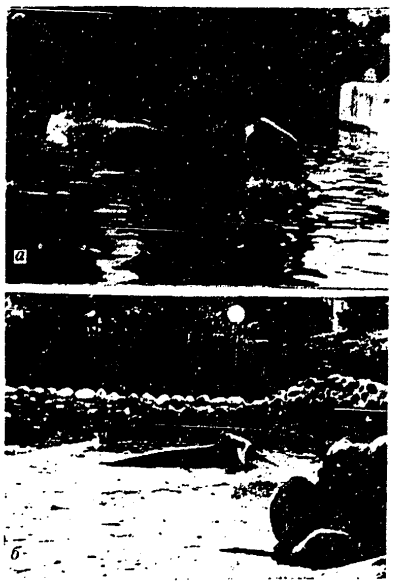

Figure 9. Killer Whale Resting in Oceanarium: a--caudal fin is half-bent; b--it touches his body

Comparing all the cases considered above to each other, one can review the different states of elasticity of the high vertical dorsal fin of the killer whale, which, on the basis of the foregoing are explained by the regulated hydroelastic effect in the fins for other species of dolphins. This follows from the general unique structure of the tissues and complex arterial-venous vessels of the fins in all species of Cetaceans. It is interesting to note that the maximum height of the dorsal fin in the killer whale does not exceed the height of the blood column corresponding to the highest arterial blood pressure of mammals, which is obviously related to the regulating role of the arteries of the large complex sangiferous vessels. However, one should also not forget the significance indicated above in the hypodermis of the fins of numerous anastomoses of various type and capillaries, the osmotic pressure in which reaches 7-8 atmospheres due to the difference of salt concentration in the arterial and venous network, as is known from hemodynamics.

APPROVED FOR RELEASE: 2007/02/08: CIA-RDP82-00850R000300060001-1

APPROVED FOR RELEASE: 2007/02/08: CIA-RDP82-00850R000300060001-1

The given facts permit one to consider the high dorsal fin of the killer whale with regard to the regulated hydroelastic effect as a type of vivid indicator of the general and energy state of the dolphin. Thus, it indicates some hypodynamics of the killer whale in an oceanarium, which occurs when the large fast ocean dolphin is placed in the restricted confines of a reservoir. Hence, it also follows that a fast dolphin cannot develop the possible maximum swimming speed in an oceanarium, which one should always keep in mind. Attention was brought to this circumstance especially in [12], where normalization of the length of maximum swimming speeds of dolphins swimming freely under natural conditions and in confinement was first proposed.

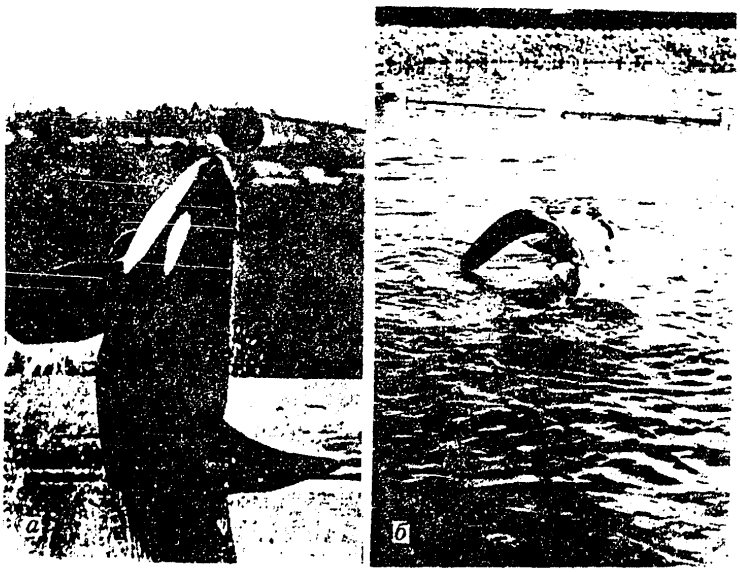

Figure 10. Trained Killer Whales in Oceanarium in Different States: a--high jump after ball (all the fins are erect and maximum elastic); b--lying in shallow water (the dorsal fin is half-bent and relaxed (rear view))

With regard to the high swimming speed of the killer whale, the fastest among dolphins, and to the large dimensions of his dorsal fin, which should be optimum in shape, it is interesting to compare the dorsal fin to that of the swordfish Xiphias gladius. The latter is the limiting case of all fast hydrobionts [13], its maximum swimming speed is double that of the killer whale, but the highest Reynolds number calculated for the total body length approaches 10^8. Nevertheless, unlike other fast fishes including tuna, the thick dorsal fin of the swordfish is not gathered in and is not even partially folded at high swimming speeds. However, this fin has good smooth "fairings" at the point where they join the body, which reduce the harmful effect of interference of their boundary layers. The nondisappearing thick dorsal fin of the swordfish is relatively low and has a large notched shape in the rear with length along the base approximately the same as the height of the fin.

APPROVED FOR RELEASE: 2007/02/08: CIA-RDP82-00850R000300060001-1

APPROVED FOR RELEASE: 2007/02/08: CIA-RDP82-00850R000300060001-1

Moreover, there are special local ampullas with mucusy substance to reduce the hydrodynamic drag of the fin on both sides of the fin and behind it in the middle of the back of the swordfish [13].

The adult killer whale doesnot have these devices. At slower swimming speeds, his high dorsal fin is triangular in shape and the height of the fin exceeds the width along the base up to 1.7-fold, which increases its aspect ratio and thus reduces the drag of the fin. However, this was possible in the presence of a hydroelastic effect in the fins of the killer whale, which is impossible in cold-blooded fish since their arterial blood pressure is an order of magnitude less than that of warm-blooded mammals. Thus, the same problem of reducing hydrodynamic drag of the vertical course stabilizer--a dorsal fin of large area--is solved by different noted methods in nature in different fast hydrodionts according to the biological characteristics of these animals and the maximum Reynolds number.

The information presented in this article can be used in hydrobionic modelling for practical purposes.

BIBLIOGRAPHY

1. Klepatskiy, A. G., M. V. Titova, S. V. Pershin et al, "Swimming Flipper," Inventor's Certificate 317390 (USSR), published in BYULLETYEN' IZOBRETENIY, No 31, 1971.

2. Pershin, S. V., A. S. Sokolov and A. G. Tomilin, "The Morphofunctional Characteristics of the Arteries and Veins of Dolphins With Regard to Locomotion," in "Tezisi dokladov IV Vsesoyuznogo soveshchaniyu po izucheniy morskikh mlekopitayushchikh" [Report Topics of the Fourth All-Union Conference on Study of Marine Mammals], Kaliningrad, 16-18 September 1969, Kaliningrad, 1969.

3. Pershin, S. V., A. S. Sokolov and A. G. Tomilin, "The Elasticity of Dolphin Fins Regulated by Special Sanguiferous Organs," DOKL. AN SSSR, Vol 190, No 3, 1970.

4. Pershin, S. V., A. S. Sokolov and A. G. Tomilin, "The Morphofunctional Characteristics of the Caudal Fins of Some Cetaceans," DOKL. AN SSSR, Vol 203, No 2, 1972.

5. Pershin, S. V., A. S. Sokolov and A. G. Tomilin, "The Phenomenon of Self-Regulation of the Hydroelasticity of Cetacean Fins: USSR Certificate No 95 for Discovery," OTKRYTIYA, IZOBRETENIY, PROMYSHLENNIYE OBRAZTSY, TOVARNIYE ZNAKI, No 23, 1971.

6. Pershin, S. V., A. S. Sokolov and A. G. Tomilin, "Self-Regulation of the Elasticity of Cetacean Fins," in "Tezisi dokladov 'Bionika-1973'" [Report Topics of "Bionics-1973"], Vol 4, Moscow, 1973.

7. Pershin, S. V., A. S. Sokolov and A. G. Tomilin, "The Biomechanical Bases of the Regulated Hydroelastic Effect in the Fins--Winged Lifting Surfaces--of Cetaceans (Dolphins and Whales)," in "Funktsional'naya morfologiya mlekopitayushchikh" [The Functional Morphology of Mammals], Leningrad, Nauka, 1974 (TR. ZOOL. IN-TA AN SSSR, Vol 4).

APPROVED FOR RELEASE: 2007/02/08: CIA-RDP82-00850R000300060001-1

APPROVED FOR RELEASE: 2007/02/08: CIA-RDP82-00850R000300060001-1

8. Pershin, S. V., Ye. P. Nosov and V. P. Isakov, "Schematic Model of the Hydroelastic Effect in the Fins of Cetaceans and Technical Use of It," in "Tezisi dokladov 'Bionika-1973'," Vol 76, Moscow, 1973.

9. Pershin, S. V., Ye. N. Nosov and V. P. Isakov, "Design of Rubber Hardware," Inventor's Certificate 318483 (USSR), published in BYULLETYEN' IZOBRETENIY, No 32, 1971.

10. Pershin, S. V., Ye. P. Nosov and V. P. Isakov, "Method of Grasping Articles," Inventor's Certificate 399449 (USSR), published in BYULLETYEN' IZOBRETENIY, No 39, 1973.

11. Pershin, S. V., Ye. P. Nosov, V. P. Isakov and K. M. Petrov, "An Airfoil," Inventor's Certificate 441188 (USSR), published in BYULLETYEN' IZOBRETENIY, No 32, 1974.

12. Pershin, S. V., "The Hydrodynamic Characteristics of Cetaceans and the Normalized Swimming Speed of Dolphins Under Natural Conditions and in Confinement," BIONIKA, No 3, 1969.

13. Pershin, S. V., "The Biohydrodynamic Phenomenon of the Swordfish as the Maximum Case of Fast Hydrobionts," BIONIKA, No 12, 1978.

14. Tomilin, A. G., "Cetaceans," in "Zveri SSSR i prilegayushchikh stran" [Animals of the USSR and Adjacent Countries], Moscow, Izd-vo AN SSSR, 1957.

15. Elsner, R., T. Pirie, D. D. Kenney and S. Schemmer, "Functional Circulatory Anatomy of Cetacean Appendages: Anatomy of Marine Mammals," Vol. 2, London, Academic Press, 1974.

16. Grieg, J. A., "Nogle notiser fraet spakhuggerstang ved Bildostrommen i januar 1904," BERGEN. MUS. AABORG, No 2, 1906.

17. Norris, K. S., "Whales, Dolphins and Porpoises," Los Angeles, University of California Press, 1966.

18. True, F. W., "Notes on a Killer Whale from the Coast of Maine," PROCEEDINGS OF THE UNITED STATES NAT. MUSEUM, Vol 27, Washington, 1904.

APPROVED FOR RELEASE: 2007/02/08: CIA-RDP82-00850R000300060001-1

APPROVED FOR RELEASE: 2007/02/08: CIA-RDP82-00850R000300060001-1

UDC 591.176

INVESTIGATING THE SKIN ELASTICITY OF LIVE DOLPHINS

Kiev BIONIKA in Russian No 13, 1979 signed to press 14 Jun 79 pp 43-52

[Article by V. V. Babenko, Institute of Hydromechanics of the Ukrainian SSR Academy of Sciences, from the collection "Bionika," Izdatel'stvo Naukova Dumka, 1,000 copies, 100 pages]

[Text] Since the bodies of marine animals moving at identical Reynolds numbers experience the same strong effect of the water medium, adaptations to these flow conditions, having identical dimensionality, were developed during evolution in the structure of their bodies or individual organs. Tested hydrodynamics equipment must be used to analyze them with regard to the difference of the force effect of flow on rigid models and living, thoroughly innervated bodies of marine animals.

This approach made it possible to formulate the principle of the receptor sensitivity of the skin of fast-swimming animals as a factor of natural selection, which determines the principles of their skin structure [1].

Investigating the interaction of flow with the bodies of marine animals also permits one to formulate in this regard the principle of automatic regulation of body characteristics and its individual parts or systems to reduce the energy expenditures when moving at typical speed for a given group of animals. Typical speed is understood as cruising speed U_{kr}, i.e., the maximum speed at which the animal moves during 15-20 minutes.

If the conditions of motion vary, the shape of the body and its configuration, the flexible rigidity of the entire body, the rigidity and mechanical properties of the skin, the elasticity and shape of the impeller, body and blood temperature, pressure in the circulatory system, thickness of the mucous sheath which plays the role of a damping surface, the production rate of mucous matter and so on are automatically regulated in the animals.

The effect of automatic regulation of the skin elasticity E of live dolphins on swimming speed U is investigated below. A physical model of the skin and a mathematical analog of the skin based on it must be developed to understand the mechanism of the interaction of live dolphin skin with the flow characteristics of the surrounding medium. A differential equation of the analog of dolphin skin is written in [9] in the form of a linear model of a viscoelastic Voight-Kelvin medium and it is written in [5] in the form of a so-called standard or generalized model of a

APPROVED FOR RELEASE: 2007/02/08: CIA-RDP82-00850R000300060001-1

APPROVED FOR RELEASE: 2007/02/08: CIA-RDP82-00850R000300060001-1

linear viscoelastic medium. A simplified mathematical analog of the skin which takes into account tension in the skin layers and bending deformations, unlike the standard model, is presented in the same paper. The diagram of the more complete analog of dolphin skin will differ significantly from the simplified diagram. Actually, if the skin structure of dolphins is considered [4, 5, 7, 14], the skin diagram presented in [5] should be supplemented in the following manner. The skin layer 4 is schematized not only by an elastic element, but also by a damper. Skin layer [5] should be schematized as an elastic element, while layer 6, the same as layer 3, should be schematized by a Voight-Kelvin element. Besides layers 5 and 6, layer 7 which is schematized by a Voight-Kelvin element should be added. Elastic connections which schematize the connective-tissue membranes are introduced parallel to the indicated elements between layers 3 and 6 and 3 and 7. It is known from polymer theory [12] that the mechanical properties of rubber can be described more fully by using nonlinear integral-differential equations of the Volterra type. There are presently no mathematical methods to describe the mechanical characteristics of filled rubber. Taking into account that tension in the skin layers and its damping properties are considerably dependent on the swimming speed of dolphins and are regulated by reflex and that the entire skin is multilayered and the upper layers have longitudinal stratification and that deformation of only individual collagenous fibers of which the skin layers consist is described by a complex nonlinear equation [16] that skin oscillations are correlated with the work of the caudal fin and are transient and that the entire skin can be simulated only by a nonlinear composite viscoelastic medium, it becomes obvious that the mathematical model of the skin cannot be solved in analytical form.

One can now find only the solution of the simplified mathematical analog by numerical methods. For example, the investigations given in [11] can be applied in first approximation to analysis of transient oscillations of the skin without regard to tension in the layers. It is concluded in this paper that dynamic interaction of the skin layers of different elasticity and oscillatory mass play a positive role, which lead to significant damping of transient oscillations.

Thus, it becomes clear that diverse experimental data on the mechanical characteristics of dolphin skins must be accumulated. Besides dynamic characteristics, it is also of interest to determine the static modulus of the elasticity of dolphin skin.

Elasticity is subordinate to Hook's law at small deformations and the principle stays the same during tension and compression [12]. Therefore, the elasticity measured in dolphins during compression with regard to the smallness of deformation characterizes the static modulus of elasticity, while measurements made with an elastometer [2] investigate the behavior of the skin described in the static Voight-Kelvin model. In this regard the results of investigations presented in this paper characterize the general static state of the entire skin without regard to its dynamic characteristics noted above.

Some results of measuring the value of E, carried out by using a specially manufactured device of the Shore hardness gauge type are presented in [2]. The parameters of elasticity k_g, which were approximately equal in value for three species of dolphins at their cruising swimming speed, were calculated from the results of these measurements for a single cross section of the body of the animals in the region of the mid-section. The modulus of elasticity was determined by using Hertz's formula, which introduced an error into the calculations that could be reduced by using the

APPROVED FOR RELEASE: 2007/02/08: CIA-RDP82-00850R000300060001-1

APPROVED FOR RELEASE: 2007/02/08: CIA-RDP82-00850R000300060001-1

dependence of the modulus of elasticity expressed in Shore units on the modulus of elasticity expressed in dimensional units, given in [13].

When working out the methods of measuring the value of E, three versions of the device were manufactured, one of which having a weak loading spring was used to measure the elasticity of the outer skin layers of the white-sided dolphin (preferably the epidermis and papillary layer), which comprised $1.4 \cdot 10^5$ N/m^2. The modulus of elasticity of the thicker skin layer measured during tension in Kramer's paper [4] comprised $1.03 \cdot 10^6$ N/m^2. The difference in the measurement results is explained by the fact that when measuring with the indicated device it is difficult to precisely estimate the thickness of the skin t on which the pressure of the measuring rod propagates, due to the possible reflex contractions of the integumental muscle and also due to the fact that Kramer measured the value of E by tension of preserved skin specimens of another species of dolphin, without taking into account the dimensions and age of the animal.

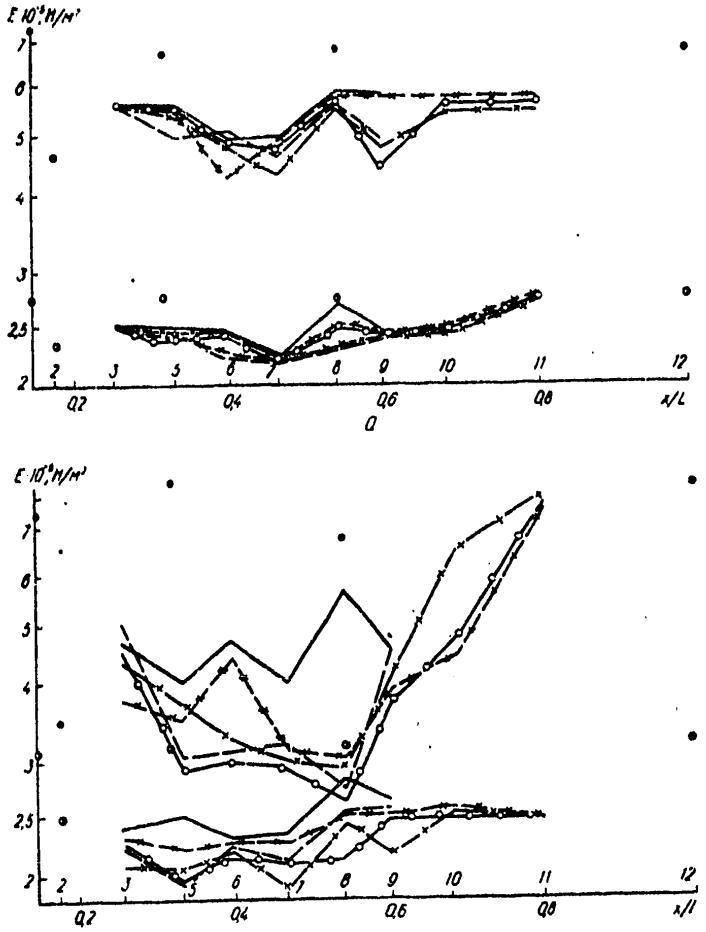

Figure 1. Distribution of Skin Elasticity Through Body of White-Sided (a) and Bottlenosed (b) Dolphins at Different Swimming Speeds

APPROVED FOR RELEASE: 2007/02/08: CIA-RDP82-00850R000300060001-1

APPROVED FOR RELEASE: 2007/02/08: CIA-RDP82-00850R000300060001-1

Using the developed device and method of conducting the experiments [2], the skin elasticity of three species of dolphins--the white-sided (Delphinus delphis), the bottlenosed (Tursiops truncatus) and finned porpoise (Phocaena phocaena)--was investigated. Data on the dimensions of the animals and the statistics of the measurement results are presented in Table 1. The skin elasticity of the white-sided and bottlenosed dolphins are presented in Figure 1, in which the numbers of the body cross-sections of the dolphin (from the top of the axis) and the distance along the body in dimensionless for x/L (on the bottom of the axis), where x is the distance from the beginning of the body and L is body length, are plotted along the x axis. A diagram of the location along the dolphin's body of these and longitudinal sections is presented in [2]. The value of E was measured along the lines of the transverse sections from top to bottom at points lying on the lines of the longitudinal sections, equally separated from each other, beginning from the line along the back denoted by the solid line, along the side, denoted by the line with circles, along the stomach, denoted by the dashed line, and along the lines located between the indicated lines from top to bottom, respectively, and denoted by a dashed line with crosses on the straight lines and with crosses between the straight lines.

Measurements of the value of E at individual points along the body, indicated in [2], are denoted by the half-shaded circles and points.

Approximate calculations showed that pressure fluctuation in the turbulent boundary layer during swimming at a speed of 10 m/s have a value on the order of $3.3 \cdot 10^3$ dynes/cm^2 and that they have a value and order less in the laminar boundary layer. During transient flow conditions in the boundary layer, the pressure fluctuations may exceed several times the value of turbulent fluctuations [10]. Analyzing the graph of variation of the skin thickness of the dolphin along the body [4], we assume that the intensity of disturbances in the boundary layer at slow swimming speed permits them to be propagated by an insignificant value t to the region of the epidermis and the papillary layer. If swimming speed increases, the kinetic energy of the disturbances of the boundary layer increases and the oscillations caused by them in the skin may propagate deeper, also penetrating the subpapillary layer. As the intensity of pressure fluctuations in the boundary layer increases, for example, during transient flow mode or with an increase of swimming speed, the fluctuations may be propagated deeper into the skin of dolphins.

The results of measuring the value of E, made with a device having normal (medium) stiffness of the spring on the assumption that these values correspond to average swimming speeds U_{sr} and characterize the elastic properties of the upper skin layers, including the subpapillary layer, are shown below in Figure 1, a and b.

Taking into account that the underlying skin layers will also respond to the increased pressure fluctuations at U_{kr} and that the skin elasticity increases to maintain its optimum stabilizing properties according to criteria of similarity [5], the values of E were measured with a device having double (strong) stiffness of the spring. These results are presented in the upper part of Figure 1, a.

The value of E of the white-sided dolphin was measured in a trained animal; therefore, the measurement errors caused by the dolphin's response to skin stimulation were insignificant. The results of measuring the value of E of a trained bottlenosed dolphin are presented in the lower part of Figure 1, b and the results of a

APPROVED FOR RELEASE: 2007/02/08: CIA-RDP82-00850R000300060001-1

APPROVED FOR RELEASE: 2007/02/08: CIA-RDP82-00850R000300060001-1

Table 1.

Species of Dolphins	Number of Dolphins Investigated	Body Length, m	Number of Measurements Made On Dolphins	Tension of Spring In Device	Comments
White-sided	4	1.4	17	Weak Medium Strong	The measurements were made at different times of the year at intervals of six months under different habitation conditions at different times of day
		1.5	1	Weak	
		1.37	1	Medium	
		1.3	2	Medium Strong	Measurements were made in morning and evening
Bottlenosed	3	1.9	3	Medium	Measurements were made at intervals of one week under different conditions of habitat
		1.79	1	Medium	
		1.7	1	Medium	
Porpoise	2	0.7	2	Strong	Measurements were made in morning and evening
		0.6	1	Strong	The animal was ill

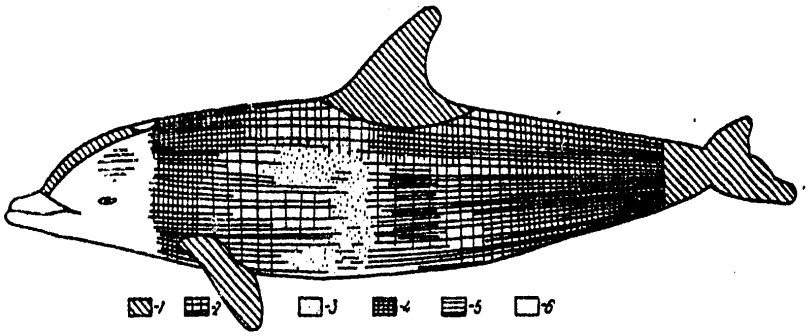

Figure 2. Topography of Skin Elasticity of White-Sided Dolphin: 1--1.9-2.0 g/mm^2; 2--1.8-1.85; 3--1.75-1.77; 4--1.85-1.9; 5--1.77-1.86; 6--not measured

APPROVED FOR RELEASE: 2007/02/08: CIA-RDP82-00850R000300060001-1

APPROVED FOR RELEASE: 2007/02/08: CIA-RDP82-00850R000300060001-1

freshly caught dolphin are presented in the upper part of this figure. The animal was excited and his muscles were tense. Therefore, the results of measurements made by the same device differ. It was assumed that the increased elasticity of the skin corresponded to U_{kr} and therefore measurements were not made on bottlenosed dolphins with the device having double spring. Data for a single dolphin, which coincide in value and nature to data for other animals, are presented in Figure 1.

Measurements showed that the skin elasticity of white-sided and bottlenosed dolphins varies smoothly along the body from top to bottom and from the nose to tail so that the softer part of the skin is located along the sides in the mid-section of the trunk. This principle is maintained in both cases--when measuring with normal and double stiffness of the spring. However, if the pressure of the measuring rod increases, the elasticity along the body varies more sharply (Figure 1, a, top). This is also discernible in Figure 1, b, which indicates that contraction of the skeletal musculature and cutaneous muscle leads to an even greater increase of skin elasticity with the same pressure of the measuring rod and that simulation of the increase of E with an increase of speed by measuring with a device having double spring stiffness was carried out correctly.

Approximately the same principles were observed in porpoises, but it was difficult to make the required number of measurements due to the fact that these dolphins respond poorly to training. Moreover, it was found that the skin elasticity of a sick dolphin is considerably less than that of a healthy animal. This is explained by the fact that the animal was weakened; therefore, the elastic characteristics of his body and integument varied.

A diagram of distribution of E along the body of the white-sided dolphin, obtained on the basis of measurements made with a device having normal spring stiffness, is presented in Figure 2. The numerical values of elasticity are expressed by pressure p of the measuring rod spring, related to the area of its tip [2]. Sections with maximum skin elasticity are noteworthy. According to morphofunctional significance, these sections experience maximum hydrodynamic pressure [3]. The caudal stem and front part of the trunk in the region of the lateral fins are exposed to lesser hydrodynamic loads; therefore, the elasticity of these sections was reduced. The mid-part of the trunk experiences the least hydrodynamic loads; therefore, the value of E in this part of the body is also least.

The skin of dolphins is similar in their mechanical properties and structure to elastomers, whose elastic properties depend not only structure, but also on thickness as well as on the mechanical properties of the substrate [12, 13]. Based on the measurements and also based on the body structure of the dolphin and its skin as a whole [7, 8, 14], one can assume by analogy with elastomers that the principles of distribution of skin elasticity along the body of three species of dolphins are determined by the difference of the skin structure along the body, its thickness and the structure of the skin substrate.

Since pressure fluctuations in the boundary layer can be compared to compressive load, and since considerable hydrostatic pressure acts on the dolphin's body when swimming at depth, then taking into account the effect of skin thickness on the results of measuring its elasticity, the elastic properties of the skin should be characterized by stiffness S, determined from the relation $S = E/t$.

APPROVED FOR RELEASE: 2007/02/08: CIA-RDP82-00850R000300060001-1

APPROVED FOR RELEASE: 2007/02/08: CIA-RDP82-00850R000300060001-1

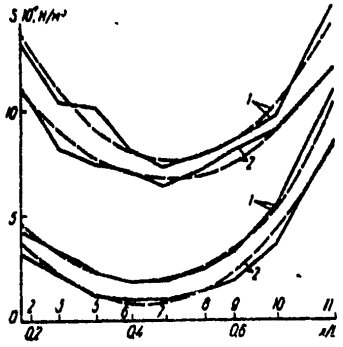

Figure 3. Distribution of Skin Stiffness of White-sided (1) and Bottlenosed (2) Dolphins at Different Swimming Speeds

The value of S was calculated by averaged values of E and t. The value of t for the white-sided dolphin was determined from data of [4] at U_{sr} with regard to the three upper skin layers and at U_{kr} with regard to the entire thickness of the skin, with the exception of the layer of the subcutaneous fatty tissue. The topography of the skin thickness of the bottlenosed dolphin was not accurately measured. The distribution of the mean values of t of the bottlenosed dolphin was interpolated on known individual sections of skin according to data of [4]. The values of t of these layers are presented in Table 2.

Table 2.

(1) Номер сечения	$t \cdot 10^3$, м			
	(2) Белобочка L=1,4 м		(3) Афалина L=1,9 м	
	(4) $U_{ср}$=6 м/с	$U_{кр}$= =7,8 м/с	$U_{ср}$= =6,9 м/с	$U_{кр}$=9 м/с
2	1,9	13	2,2	17
3	2,4	17	2,7	21
5	2,4	25	2,7	28
6	2,8	26	3,1	30
7	3,0	26	3,3	28
9	2,8	17	3,1	21
10	2,5	10	2,8	14
11	1,8	5	2,1	9

Key:
1. Number of cross section
2. White-sided
3. Bottlenosed
4. M/s

The results of calculating the value of S at U_{sr} (top) and at U_{kr} (bottom) are presented in Figure 3. The solid lines denote the results of calculations while the dashed lines denote approximation of these calculations by formulas for the upper curves:

APPROVED FOR RELEASE: 2007/02/08: CIA-RDP82-00850R000300060001-1

APPROVED FOR RELEASE: 2007/02/08: CIA-RDP82-00850R000300060001-1

$$1 - S \cdot 10^{-7} = 67 \frac{x}{L}\left(\frac{x}{L} - 0{,}96\right) + 23; \tag{1}$$

$$2 - S \cdot 10^{-7} = 48{,}7 \frac{x}{L}\left(\frac{x}{L} - 0{,}94\right) + 17{,}5; \tag{2}$$

for lower curves:

$$1 - S \cdot 10^{-7} = 49{,}4 \frac{x}{L}\left(\frac{x}{L} - 0{,}84\right) + 10{,}5; \tag{3}$$

$$2 - S \cdot 10^{-7} = 53 \frac{x}{L}\left(\frac{x}{L} - 0{,}84\right) + 10. \tag{4}$$

The value of S along the body of dolphins varies with the same regularity as elasticity, but more sharply and stiffness varies according to parabolic functions of the same type at different swimming speeds. The value of S of the white-sided and bottlenosed dolphin varies with practically the same regularity at U_{kr}. Formulas (1)-(4) apparently limit the optimum range of variation of S at typical swiming speeds.

For simplicity the curves located on the bottom of Figure 3 can be approximated by straight lines from the left for the white-sided dolphin

$$S \cdot 10^{-7} = -11 \frac{x}{L} + 6; \tag{5}$$

for the bottlenosed dolphin

$$S \cdot 10^{-7} = -10{,}5 \frac{x}{L} + 4{,}8 \tag{6}$$

and from the right for the white-sided dolphin

$$S \cdot 10^{-7} = 32 \frac{x}{L} - 16, \tag{7}$$

for the bottlenosed dolphin

$$S \cdot 10^{-7} = 31 \frac{x}{L} - 17. \tag{8}$$

Averaging of expressions (5) and (6) yields the formula

$$S \cdot 10^{-7} = -10{,}8 \frac{x}{L} + 5{,}4, \tag{9}$$

and of expressions (7) and (8) yields the formula

$$S \cdot 10^{-7} = 31{,}5 \frac{x}{L} - 16{,}3. \tag{10}$$

Experimental investigation of the hydrodynamic stability during flow over damping surfaces which simulate the skins of dolphins showed [6] that stabilization of the boundary layer depends on the surface configuration and the mechanical properties of the surfaces characterized by criteria of similarity. One of the criteria is the parameter of elasticity

APPROVED FOR RELEASE: 2007/02/08: CIA-RDP82-00850R000300060001-1

APPROVED FOR RELEASE: 2007/02/08: CIA-RDP82-00850R000300060001-1

$$k_S = S \frac{\nu}{\rho} \frac{1}{U^3}, \qquad (11)$$

where ν and ρ are the coefficient of kinematic viscosity and the density of the fluid, respectively. The distribution of case of S along the body (Figure 4) of white-sided (solid lines) and bottlenosed (dashed lines) dolphins for U_{sr} (top) and U_{kr} (bottom) was calculated using the data of Figure 3 and Table 2 according to formula (11). The range of optimum values of k_S found by Gyorgyfalvy's calculating method [5], is cross-hatched in Figure 4. The value of k_S along the entire body length has nonoptimum values when swimming at U_{kr} and has optimum values in the mid-section of the body when swimming at U_{kr}.

The value of k_S of the white-sided dolphin is found at the beginning of the body outside the optimum zone, but the negative pressure gradient on the body of the dolphin is of important significance at this location to stabilize the boundary layer [3]. The stem of the dolphin, being part of the impeller, makes an oscillatory motion and flow over it is distinct from flow over the mid-section of the body.

It is obvious that k_S has an optimum value along the entire length of the body when swimming speed increases up to maximum speeds.

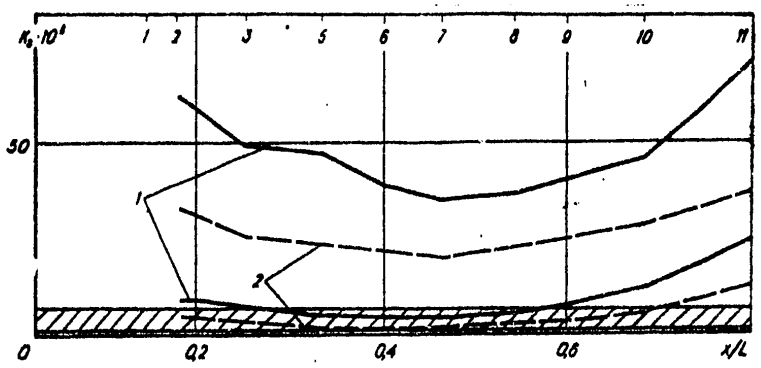

Figure 4. Distribution of Parameter of Elasticity Along Body of White-Sided (1) and Bottlenosed (2) Dolphins

Relation (11) indicates that the value of S should vary with variation of swimming speed to maintain the value of k_S in the range of optimum values. To check this proposition, let us carry out the following calculations for cross-section 7 of the body of the white-sided dolphin. The optimum value of k_S comprises $3.18 \cdot 10^5$ along the corresponding lower curve of Figure 4 for this cross-section. The optimum value of $S = 6.8 \cdot 10^6$ H/m^3 for $U_{sr} = 6$ m/s according to formula (11), whereas it comprises $7.3 \cdot 10^7$ H/m^3 according to the data of Figure 3. The corrected optimum value of S with regard to the skin difference according to Table 2 comprises $5.67 \cdot 10^7$ H/m^3. The difference of the measured and optimum value of S is equal to

$$\Delta = \frac{7{,}3 \cdot 10^7 - 5{,}67 \cdot 10^7}{7{,}3 \cdot 10^7} \cdot 100\ \% = 22{,}4\ \%.$$

APPROVED FOR RELEASE: 2007/02/08: CIA-RDP82-00850R000300060001-1

APPROVED FOR RELEASE: 2007/02/08: CIA-RDP82-00850R000300060001-1

Similar calculations for the bottlenosed dolphin yield a deviation of 40 percent.

Having expressed relation (11) by Reynolds number, in [18] Kramer proposed relations which determined the principle of variation of stiffness along the body. These relations differ from formulas (1)-(10) by the fact that the value of S decreases monotonically as x increases with respect to Kramer's relations. The deviation with the measurements is explained by the fact that the caudal part of the trunk of dolphins is mobile and is washed by a transient flow.

Calculations carried out by Kramer's formulas showed for sections 2 and 7 of the white-sided and bottlenosed dolphins that the distribution of S along the body (Figure 3) does not satisfy the relations proposed by Kramer at U_{Sr}, but they do satisfy the relations at U_{kr}.

The hydrodynamic principles considered in [3], on the basis of which the quasi-steady approach should be applied only to the body length in the region of sections 2-8, should be taken into account when analyzing the investigations. Actually, the nose part of the body undergoes large dynamic and tangent stresses, has a specific frontal projection affecting the skin thickness and makes small oscillatory movements. The caudal part of the body is part of the impeller with increased dynamic pressure and variable flow speeds.

Based on the foregoing, one can make the following conclusions.

1. Automatic regulation of the stabilizing properties of the skin is established in the skin structure of dolphins. When speed increases, the pressure fluctuations, which penetrate to the deeper layers of the skin, increase. At the same time the stress of the skeletal, motor and cutaneous musculature increases [1, 7, 8].

Skin elasticity increases and its thickness decreases in the region of the cutaneous muscle due to the specific structure of skins [7, 8, 14], while its diameter decreases in the mid-section of the body. Thus, measurements made by using a belt placed on the dolphin's body in front of the dorsal fin showed that the body diameter in this region decreased by 4-8 mm as a function of the size and species of dolphin when moving at high speeds or accelerations. If one takes into account that the skin elasticity does not vary with an increase of speed, then a decrease of skin thickness by approximately 2 mm leads to an increase of its stiffness by 10-15 percent. The difference of submersion of the rod of the measuring device into the dolphin's skin comprised an average of 3 mm when measuring elasticity with a device having single and double springs. If one assumes that the decrease of body diameter is related both to a decrease of skin thickness and to the flexibility of the skeleton, the results of measuring skin elasticity are in good agreement with the data of the decrease of body diameter when swimming speeds increase. Calculations show that it is sufficient to vary the stiffness of the skin by 20-40 percent to maintain the optimum value of k_S over a wide range of cruising speeds by dolphins. Variation of elasticity of the body, being a skin substrate, itself affects the stiffness of the skin.

2. Measurements showed that the value of S is more strongly dependent on t than on E. The values of t and E are varied simultaneously by using the cutaneous muscle, which automatically affects the depth of propagation of the pressure fluctuations in the skin of dolphins and the phase velocity of oscillations, according to oscillation theory.

APPROVED FOR RELEASE: 2007/02/08: CIA-RDP82-00850R000300060001-1

APPROVED FOR RELEASE: 2007/02/08: CIA-RDP82-00850R000300060001-1

3. During slow swimming when the dolphin's body is relaxed, the principle of distribution of skin stiffness along the body is optimum for stabilization of the boundary layer on the assumption of uniform distribution of the damping properties of the skin along the body even at nonoptimum values of parameter k_S.

BIBLIOGRAPHY

1. Agarkov, G. B., V. V. Babenko and Z. I. Ferents, "Innervation of the Skin and Cutaneous Musculature of the Dolphin With Regard to the Hypothesis of Flow Stabilization in the Boundary Layer," in "Problemy bioniki" [Problems of Bionics], Kiev, Naukova Dumka, 1973.

2. Babenko, V. V., N. A. Gnitetskiy and L. F. Kozlov, "Preliminary Results of Investigating the Elastic Properties of the Skin of Live Dolphins," BIONIKA, No 3, 1969.

3. Babenko, V. V. and O. D. Nikishova, "Some Hydrodynamic Principles of the Skin Structure of Marine Animals," BIONIKA, No 10, 1976.

4. Babenko, V. V. and R. M. Surkina, "Determination of the Parameter of the Oscillating Mass of Skin of Some Marine Animals," BIONIKA, No 5, 1971.

5. Babenko, V. V., "Main Characteristics of Flexible Coverings and Criteria of Similarity," BIONIKA, No 5, 1971.

6. Babenko, V. V. and L. F. Kozlov, "Experimental Investigation of the Hydrodynamic Stability on Stiff and Elastic-Damping Surfaces," IZV. AN SSSR. MEKHANIKA ZHIDKOSTI I GAZA, No 1, 1973.

7. Babenko, V. V. and R. M. Surkina, "Some Hydrodynamic Characteristics of Swimming by Dolphins," BIONIKA, No 3, 1969.

8. Babenko, V. V., L. F. Kozlov and S. V. Pershin, "Variable Damping of the Dolphin Skin at Different Swimming Speeds," BIONIKA, No 6, 1972.

9. Voropayev, G. A. and V. V. Babenko, "Absorption of Fluctuating Energy by a Damping Covering," BIONIKA, No 9, 1975.

10. Kozlov, L. F., "Investigating the Transition of the Laminar Boundary Layer to Turbulent Boundary Layer on a Plate in an Experimental Basin," GIDROMEKHANIKA, No 17, 1971.

11. Nguen Van Dao, "Transient Oscillations of a Dynamic System With Damper," IZV. AN SSSR. MEKHANIKA ZHIDKOSTI I GAZA, No 4, 1965.

12. Poturayev, V. N., V. I. Dyrda and I. I. Krush, "Prikladnaya mekhanika reziny" [Applied Mechanics of Rubber], Kiev, Naukova Dumka, 1975.

13. Scott, J. R., "Fizicheskiye ispytaniya kauchuka i reziny" [Physical Tests of Latex and Rubber], Moscow, Khimiya, 1968.

APPROVED FOR RELEASE: 2007/02/08: CIA-RDP82-00850R000300060001-1

APPROVED FOR RELEASE: 2007/02/08: CIA-RDP82-00850R000300060001-1

14. Sokolov, V. Ye., "The Skin Structure of Some Cetaceans," Report 2, NAUCH. DOKL. VYSSH. SHKOLY. BIOLOGICHESKIYE NAUKI, No 3, 1962.

15. Gyorgyfalvy, D., "The Possibilities of Drag Reduction By the Use of Flexible Skin," AIAA PAPER, No 66, 1966.

16. Flisen, M., M. Magi, L. Sonnerup and A. Viidik, "Rheological Analysis of Soft Collagenous Tissue," J. BIOMECH., Vol 2, No 1, 1969.

17. Kramer, M. O., "Hydrodynamics of the Dolphin," ADV. HYDROSCI., Vol 2, No 1, 1965.

18. Kramer, M. O., "Improvements in Means for Reducing Frictional Drag in Fluids," Patent 864593 (United States), Print, 1961.

APPROVED FOR RELEASE: 2007/02/08: CIA-RDP82-00850R000300060001-1

APPROVED FOR RELEASE: 2007/02/08: CIA-RDP82-00850R000300060001-1

UDC 599.53

INVESTIGATING THE PROPAGATION SPEED OF OSCILLATIONS ON THE SKIN OF THE DOLPHIN

Kiev BIONIKA in Russian No 13, 1979 signed to press 14 Jun 79 pp 52-58

[Article by S. M. Kidun, Physicomechanical Institute of the Ukrainian SSR Academy of Sciences, L'vov, from the collection "Bionika," Izdatel'stvo Naukova Dumka, 1,000 copies, 100 pages]

[Text] One of the important and informative parameters which characterize the properties of the dolphin skin is the rate of propagation of oscillations. When a dolphin moves in water, his skin is in complex interaction with the water flow. It is reported in [1, 8, 10, 13] that the dolphin's skin is capable of providing a laminar mode of flow at high speed or of stopping turbulent flow in ordered vortices [9, 11, 12].

A number of papers [2-4, 6] has been devoted to consideration of the skin as an elastic-damping covering. Mechanical models and linearized schemes of displacement of the skin upon interaction with the flow, on the basis of which such parameters as elasticity, tension and damping properties of the skin are calculated, are presented in them. However, it is difficult or almost impossible to determine them experimentally during motion on live dolphins without preparation of the skin, as pointed out in these papers. It is also noted that one of the indirect parameters which characterize the properties of the skin can be the rate of propagation of oscillations.

The skin structure of the dolphin is described in [14]. The total thickness of the skin fluctuates from 20 to 60 mm as a function of the location on the body. The skin consists of an upper layer of epidermis, the papillary, subpapillary and reticular layer of the dermis, the connective-tissue layer, the cutaneous musculature (cutaneous muscle) and the subcutaneous fatty tissue. The cutaneous muscle is firmly connected to the dermis and rests on the fatty tissue. The fatty tissue is a soft and pliable formation which provides mobility of the skin in all directions. The skin is connected by tendons to the skeleton and its musculature at separate points of the body [15].

It is pointed out in [15] that formation of large longitudinal folds or several oblique folds on the side from the right and left and transverse folds below the lower mandible, on the chest and stomach by using the dolphin's cutaneous musculature. Essapian's data that skin folds of different size, oblique and transverse on the lateral surface, below the lower mandible, on the breast and stomach were detected by using underwater movie filming in the case of short or long propelling motions of the dolphin and also during a sudden stop after these motions. Some of

APPROVED FOR RELEASE: 2007/02/08: CIA-RDP82-00850R000300060001-1

APPROVED FOR RELEASE: 2007/02/08: CIA-RDP82-00850R000300060001-1

them are formed during time on the order of 1/4 second and disappear within 3/4 second and others are maintained for 2-3 seconds. In the opinion of the author of [15], these data require experimental checking, consisting in investigation of the conditions of formation of the folds, the nature and direction of propagation, measurement of the height and width of the folds and study of their effect on reduction of hydrodynamic drag.

Thus, to study the properties of the dolphin skin and to determine its functional role, one can study the parameters of propagation of surface oscillations along the skin and can investigate the behavior of the skin during its free motion in water. The main parameter of surface oscillations of the skin is the rate of propagation and damping of oscillations with distance.

The results of instrument measurements of the rate of propagation and damping of induced oscillations on the skin of live dolphins, at a state of rest, and also the parameters of freely occurring oscillations on the skin during motion of the dolphin in water, which we carried out, are presented in this paper.

Ya. Ye. Belen'kiy and the author proposed that the parameters of induced oscillations on the dolphin skin be measured. The rate of propagation was measured by the phase method with variable base [7]. Oscillations were stimulated on the skin by a rod with a lunate disc tip of an electrodynamic exciter. The phase intervals, multiples of π, were measured by a probe oscillation pickup with pre-amplifier and distance meter and were recorded by a phase-coincidence indicator. The measurements were made in the frequency range from 50 to 400 Hz on the bottlenosed dolphin.

It was established during the measurements that surface oscillations propagating in all directions from the point exciter in the form of travelling waves are induced on the skin in the investigated frequency range. Travelling waves occur on the skin of both live and dead dolphins.

The experiment showed that the rate of propagation of oscillations is different at different locations of the skin. A graph of the rate of propagation of oscillations on the skin of one side of a dolphin is presented in Figure 1, where the coordinates of projection of one side of the skin are plotted along the x and y axes and the value of velocity is plotted along the z axis. It is obvious from this figure that the velocity on the skin of the head (Section 4) is relatively high, it drops in the region of the neck (Section 6), again increases from the center of the body (Sections 8 and 9) and then drops slightly. It increases at the beginning of the caudal stem and further along the stem.

Variation of velocity along lines a and b (Figure 1) is less compared to variation of velocity along lines c, d and e, located nearer the dolphin's stomach.

This pattern is somewhat disrupted for some dolphins due to the presence of defects on the skin in the form of scars, wounds or cuts. A reflection of oscillations was observed at these points, which led to formation of standing waves. It is interesting to note that the rate of propagation of surface oscillations, as shown in Figure 1, varies from 4 to 12 m/s, i.e., it lies within the range of swimming speeds of dolphins. For comparison let us point out that the rate of propagation of oscillations on the tensed muscle of the human shoulder is on the order of 25-30 m/s.

APPROVED FOR RELEASE: 2007/02/08: CIA-RDP82-00850R000300060001-1

APPROVED FOR RELEASE: 2007/02/08: CIA-RDP82-00850R000300060001-1

The rate of propagation of oscillations is not dependent on the direction of propagation. The rate was measured at a frequency of 200 Hz. The relative error of measuring the rate, which consisted of the error of reading the intervals of multiples of π and the error of phase coincidence indication, did not exceed 7-10 percent. The data presented in Figure 1 on the rate of propagation of oscillations along the skin are an averaged pattern for six adult bottlenosed dolphins. Their body length was in the range from 1.8 to 2.5 meters.

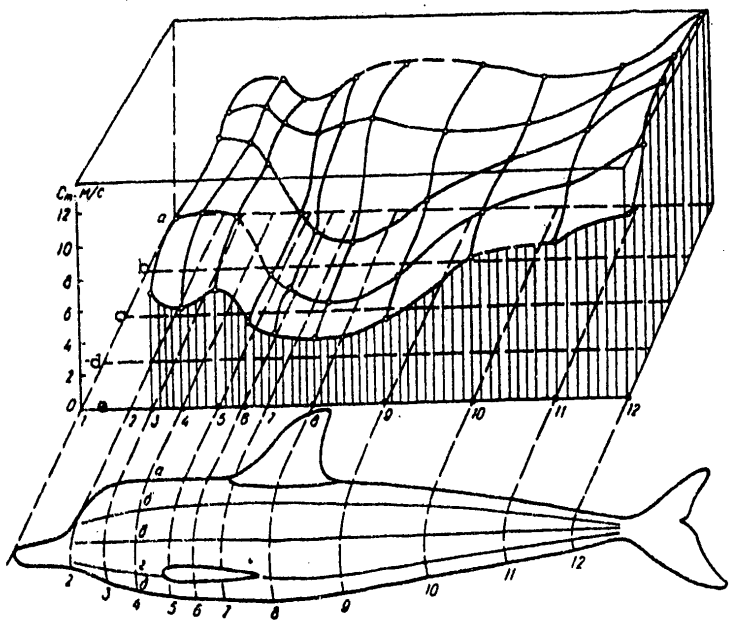

Figure 1. Distribution of Phase Velocity of Induced Oscillations of Skin on Body of Bottlenosed Dolphin. The diagram for conducting the measurements is the same as in [4].

The damping of oscillations on the skin of live dolphins was measured by the same method in the same frequency range. Oscillations were excited on the skin by using an electrodynamic exciter; the wavelength was measured by the phase method and damping of the oscillations was measured by the amplitude-comparison method.

Measurements showed that the value of the logarithmic decrement of attenuation is hardly dependent on frequency in the frequency range of 50-400 Hz and lies in the range of 0.71 to 0.81 for the skin of an immobile live dolphin, i.e., at a distance equal to one wavelength, and the oscillation amplitude is attenuated by a factor of 2-2.5.

Besides measuring the parameters of induced oscillations on the skin of an immobile dolphin, the oscillations of the skin of the dolphin moving freely in the water were recorded. The oscillations were transmitted in the form of electric signals

APPROVED FOR RELEASE: 2007/02/08: CIA-RDP82-00850R000300060001-1

APPROVED FOR RELEASE: 2007/02/08: CIA-RDP82-00850R000300060001-1

from the dolphin by a thin flexible shielded cable. The dolphin was placed in an open shore cage measuring 6 X 30 meters. The vibration sensor from which the signals were transmitted by flexible cable to the receiving-recording apparatus was placed on it. A belt was attached to the dolphin in front of the dorsal fin. A probe vibration pickup was placed on one side in the square between sections 6 and 7 and longitudinal lines b and c (see Figure 1) so that the vibration pickup probe lay against the dolphin's skin and was located in front of the belt. A communications cable was attached to the belt on the other opposite side.

The dolphin's speed was estimated visually. Sections of free swimming, acceleration and slowing of the dolphin were noted. Oscillations of the skin were recorded when the dolphin was moving in water at slow speed and when it was in a state of rest (Figure 2). The oscillations were pulse transmissions, single or group, following one after the other with period of 0.1-0.12 second, length of 0.035-0.09 second and charging frequency of 130-140 Hz. There were no jerks of any kind in the motion of the animal or jerking of the communications cable during recording.

It was decided to use acceleration in the open cage during a jump over a movable screen barrier to ensure rapid motion of the dolphin in water. To do this, at the beginning of the experiment the barrier in the cage was moved in a direction where the dolphin was located. The dolphin, seeing a reduced space in the cage, accelerated and jumped over the barrier. The barrier was then moved in the opposite direction and the dolphin made a second jump in the opposite direction. The dolphin subsequently learned the problem and jumped at the instructions of the experimenter. The height reached by the dolphin during the jump above the water reached 1.5-2 meters. During the jump the dolphin emerged from the water at approximately an angle of 45-50° at a speed on the order of 8-9 m/s.

It is obvious from the oscillogram of Figure 3 that the length of the entire jump is equal to approximately 1.0 second. The frequency of skin oscillations is variable and is within the range of 115 to 230 Hz. The frequency of oscillations during acceleration increases, is then maintained relatively constant and then drops. There are special points on the oscillogram where the phase of oscillations changes by 180°. These points correspond to the approximate time the animal enters the water during the jump.

Approximately 10 jumps were recorded during the experiment. To ascertain the reliability of the data, the effect of jerks and bends of the conducting cable and the effect of water flow on the vibration pickup were investigated after completion of the experiments. The investigations showed that throws of the pickup, bending of the cable and the effect of water flow were not recorded by the pickup.

The detected oscillations may be generated by the central nervous system or locally due to autooscillations of the skin during motion. Since the rate of propagation of the electric pulses in the muscular tissues of animals is within the range of 15-18 m/s, the time of passage through two structures, i.e., a single wavelength, will be equal to 0.008-0.0055 second with spacing of 5-6 cm of alteration of skin structures, which corresponds to a frequency on the order of 125-180 Hz. This provides the basis to assume that the detected oscillations can be excited by the nervious system. On the other hand, it must be noted that the frequency of the energy-bearing fluctuations of velocity in the turbulent layer is within the range of 100-200 Hz. It is not excluded that these fluctuations may create surface oscillations of the skin.

APPROVED FOR RELEASE: 2007/02/08: CIA-RDP82-00850R000300060001-1

APPROVED FOR RELEASE: 2007/02/08: CIA-RDP82-00850R000300060001-1

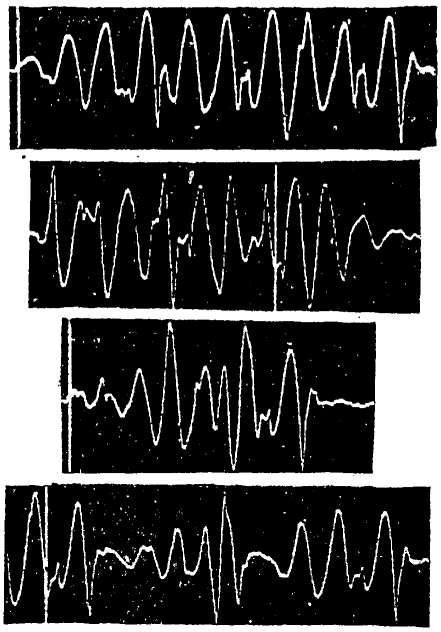

Figure 2. Oscillogram of Skin Oscillations of Dolphin During Slow Swimming (the time marks correspond to 0.1)

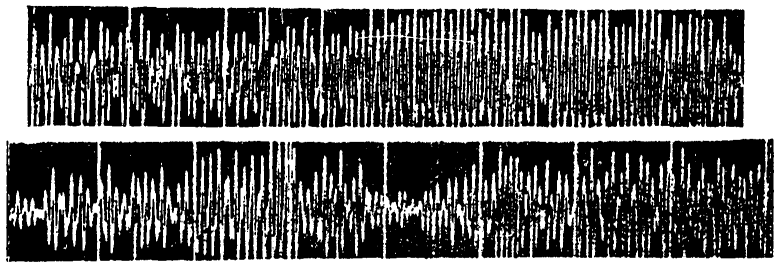

Figure 3. Oscillogram of Skin Oscillations of Dolphin During Jump

It is of interest to compare the distribution of the rate of surface oscillations on the dolphin skin (Figure 1) to distribution of the modulus of elasticity of the skin [4] and the distribution of the total thickness of the skin [5].

It is obvious from Figure 4 that the rate of propagation of oscillations for longitudinal line c of the dolphin skin clearly correlates the modulus of elasticity and the total thickness of the skin. As elasticity increases and the skin thickness decreases, the rate of propagation of oscillations increases. Using the data of the total thickness of the skin and determining the average density by the density

APPROVED FOR RELEASE: 2007/02/08: CIA-RDP82-00850R000300060001-1

APPROVED FOR RELEASE: 2007/02/08: CIA-RDP82-00850R000300060001-1

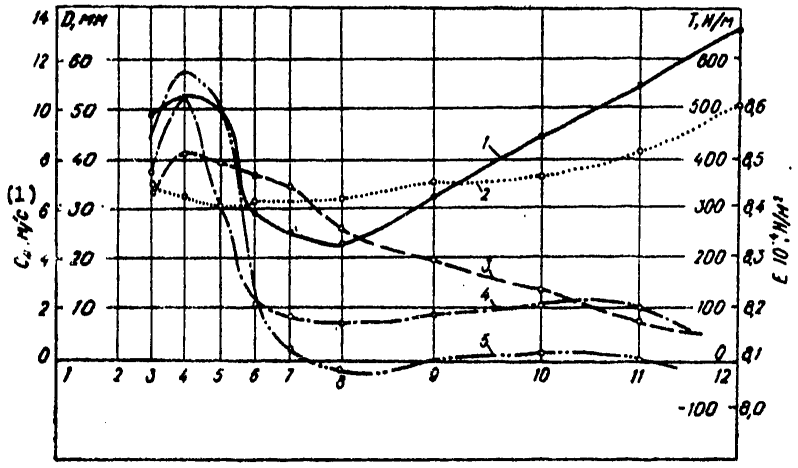

Figure 4. Dependence of Phase Rate of Induced Oscillations of Dolphin Skin on Its Mechanical Characteristics: 1--value c_m; 2--modulus of elasticity E; 3--thickness D; 4--static tension T; 5--total tension of skin during motion

Key:
1. M/s

of individual layers [5], we find the distributed mass of the skin for line c (see Figure 1). According to the expression taken from [2] for the rate of propagation of oscillations, one can calculate the tension of the skin from the relation

$$T = c_m^2 M, \quad (1)$$

where T is the tension of the skin, H/m, c_m is the rate of propagation of oscillations, m/s, and M is the distributed mass of the skin, kg/m^2.

The tension of the skin was then calculated from experimental data on the rate of propagation of oscillations and on the distributed mass of the skin. The calculated tension is static since it characterizes the skin of the dolphin in a state of rest. It is determined for line c of one side of the skin (curve 4 of Figure 4). The amount of tension is within the range from 54 to 502 H/m. On the other hand, the value of dynamic tension occurring during motion in water for high speed, according to [2], is equal to 80.1 H/m for the bottlenosed dolphin.

The total tension, added from static and dynamic tension, is of greatest interest for analyzing skin deformation. Due to the effect of dynamic tension, the skin, being reinforced in the region of the head, the front flippers and on the chest [15], is subjected to tension. Tension moves the skin with respect to the skeleton and the skeletal musculature due to the presence of the subcutaneous fatty tissue. However, the skin is attached to the skeletal musculature in the region of the dorsal fin and on the caudal stem and cannot be moved [15]. This leads to compression of

APPROVED FOR RELEASE: 2007/02/08: CIA-RDP82-00850R000300060001-1

APPROVED FOR RELEASE: 2007/02/08: CIA-RDP82-00850R000300060001-1

it on the section between the dorsal fin and the caudal fin. Thus, variation of the sign of dynamic tension in Sections 6-7 of the dolphin skin must be taken into account when adding the tension (see Figure 1).

It is obvious from Figure 4 that total tension is reduced in the region of transverse sections 7-10 to compression, and this may lead to formation of oblique and transverse folds on the sides and stomach of the dolphin. Hardly tensed and compressed skin can easily be deformed due to the effect of flow and can be controlled by the cutaneous muscle. However, fold formation was not detected in experiments in swimming dolphins.

Let us compare the value of the logarithmic decrement of attenuation which we measured to data presented in [2]. According to expression(6) [2], the logarithmic decrement of attenuation Δ can be determined from the relation

$$\Delta = \pi K_\eta, \tag{2}$$

where K_η is the damping parameter. According to data of [2], $K_\eta = 1.37$ and $\Delta = 4.3$ for the bottlenosed dolphin at low speed and $K_\eta = 0.13$ and $\Delta = 0.4$ at high speed, i.e., the oscillations are damped by a factor of 73 for low speed at distance equal to one wavelength, while they are damped by a factor of 1.5 for high speed.

The extent of attenuation, according to [2], shows that oscillations are essentially not propagated at low speed, which does not agree with data of our experiment. The investigations which we carried out showed that even for a dolphin in a state of rest, oscillations on the skin are propagated with damping by no more than a factor of 2-2.5. Hence, it follows that the damping properties during variation of speed do not vary over a wide range, and are close to values corresponding to high swimming speed even in a state of rest.

Thus, the experimental material indicates correlation relations between the structure of the skin and parameters which determine the state of the skin during motion of the dolphin. The material does not exclude the possibility of formation of the corresponding mechanism on the skin of the dolphin, which may contribute to a decrease of its resistance to motion in the water.

BIBLIOGRAPHY

1. Babenko, V. V., N. A. Gnitetskiy and L. F. Kozlov, "Preliminary Results of Investigating the Elastic Properties of the Skin of Live Dolphins," BIONIKA, No 3, 1969.

2. Babenko, V. V., "Some Mechanical Characteristics of the Skin of Dolphins," BIONIKA, No 5, 1971.

3. Babenko, V. V. and R. M. Surkina, "Determining the Parameter of the Oscillating Mass of the Skins of Some Marine Animals," BIONIKA, No 5, 1971.

4. Babenko, V. V., "The Main Characteristics of Flexible Coverings and Criteria of Similarity," BIONIKA, No 5, 1971.

APPROVED FOR RELEASE: 2007/02/08: CIA-RDP82-00850R000300060001-1

APPROVED FOR RELEASE: 2007/02/08: CIA-RDP82-00850R000300060001-1

5. Babenko, V. V., L. F. Kozlov and S. V. Pershin, "Variable Damping of the Skin of Dolphins at Different Swimming Speeds," BIONIKA, No 6, 1972.

6. Babenko, V. V. and O. D. Nikishova, "Some Hydrodynamic Principles of the Skin Structure of Marine Animals," BIONIKA, No 10, 1976.

7. Brazhnikov, N. I., "Ul'trazvukovaya fazometriya" [Ultrasonic Phase Measurement], Moscow, Energiya, 1968.

8. Voropayev, G. A. and V. V. Babenko, "Absorption of Pulsating Energy by a Damping Covering," BIONIKA, No 9, 1957.

9. Kozlov, L. F. and A. Ya. Oleynik, "Some Results of Hydrobionic Investigations," BIONIKA, No 9, 1975.

10. Merkulov, V. I., "Flow of a Viscous Fluid Along a Travelling Wave," IZV. SO AN SSSR. SER. TEKHN. NAUK, Issue 2, No 8, 1967.

11. Merkulov, V. I. and Yu. N. Savchenko, "Experimental Investigation of Fluid Flow Along a Travelling Wave," BIONIKA, No 4, 1970.

12. Merkulov, V. I., "A Travelling Wave on an Elastic Body Moving in an Ideal Fluid," BIONIKA, No 4, 1970.

13. Pershin, S. V., "Self-Adjustment of Skin Damping and Reduction of Hydrodynamic Drag During Active Swimming of Cetaceans," BIONIKA, No 10, 1976.

14. Surkina, R. M., "Structure of the Connective-Tissue Stroma of the Skin of Dolphins," in "Mekhanizmy peredvizheniya i orientatsii zhivotnykh" [Mechanisms of Motion and Orientation of Animals], Kiev, Naukova Dumka, 1968.

15. Surkina, R. M., "The Structure and Function of the Cutaneous Musculature of Dolphins," BIONIKA, No 5, 1971.

APPROVED FOR RELEASE: 2007/02/08: CIA-RDP82-00850R000300060001-1

APPROVED FOR RELEASE: 2007/02/08: CIA-RDP82-00850R000300060001-1

UDC 574.6:532.5

SOME RESULTS OF SPECTRAL ANALYSIS OF FLUCTUATIONS IN THE BOUNDARY LAYER OF CETACEANS

Kiev BIONIKA in Russian No 13, 1979 signed to press 14 Jun 79 pp 58-62

[Article by A. A. Vishnyakov, L. F. Kozlov and V. M. Shakalo, Institute of Hydromechanics of the Ukrainian SSR Academy of Sciences, from the collection "Bionika," Izdatel'stvo Naukova Dumka, 1,000 copies, 100 pages]

[Text] Telemetry investigations of the boundary layer of cetaceans showed that the flow over a bottlenosed dolphin is turbulent or transient from laminar to turbulent. A significant decrease of the level of the longitudinal component of velocity fluctuations by the boundary layer of the bottlenosed dolphin was also established [1, 3]. In this regard further investigations of the structure of the boundary layer of cetaceans are of great interest. One of the methods of investigating the structure of the layer is spectral analysis of velocity fluctuations in the boundary layer. The longitudinal component of the velocity fluctuations in the boundary layer were measured to carry out this analysis on the Black-Sea bottlenosed dolphin.

The measuring apparatus was developed at the Institute of Hydromechanics of the Ukrainian SSR Academy of Sciences on the basis of a wire thermoanemometer operating by a scheme with constant current intensity and a velocity meter in the form of a small vane. The sensors (thermoanemometer and vane) were attached to the bottlenosed dolphin's body by an elastic belt. The design of the thermoanemometer provided suspension of a heated filament in the boundary layer of the animal at a constant distance from the body surface equal to 1 mm with the required degree of accuracy. The longitudinal coordinate of the measurement point in the boundary layer comprised 1,250 mm. The method of measurements provided apparatus and analytical compensation of errors arising during measurement of fluctuating characteristics using the wire thermoanemometer operating by a scheme with constant current intensity.

The animal's swimming speed sensor contained a microlog of type Kh-6M, in which a variable electrolytic contact was used as the rotational speed to electric value converter.

The entire measuring complex installed on the bottlenosed dolphin was connected to on-shore recording apparatus by a thin flexible cable. The cable and apparatus had no significant effect on swimming of the cetacean and the hydrodynamic characteristics being measured. The information coming in from the sensors was converted and was recorded in encoded form on magnetic tape.

APPROVED FOR RELEASE: 2007/02/08: CIA-RDP82-00850R000300060001-1

APPROVED FOR RELEASE: 2007/02/08: CIA-RDP82-00850R000300060001-1

The measurements were made on the bottlenosed dolphin in a marine basin measuring 80 X 3.5 X 3 meters surrounded by nets. The animal on which the investigations were made underwent special training, as a result of which it swam freely and naturally in this basin with the apparatus attached to it and developed a speed from 0.3 to 5.5 m/s.

The information recorded on the magnetic tape was reproduced and analyzed in a special electronic device and was then recorded on 35-millimeter movie film in the form of synchronous oscillograms of the bottlenosed dolphin's swimming speed, speed fluctuations and a monitoring-calibrating signal. The oscillogram of the cetacean's swimming was a recording of pulses whose repetition rate was proportional to speed and was used to construct the graph dependence of the given speed on time. The period of averaging the pulses comprised 0.1 second.

A model of the dolphin's swimming, containing segments of motion at high and low speed and at different acceleration, including when the animal swam against the current in the boundary layer (Figure 1), was selected for spectral analysis. The location and length of the analysis segments and also the transient nature on the selected segment are shown here.

The flow over the dolphin in the considered model was transient and turbulent. The beginning and end of transition for the measurement point corresponded to the dolphin's average swimming speeds $U_{\infty Sr}$ = 0.1 and 2.3 m/s ($Re_x = 10^5$ and $2.3 \cdot 10^6$, respectively).

Segments of uniform, accelerated and slowed motion in fluctuations of the dolphin's swimming speed, caused by work of its caudal stem, was subjected to spectral analysis. These fluctuations, as is known [2], have the greatest effect on the intensity of speed fluctuations and other transient processes in the animal's boundary layer. Since the frequency of oscillations of this type comprised 1-1.2 Hz for the selected segments, the length of the analysis segments should be very short. The kinematic characteristics of the segments are presented in the table.

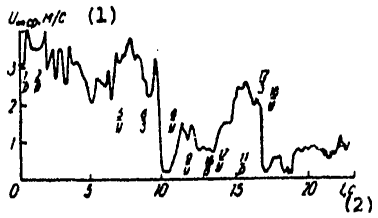

Figure 1. Model of Bottlenosed Dolphin's Gliding Speed. The number of the segment according to the table is included in the numerator and uniform motion (r), acceleration (u) and slowing (z) are included in the denominator.

Key:
1. M/s
2. Seconds

APPROVED FOR RELEASE: 2007/02/08: CIA-RDP82-00850R000300060001-1

APPROVED FOR RELEASE: 2007/02/08: CIA-RDP82-00850R000300060001-1

The information required to analyze these short segments of the model was taken by reproducing the corresponding segment of a continuous magnetic recording on a tape recorder of type AT. The operating principle of the tape recorder included continuous removal of signals from the selected segment of fixed magnetic tape using rotating magnetic playback heads. The length of the recording segment from which the information was read was reduced to 0.4 second.

Spectral analysis of the reproduced signal was carried out on a spectral analyzer of type 2107 of the Bruell and Kjer Company (Denmark) in the 1/4-octave band. An eightfold transposition of the signal was reproduced on the 2107 apparatus to analyze low frequencies of the spectrum. The total level of equipment noise during playback and analysis was 20 dB below the level of the analyzed signal.

The authors investigated the low-frequency, most energy-carrying part of the spectrum in the band to 625 Hz. This consideration provides a sufficiently true idea of the nature of the energy spectrum of the dolphin's boundary layer. This follows from analysis of both the high-frequency spectrum of pressure fluctuations in the bottlenosed dolphin's boundary layer, found in [3], and of the theoretical spectrum in the high-frequency range [5]. The spectral graphs of the longitudinal components of the speed fluctuations obtained by the author in the bottlenosed dolphin's boundary layer, recalculated to the 1-Hz band with respect to the same initial level, are presented in Figure 2. For better illustration, the x-axes in this figure are shifted by some distance from each other. The origin of the coordinate system for each spectrum is denoted on the y axis by an arrow with the number of the segment. The scale line of the level of spectral components is drawn in decibels parallel to it.

The spectra of the longitudinal component of speed fluctuations are cut off and are distinguished by significant variability. It was possible to establish as a result of the analysis that the number of extreme values in the spectra and their frequency and amplitude are determined by the effect of instability, the average swimming speed of the animal, the flow conditions in his boundary layer and moreover, depend on whether the animal affects the flow characteristics in the boundary layer or not.

The effect of instability was manifested in the fact that, upon acceleration during the dolphin's swimming speed fluctuations caused by the work of his caudal fin, extreme values appeared in the range of turbulent and transient modes at frequency of 31-33 Hz, which were only in the transient mode during uniform motion and which generally disappeared upon slowing down. Extreme value of the spectrum whose frequency comprised 10-13 Hz was observed in the transient flow mode upon acceleration. The extreme value disappeared during uniform motion and slowing down. Since this frequency is contained quite satisfactorily in the range of instability according to Schubauer-Scramstad-Tolmin [5], the given spectral peak is obviously determined by the more vigorous increase of unstable fluctuations on the accelerated laminar segments of the transient mode than during uniform and slowed motion.

An extreme value of the spectrum at frequency of 25 Hz, which could easily appear according to [4], during formation of vortex strands in the layer, was observed in the dolphin's boundary layer at the beginning of transition of the laminar flow mode upon acceleration (segment 18). This peak disappeared with further development of the accelerated transient mode and an extreme value appeared in the spectrum at frequency of 150 Hz, obviously indicating, according to [4], the breakdown of vortex strands and the beginning of turbulent spot formation. This extreme value

APPROVED FOR RELEASE: 2007/02/08: CIA-RDP82-00850R000300060001-1

APPROVED FOR RELEASE: 2007/02/08: CIA-RDP82-00850R000300060001-1

(1) Обозначение участка	(2) Характер плавания животного	(3) $U_{\infty\ ср}$, м/с	(4) a, м/с^2	(5) Параметр нестационарности $N=a\frac{\delta}{U_{\infty}^2{}_{ср}}$	(6) Эффект воздействия $K=\frac{\delta_{без\ возд.}}{\delta_{с\ возд.}}$
1	Равномерное движение (7)	3,4	0	0	1
2	То же (7)	2,7	0	0	2,8
5	Ускорение (8)	3,2	1,6	0,03	1
6	Замедление (9)	2,7	—2,3	—0,063	1
7	Ускорение (8)	0,4	3	0,05	1
9	То же (8)	1,3	1,6	0,34	1
11	Равномерное движение (7)	3,7	0	0	1,3
12	Замедление (9)	0,4	—4	—0,7	1
16	Равномерное движение (7)	0,8	0	0	1
17	Ускорение (8)	1,2	3,6	0,06	1
18	То же (8)	0,3	3,6	0,04	1

Key:

1. Notation of segment
2. Nature of animals swimming
3. M/s
4. M/s^2
5. Parameter of instability
6. Effect
7. Uniform motion
8. Acceleration
9. Slowing

disappeared at a specific stage of development of the accelerated turbulent boundary layer. A similar pattern should be observed in the range speed fluctuations of the transient mode of the dolphin during uniform and slowed motion.

The effects on the characteristics of the boundary layer produced by the bottlenosed dolphin were established by a significant reduction (by a factor of more than 2) of the degree of turbulence of the longitudinal component of speed fluctuations in the boundary layer. The range of speed fluctuations corresponding to this mode is found in segment 2.

The characteristic feature of the spectrum during the effect on the characteristics of the boundary layer compared to that in the absence of the effect mentioned above (segment 1) is the significant energy concentration at frequency of approximately 50 Hz with a simultaneous decrease of the adjacent spectral level in the frequency range from 20 to 150 Hz. The range of speed fluctuations has similar, but no less marked changes with lesser effectiveness of this effect (segment 11).

Some energy concentration at 50-56 Hz is generally inherent to most spectra of speed fluctuations. It was established in this case that the extreme value of the envelopes corresponding to frequency of 50 Hz is not the setting of the commercial frequency of the electrical system to which the electronic recording apparatus used in the experiments was connected. The presence of an extreme value at 50-56 Hz apparently indicates some initial adjustment of the mechanism on the characteristics of the dolphin's boundary layer, which became maximum effective under specific conditions.

It should be noted that the spectra of speed fluctuations in the dolphin's boundary layer, obtained by the authors, are in good agreement with corresponding spectra of

APPROVED FOR RELEASE: 2007/02/08: CIA-RDP82-00850R000300060001-1

APPROVED FOR RELEASE: 2007/02/08: CIA-RDP82-00850R000300060001-1

pressures during active and passive swimming of this same species of bottlenosed dolphin obtained in [3].

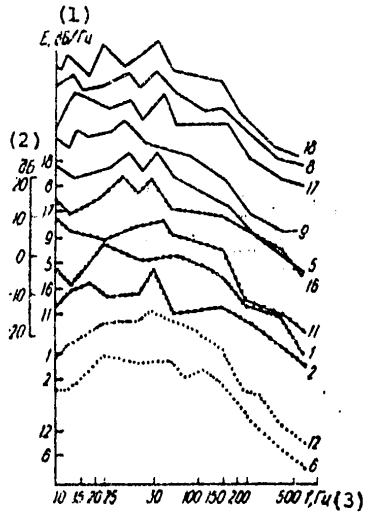

Figure 2. Combined Spectra of Longitudinal Speed Component in Boundary Layer of Bottlenosed Dolphin

Key:
1. dB/Hz
2. dB
3. Hz

BIBLIOGRAPHY

1. Kozlov, L. F. and V. M. Shakalo, "Some Results of Measuring the Speed Fluctuations in the Boundary Layer of Dolphins," BIONIKA, No 7, 1973.

2. Kozlov, L. F., V. M. Shakalo, L. D. Bur'yanova and N. N. Vorob'yev, "The Effect of Instability on the Flow Mode in the Boundary Layer of the Black-Sea Bottlenosed Dolphin," BIONIKA, No 8, 1974.

3. Romanenko, Ye. V., "The Hydrodynamics of Fish and Dolphins," MORSKOYE PRIBOROSTROYENIYE, No 1, 1972.

4. Shklyarevich, A. I. and V. A. Tetyanko, "Experimental Investigation of Natural Transition in the Boundary Layer," TR. LENINGR. KORABLESTROIT. IN-TA, No 69, 1970.

5. Shlikhting, G., "Teoriya progranichnogo sloya" [Boundary Layer Theory], Moscow, Nauka, 1969.

APPROVED FOR RELEASE: 2007/02/08: CIA-RDP82-00850R000300060001-1

APPROVED FOR RELEASE: 2007/02/08: CIA-RDP82-00850R000300060001-1

UDC 597.587.2

DISTRIBUTION OF BODY MASS AND RED MUSCLES OF THE TUNA ALONG ITS LENGTH

Kiev BIONIKA in Russian No 13, 1979 signed to press 14 Jun 79 pp 62-65

[Article by V. Ye. Pyatetskiy, Institute of Hydromechanics of the Ukrainian SSR Academy of Sciences, from the collection "Bionika," Izdatel'stvo Naukova Dumka, 1,000 copies, 100 pages]

[Text] The common bluefin tuna (Thunnus thunnus) is one of the representatives of the Scombridae family, consisting of nine genera. Most representatives of the family have innate fast swimming speeds. The tuna is a typical ocean predator feeding mainly on small fish and squid. The area of distribution is the tropical, subtropical and partially the temperate regions of the world ocean. It reaches a length of more than 3.5 meters and a mass of more than 700 kg [2]. An intensive water flow through the gills is required for normal supply of oxygen to the blood of the tuna and this can be achieved only during motion. The precise value of the swimming speed of the tuna is not yet known. However, observations show that shoals of these animals in their search for food are capable of travelling ocean distances of thousands of kilometers within several days and not a single fishing vessel is capable of overtaking them.

Data from the literature are known [3], according to which the instantaneous swimming speed of a yellowfin tuna caught on a hook comprises 74.59 km/hr (21.11 body lengths per second), while that of the wahoo comprises 77.05 km/hr (18.93 body lengths per second). The measurements were made by using an electromagnetic marker with oscillograph recording by the rate of payout of the fishing line, marked every inch of its length by a special paint. Speed "explosions" were observed only during the first 10-20 seconds after the fish was caught on the hook and then its value decreased significantly. It is assumed that the results do not exhaust all the energy capabilities of these fast-swimming marine animals. Therefore, study of the bioenergetic characteristics of their motion, body shape, specifics of functioning of the muscular system and the topography of its distribution is of interest.

The results of investigations to determine the distribution of the entire mass of red muscles along the body of the common bluefin tuna (female, 857 mm long and with mass of 11,815 grams) are presented below. The method of conducting the experiment included the following: an animal's body with known total length L and mass Q, frozen in the suspended state on the front part of the body was cut by using a sharp thin-bladed knife into approximately n-equal length parts (in the given case n = 31) (Figure 1). The mass q_n and length Δl_n of each part was determined. The dimensionless coordinate of the mid-length of each section and the specific mass q_n^1 (g/mm)

APPROVED FOR RELEASE: 2007/02/08: CIA-RDP82-00850R000300060001-1

APPROVED FOR RELEASE: 2007/02/08: CIA-RDP82-00850R000300060001-1

per unit of length were determined. A graph of the dependence of these values was constructed from the data and the dimensionless coordinate of the mid-length of each section was plotted along the x axis and the specific mass was plotted along the y axis. The simple method of finding the mean values of two adjacent points on the x and y axes was used to smooth out the resulting curve. This procedure was accomplished graphically by joining these points by a straight line and finding its middle, which was taken as the point belonging to the smoothed curve. The area bounded by the curve plotted in this manner and by the x axis is equal to the mass of the tuna with regard to the scale used, which was used as one of the criteria for evaluating the reliability of graphic representation of the considered dependence.

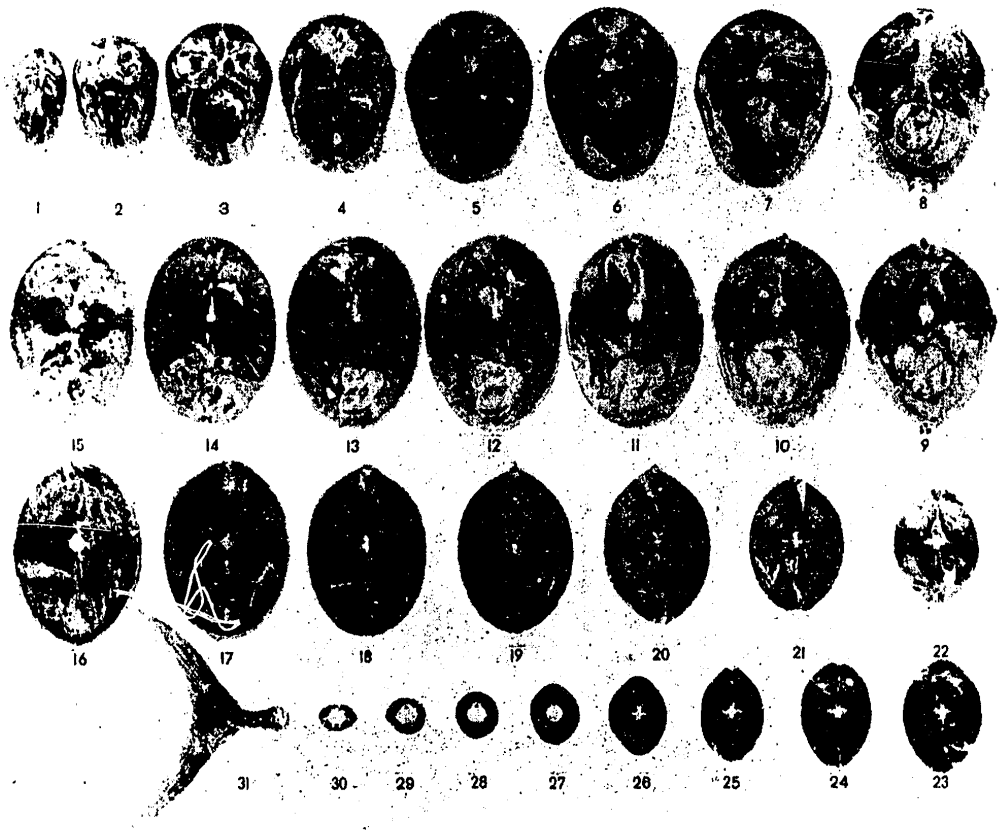

Figure 1. Transverse Sections of Tuna Body

The dimensionless value q_p/Q of mass was determined on the basis of these data at each point of the mid-length of 20 arbitrarily taken calculated sections along the length of the body. All the calculations were made in tabular form and the results are reduced to a table in dimensionless form and are presented in Figure 2 (curve 1).

APPROVED FOR RELEASE: 2007/02/08: CIA-RDP82-00850R000300060001-1

APPROVED FOR RELEASE: 2007/02/08: CIA-RDP82-00850R000300060001-1

Measured Value	Number of Sections								
	1	2	3	4	5	6	7	8	9
x_i	0.05	0.10	0.15	0.20	0.25	0.30	0.35	0.40	0.45
$x_i - (\Delta l/2L)$	0.025	0.075	0.125	0.175	0.225	0.275	0.325	0.375	0.425
Body mass, g q_p	111.4	330.0	531.3	719.9	899.9	1,067.0	1,204.1	1,229.8	1,208.4
q_p/Q	0.09	0.27	0.44	0.60	0.76	0.90	1.01	1.04	1.02
v_{pY}	90.0	278.5	479.9	698.9	899.9	1,105.5	1,255.5	1,225.5	1,221.2
v_{pY}/Q	0.07	0.23	0.40	0.59	0.76	0.93	1.03	1.06	1.03
Mass of red muscles, g v_{pY}	--	--	--	--	4.29	30.00	72.85	128.55	171.40
v_{pY}/Q	--	--	--	--	0.003	0.025	0.061	0.108	0.145

Measured Value	Number of Sections										
	10	11	12	13	14	15	16	17	18	19	20
x_i	0.50	0.55	0.60	0.65	0.70	0.75	0.80	0.85	0.90	0.95	1.0
$x_i - (\Delta l/2L)$	0.475	0.525	0.575	0.625	0.675	0.725	0.775	0.825	0.875	0.925	0.975
Body mass, g q_p	1,122.7	964.1	797.0	621.3	437.1	257.1	141.4	77.1	47.1	34.3	12.9
q_p/Q	0.95	0.81	0.67	0.52	0.36	0.21	0.11	0.06	0.03	0.02	0.01
v_{pY}	131.3	981.3	809.9	629.9	432.8	270.0	145.7	81.4	42.9	25.7	8.6
v_{pY}/Q	0.95	0.83	0.68	0.53	0.36	0.22	0.12	0.06	0.03	0.02	0.007
Mass of red muscles, g v_{pY}	154.26	102.84	64.28	34.28	12.86	--	--	--	--	--	--
v_{pY}/Q	0.130	0.087	0.054	0.029	0.010	--	--	--	--	--	--

APPROVED FOR RELEASE: 2007/02/08: CIA-RDP82-00850R000300060001-1

APPROVED FOR RELEASE: 2007/02/08: CIA-RDP82-00850R000300060001-1

The entire volume of the animal's body and also the volume of its red muscles was determined in a similar manner. To do this, the areas of the entire cross-section and part of this cross-section occupied by the red muscles were determined by the planimetric method from photographs of its transverse sections made in known scale (see Figure 1). Graphical smoothing of the distribution curve of the entire body volume and the volume of the red muscles along the length was then carried out and these functions were then reduced to dimensionless form. As in the previous case, these functions are presented with regard to specific weight in the form of curves in Figure 2 (curve 2 is distribution of the entire body mass and curve 3 is the mass of the red muscles) for convenience of checking the plotting of the curves and also for clarity of analyzing the results obtained. The specific weight of the tuna is $\gamma = 1.02$ g/mm^3 [1].

The error of the results is found in the range of 2.5-3 percent. It follows from consideration of curves 1 and 2 that the greatest mass of the tuna is concentrated in the section located from the nose at a distance of (0.35-0.40) L. The mass of the red muscles comprises 6.5 percent of the entire body mass and its distribution curve along the length of the tuna has a maximum at distance of (0.42-0.43) L from the nose. To find the distribution of the volume of the tuna's body along its length, the y axes of curve 2 should be separated by the value of the tuna's specific weight, taken as equal to $\gamma = 1.02$ in the given case. The distribution of the volume of the red muscles is also determined in similar fashion by curve 3. One can conclude from the disposition of curves 1 and 2 that the center of gravity of the tuna's body volume and the center of gravity of its mass practically coincide.

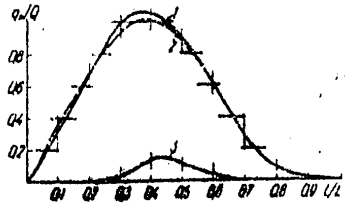

Figure 2. Distribution of Body Mass and Red Muscles Along Length of Tuna

The given results can be used as input data when studying different problems related to the hydrodynamics and bioenergetics of swimming of these animals.

BIBLIOGRAPHY

1. Alyev, Yu. G., "Nekton" [Nekton], Kiev, Naukova Dumka, 1976.

2. "Tekhnokhimicheskiye svoystva okeanskikh ryb. Spravochnik" [The Technical and Chemical Properties of Ocean Fishes. Handbook], Moscow, Pishchevaya promyshlennost', 1972.

3. Walters, V. and H. L. Firstine, "Measurements of Swimming Speeds of Yellowfin Tuna and Wahoo," NATURE, Vol 202, No 4928, 1964.

APPROVED FOR RELEASE: 2007/02/08: CIA-RDP82-00850R000300060001-1

APPROVED FOR RELEASE: 2007/02/08: CIA-RDP82-00850R000300060001-1

UDC 599.53:591.485

THE ROLE OF HEARING MECHANISMS IN THE SPATIAL ORIENTATION OF ANIMALS

Kiev BIONIKA in Russian No 13, 1979 signed to press 14 Jun 79 pp 65-68

[Article by V. A. Saprykin, E. A. Levin and V. A. Protasov, Sevastopol', from the collection "Bionika," Izdatel'stvo Naukova Dumka, 1,000 copies, 100 pages]

[Text] The role of hearing mechanisms in determining the speed of sound sources during spatial orientation of animals has not been adequately studied. Promising in this regard is investigation of such highly specialized animals as dolphins in which spatial orientation is accomplished primarily due to the use of hearing mechanisms. There are very few publications directly devoted to consideration of the given problem.

It is known that the motion of the body in a fluid is accompanied by radiation of sound--a noise signal in a specific frequency band. In this case the signal in the spectrum may contain discrete components of considerable amplitude [3]. The motion of the sound source with respect to the receiver leads to variations of the parameters of the acoustic field being recorded. One may assume that the animals use a goniometric discrimination mechanism based on analysis of the change of direction toward a moving object per unit time when determining the speed of a sound source in water. Along with the foregoing, use of a frequency analysis mechanism is possible where information about the speed of motion can be obtained by analyzing the shift of the spectral characteristics of noise radiation in time, determined by the Doppler effect, is possible. The combined use of the given mechanisms is also possible. In this case sequential analysis of the signal spectrum permits one to determine both the radial and the absolute speed of an object.

The relationship between the velocity of a sound source and the extent of displacement of the signal frequency spectrum can be described by using the following function (let us consider the source a point source and one emitting a tonal frequency signal f_0) [2]:

$$V = \sqrt{\frac{hc\left|\frac{df_{\text{д}}}{dt}\right|_{\text{макс}}}{2\lambda f_0}}, \qquad (1)$$

where h is the minimum distance between the sound source and the receiver (Figure 1), c is the speed of propagation of acoustic waves in the medium and $|df_d/dt|_{maks}$ is the maximum value of the absolute derivative of the signal frequency of a moving tonal sound source in time in the readout system of a fixed receiver.

APPROVED FOR RELEASE: 2007/02/08: CIA-RDP82-00850R000300060001-1

APPROVED FOR RELEASE: 2007/02/08: CIA-RDP82-00850R000300060001-1

The given expression was found by transformation of the well-known formula which expresses the dependence of the frequency of a tonal signal source moving at constant velocity upon reception of radiation at a fixed point on the speed and direction to the reception point (the Doppler effect) [3]:

$$f_{\text{п}} = \frac{f_0}{1 - \frac{V}{c}\sin\alpha}. \qquad (2)$$

Here α is the angle between the perpendicular to the trajectory of motion from the reception point and the direction toward the sound source (see Figure 1):

$$\alpha = \arcsin \frac{Vt}{\sqrt{V^2t^2 + h^2}}.$$

In the other case, according to known values of Doppler frequencies f_{d1} and f_{d2} and the direction toward the sound source (which are determined by the values of angles α_1 and α_2) at different moments of time, making use of formula 2, to calculate the speed of the source we find the expression

$$V = \frac{f_{\text{п}_1} - f_{\text{п}_2}}{f_{\text{п}_2}\sin\alpha_1 - f_{\text{п}_1}\sin\alpha_2}. \qquad (3)$$

One can also cite other examples which illustrate the possibility of using the Doppler effect to determine the speed of the sound source. It is significant that the time shift of the frequency signal spectrum (or its derivative) must be determined when using similar methods of estimating speed. Under real conditions when a body is moving in an aqueous medium, a noise signal is emitted in the frequency band; therefore, the speed of motion can be determined both by analysis of the discrete components of the signal spectrum and by the integral characteristics of noise emission.

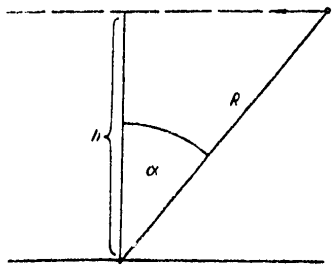

Figure 1. Diagram of Measuring Speed of Sound Source

Let us assume that animals, specifically dolphins, use the frequency analysis mechanism along with goniometric methods. To confirm the indicated hypothesis,

APPROVED FOR RELEASE: 2007/02/08: CIA-RDP82-00850R000300060001-1

APPROVED FOR RELEASE: 2007/02/08: CIA-RDP82-00850R000300060001-1

one must investigate the resolution of the dolphin's auditory analyzer when distinguishing frequency deviation as a factor which determines the possibility of estimating the values of Doppler frequency shifts. Paper [4] is devoted to this problem. The investigations were carried out on the common porpoise Phocaena phocaena. The threshold value of frequency deviation (the minimum distinguishable value of tonal signal frequency variation) in the given animal did not exceed 0.5 percent of the carrier frequency in the entire frequency range perceived by the porpoise. However, these data cannot be used to construct the possible functional model of the hearing mechanism of the dolphin when determining speed since 2-4 Hz or more were found for the modulation frequencies, whereas under real conditions variation of signal frequency occurs much more slowly.

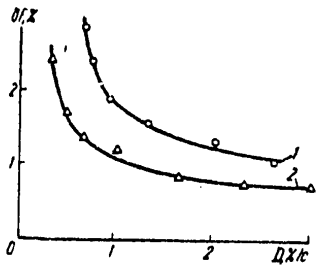

Figure 2. Dependence of Threshold Values of Frequency Deviation δF on Deviation Rate D for Different Values of Carrier Frequency: 1--2 kHz; 2--20 kHz

The differential thresholds of the hearing of dolphins by the rate of frequency deviation (the value of frequency deviation per unit time) at infrasonic modulation frequencies were studied in the experiments. The investigations were carried out by using the conditioned reflex method on two adult females of the bottlenosed dolphin Tursiops truncatus, well adapted to confinement conditions. The animals were located in a net enclosure and were taught to approach a permanent feeding spot upon presentation of a positive conditioned stimulus and to return to their initial position. A tonal signal was presented constantly to the dolphins during this entire experiment and the modulation of this tone was a positive conditioned stimulus. Modulation was accomplished by transmission of sawtooth voltage pulses to the tonal signal generator input, which provided frequency modulation by the law of variation of the modulating voltage. The pulse amplitude and length characterized the extent of deviation and the rate of its variation per unit time.

The experimental data are presented in Figure 2, from which it is obvious that there is a threshold value of the rate of deviation for each carrier frequency at which the dolphin no longer distinguishes the tonal and frequency-modulated signals. The probability of an error in discrimination of these signals depends on the rate of frequency deviation (Figure 3).

The results of investigating the differential thresholds of hearing permit one to distinguish zones where the dolphins possibly use the frequency analysis mechanism at specific ratios between the speed of the sound source, the direction toward it and the distance to the source. Differentiating both sides of equality (2) by time, we find a relation which links the indicated parameters:

APPROVED FOR RELEASE: 2007/02/08: CIA-RDP82-00850R000300060001-1

APPROVED FOR RELEASE: 2007/02/08: CIA-RDP82-00850R000300060001-1

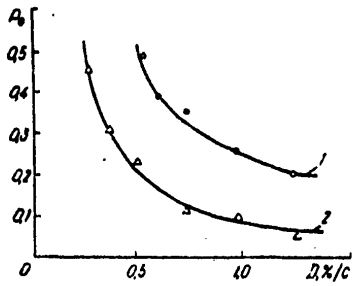

Figure 3. Dependence of Probability of Errors in Discrimination of Tonal and Frequency-Modulated Signals P_0 on Rate of Deviation D at Different Values of Carrier Frequency: 1--2 kHz; 2--20 kHz

$$\frac{1}{f_A}\cdot\frac{df_A}{dt}=\frac{1}{R}\frac{\frac{V^2}{c}\cos\alpha}{\left(1-\frac{V}{c}\sin\alpha\right)^2},$$

where $(1/f_d)(df_d/dt)$ is the rate of frequency deviation and R is the distance to the sound source.

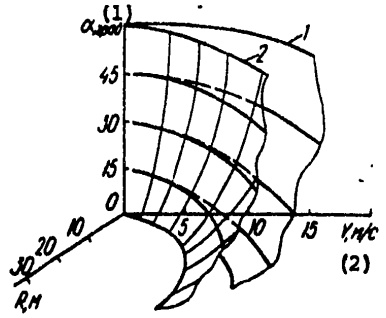

Figure 4. Division of Space (R, V and α) By Surfaces of Threshold Values Into Zones of Use of Different Mechanisms to Determine Speed: 1--2 kHz; 2--20 kHz

Key:
1. Degree
2. M/s

Using data from the literature [1] on the capability of dolphins to distinguish directions toward a sound source and the results of the authors' investigations, one can determine the regions in which simultaneous use of goniometric mechanisms for determination of speed and mecahnisms based on frequency analysis is possible (Figure 4).

APPROVED FOR RELEASE: 2007/02/08: CIA-RDP82-00850R000300060001-1

APPROVED FOR RELEASE: 2007/02/08: CIA-RDP82-00850R000300060001-1

The use of the indicated mechanisms as those which utilize different channels for obtaining information (goniometric and frequency) increases the operating efficiency of the auditory system of animals when determining the speed of sound sources and in spatial orientation.

BIBLIOGRAPHY

1. Bel'kovich, V. M. and N. A. Dubrovskiy, "Sensornyye osnovy orientatsii kitoobraznykh" [The Sensory Bases of the Orientation of Cetaceans], Leningrad, Nauka, 1976.

2. Kotel'nikov, V. A. et al, "Investigating the Doppler Effect to Determine the Orbital Parameters of Artificial Earth Satellites," RADIOTEKHNIKA I ELEKTRONIKA, Vol 3, No 7, 1958.

3. Miniovich, I. Ya., A. D. Pernik and V. S. Petrovskikh, "Gidrodinamicheskiye istochniki zvuka" [Hydrodynamic Sources of Sound], Leningrad, Sudostroyeniye, 1972.

4. Supin, A. Ya., and M. N. Sukhoruchenko, "Characteristics of the Acoustic Analyzer of the Common Porpoise Phocaena phocaena," in "Morfologiya, fiziologiya i akustika morskikh mlekopitayushchikh" [The Morphology, Physiology and Acoustics of Marine Mammals], Moscow, Nauka, 1974.

APPROVED FOR RELEASE: 2007/02/08: CIA-RDP82-00850R000300060001-1

APPROVED FOR RELEASE: 2007/02/08: CIA-RDP82-00850R000300060001-1

UDC 599.53:591.422-23

MORPHOFUNCTIONAL ANALYSIS OF THE LIGAMENT-ARTICULAR APPARATUS OF THE LARYNX AND TRACHEA OF DOLPHINS

Kiev BIONIKA in Russian No 13, 1979 signed to press 14 Jun 79 pp 69-73

[Article by A. P. Manger and I. V. Karysheva, Institute of Zoology of the Ukrainian SSR Academy of Sciences, from the collection, "Bionika," Izdatel'stvo Naukova Dumka, 1,000 copies, 100 pages]

[Text] Adaptation of Cetaceans to an aqueous medium while retaining pulmonary respiration became possible due to the significant morphological changes which occurred in the respiratory system and specifically in the larynx and trachea. However, the data of the literature [1, 3-8] has far from exhausted the problems of the anatomical characteristics of the indicated organs until now and they contain significant morphological errors. This is related, for example, to the ligament-articular system of the larynx and trachea of dolphins, detailed study of which improves the understanding of many problems of their functioning. Moreover, a similar investigation may serve to a known degree as an objective criterion in problems of simulating these important sections of air passages.

P. F. Lesgaft devoted much attention to the joint relief in his functional constructions. He assumed that the joint relief is of decisive significance to determine the joint function. Lesgaft proceeded in this case from the dialectic-materialistic understanding of shape and function as two interrelated and mutually determined aspects of the same process. It was always emphasized in his papers on functional anatomy that "reading" the function by the shape of the joint surfaces is of special significance for understanding the joints. We were guided by this very principle in our investigations.

Typical joints with articular capsules in the larynx of dolphins are formed between the thyroid and cricoid and the cricoid and arytenoid cartilages.

The cricoid-thyroid joint (Figures 1 and 2) is formed at the location where the caudal horns of the thyroid cartilage come into contact, having on their thickened ends articulate cricoid surfaces with articulate thyroid surfaces arranged along the sides of the plate of the cricoid cartilage. The articular surfaces correspond completely to each other in size and configuration, i.e., they are congruent. The joint capsule is difficult to stretch and is attached along the edge of the articular surfaces and it also encompasses the peak on the caudal horn of the thyroid cartilage. The cricoid-thyroid joint should be related in shape and configuration

APPROVED FOR RELEASE: 2007/02/08: CIA-RDP82-00850R000300060001-1

APPROVED FOR RELEASE: 2007/02/08: CIA-RDP82-00850R000300060001-1

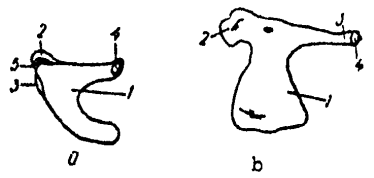

Figure 1. Ligament-Articular Apparatus of Dolphin Larynx: a--cricoid cartilage: 1--plate; 2--coracoid process; 3--arytenoid articular surface; 4--thyroid articular surface; 5--beak ligament; b--thyroid cartilage: 1--plate; 2--anterior horn; 3--caudal horn 4--cricoid articular surface

of the articular surfaces to flat or stiff joints with limited volume of motions and with a single rotational axis around the longitudinal horizontal axis. Both joints function simultaneously, determining the possibility of making the following motions due to the effect of contract of a number of muscles: deflection of the thyroid cartilage ventrally and dorsally. In the first case some opening of the entrance to the larynx is possible and in the second case tighter closing of it is possible due to the fact that the epiglottis joined to it moves together with the thyroid cartilage, thus changing the distance between the epiglottis and the arytenoid cartilages. The articular capsule is attached by horny-cricoid ligaments, among which the lateral and dorsal can be distinguished (Figures 2-5).

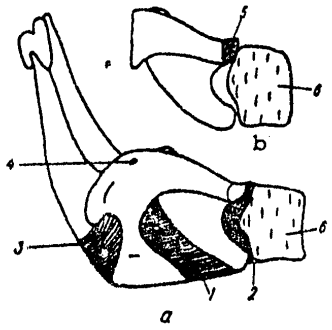

Figure 2. Ligament-Articular Apparatus of Dolphin Larynx: 1--cricoid-thyroid ligament; 2--cricoid-tracheal ligament; 3--thyroid-epiglottal ligament; 4--thyroid opening; 5--lateral horny-cricoid ligament; 6--trachea

The cricoid-arytenoid joint (Figures 4 and 6) is paired and is formed between the convex articular arytenoid surfaces located on the front edge of the plate of the cricoid cartilage and by convex articular cricoid fossae at the bases of the arytenoid cartilages. The articular surfaces have an ellipsoid shape and correspond to each other. The articular capsule is rather easily stretched and is attached along the edges of the articular surfaces. The articular capsule is thickened on the dorsal side since the dorsal cricoid-arytenoid ligament is entwined into it

APPROVED FOR RELEASE: 2007/02/08: CIA-RDP82-00850R000300060001-1

APPROVED FOR RELEASE: 2007/02/08: CIA-RDP82-00850R000300060001-1

(see Figure 3, 2). The cricoid-arytenoid joint, based on the shape of the articular surfaces, should be related to ellipsoid joints with the possibility of moving around two mutually perpendicular axes: the horizontal lying in the sagittal plane and the vertical. Both joints function simultaneously, determining the deflection of the arytenoid cartilages ventrally and dorsally around the horizontal axis and rotation of the arytenoid cartilages laterally and medially around the vertical axis. In the first case opening of the entrance to the larynx (upon deflection of the cartilages dorsally) or tighter closing of it (upon deflection of the cartilages ventrally) are possible due to the effect of a number of muscles. Upon movement of the arytenoid cartilages around the vertical axis, rotation of the latter in lateral directions opens the entrance to the larynx and on the contrary bringing the cartilages to each other accomplishes tighter closing of it. The cricoid-arytenoid joint is very similar in the entire shape of the articular surfaces to the atlantal-occipital joint in land mammals, but with more restricted span of movements.

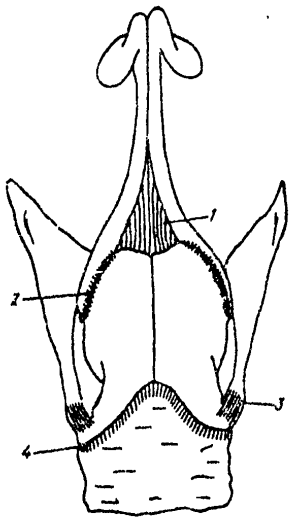

Figure 3. Ligament-Articular Apparatus of Dolphin Larynx: 1--interarytenoid fissure; 2--dorsal cricoid-arytenoid ligament; 3--dorsal horny-cricoid ligament; 4--cricoid-tracheal ligament

If the articulations with joint process described above are interrupted, the connection between the base of the epiglottis and the front edge of the body of the thyroid cartilage can be confidently related to the synchondroses, i.e., to the cartilaginous accretions (see Figure 5). This connection is very strong and almost excludes the possibility of the epiglottis moving with respect to the thyroid cartilage. At the same time if a number of muscles contract, the epiglottis-thyroid cartilage system may move in the cricoid-thyroid joint. Separation of the epiglottal cartilage from the arytenoid cartilage or closer approach of them then becomes possible. In the first case the thyroid cartilage together with the epiglottis is deflected ventrally, thus opening the entrance to the larynx. In the second case

APPROVED FOR RELEASE: 2007/02/08: CIA-RDP82-00850R000300060001-1

APPROVED FOR RELEASE: 2007/02/08: CIA-RDP82-00850R000300060001-1

APPROVED FOR RELEASE: 2007/02/08: CIA-RDP82-00850R000300060001-1

APPROVED FOR RELEASE: 2007/02/08: CIA-RDP82-00850R000300060001-1

the epiglottis-thyroid cartilage system is deflected dorsally, which provides tighter closing of the entrance to the larynx.

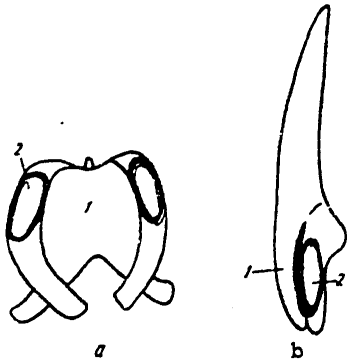

Figure 4. Ligament-Articular Apparatus of Dolphin Larynx: a--cricoid cartilage: 1--plate; 2--arytenoid articular surface; b--arytenoid cartilage: 1--vocal chord process; 2--cricoid articular surface

Anatomical investigation of the ligament apparatus made it possible to establish that there is no hyothyroid ligament in the dolphin larynx, which exists in most land mammals. We feel this is explained by the fact that the thyroid cartilage is almost completely adjacent with its front edge to the large horn of the hyoid bone with regard to the almost complete absence of a neck region. At the same time the thyroid-epiglottal ligament, especially well marked in the bottlenosed and white-sided dolphins (see Figure 5, 3), achieves significant development in dolphins. This ligament is stretched between the cranial horns of the thyroid cartilage and the lateral plates of the epiglottis, filling the anterior-lateral thyroid notches. The thyroid-epiglottal ligament in the porpoise and sometimes in the bottlenosed dolphin is sometimes pierced approximately in the middle by an opening which passes through the inner branch of the cranial laryngeal nerve and the cranial laryngeal artery.

The cricoid-thyroid ligament is stretched between the half-arcs of the cricoid and rear edge of the thyroid cartilages (see Figure 5, 1). It is rather easy to stretch and has a yellowish color since it contains a large number of elastic fibers. The lateral edges of this ligament change without a sharp boundary to the inner surface of the laryngeal cartilages, participating in formation of the elastic interlayer between them and the mucous membrane. Since the ring of the cricoid cartilage is not closed in dolphins, the ventral ends of the arcs are connected to each other by an easily stretchable transverse ligament (see Figure 5, 2).

Thus, the openness of the cartilaginous ring and also the presence of a large number of elastic fibers in the cricoid-thyroid transverse cricoid ligaments of the larynx permit one to assume significant stretching of the ventral wall of the larynx.

APPROVED FOR RELEASE: 2007/02/08: CIA-RDP82-00850R000300060001-1

APPROVED FOR RELEASE: 2007/02/08: CIA-RDP82-00850R000300060001-1

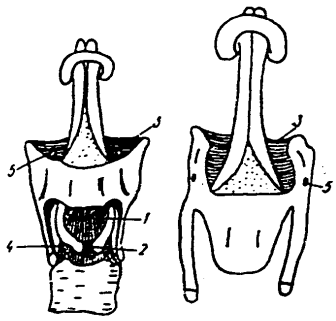

Figure 5. Ligament-Articular Apparatus of Dolphin Larynx: 1--cricoid-thyroid ligament; 2--transverse cricoid ligament; 3--thyroid-epiglottal ligament; 4--cricoid-tracheal ligament; 5--thyroid opening

The anterior edge of the cricoid cartilage is connected to the first ring of the trachea by the cricoid-tracheal ligament (see Figure 3, 4 and Figure 5, 4). The fibers of this ligament are entwined on the ventral side into the transverse cricoid ligament. On the whole the cricoid-tracheal ligament, as described above, is stretchable and provides some mobility of the larynx with respect to the trachea. The ligaments of the cricoid cartilage are also related to the small connective-tissue membrane stretched between the tip of the beak and the anterior edge of the plate of the cricoid cartilage (see Figure 1, 2).

Figure 6. Cricoid-Arytenoid Joint of White-Sided Dolphin (the thyroid cartilage is removed. Photo was taken from a preparation)

APPROVED FOR RELEASE: 2007/02/08: CIA-RDP82-00850R000300060001-1

APPROVED FOR RELEASE: 2007/02/08: CIA-RDP82-00850R000300060001-1

Based on the data on the anatomy of the ligament-articular apparatus, one can conclude that the greatest motions in the laryngeal stroma of dolphins is possible in the cricoid-arytenoid joint related to two-axis ellipsoid joints. It is obvious that movements of the arytenoid cartilagesplay the main role in opening and closing of the entrance to the larynx. The cricoid-thyroid joint, being a single-axis joint difficult to stretch, apparently plays a supplementary role with respect to the cricoid-arytenoid joint. At the same time complete opening or closing of the entrance to the larynx can be accomplished only with the combined interaction of both joints functioning simultaneously due to the contraction of one or another muscles of the laryngeal musculature. The morphology of the ligament apparatus of the larynx of dolphins indicates the possibility of considerable stretching of the ventral wall of the larynx due to the effect of through flow of air.

The ligament apparatus of the dolphin trachea is characterized by the absence of a longitudinal membrane which closes the half-ring of the trachea on the dorsal side in most mammals. This is related to the fact that the tracheal rings of dolphins are complete and frequently are superimposed on each other, forming a flexible descending tube.

As already pointed out, the cricoid-tracheal ligament, which provides some mobility of the larynx with respect to the trachea, is most marked in the porpoise. The ligaments between separate rings of the trachea and the major bronchi (circular) consists of rough fibrous connective tissue difficult to stretch, which corresponds to an even greater degree to the structural strength of the trachea.

The indicated characteristics in the structure of the trachea of the porpoise obviously have a clearly marked adaptive nature since the animal catches and swallows whole prey when located under the water surface. It is natural to assume in this case that passage of food (most frequently fish) through the food tract would significantly deform the trachea with soft membranous part, thus creating specific difficulties for the dolphin to inhale, exhale, sometimes following immediately after swallowing the prey.

BIBLIOGRAPHY

1. Kleynenberg, S. Ye., A. V. Yablokov, V. M. Bel'kovich and V. M. Tarasevich, "Belukha: Opyt monograficheskogo opisaniya vida" [The Beluga: Experience of Monographic Description of a Species], Moscow, Nauka, 1964.

2. Lesgaft, P. F., "Osnovy teoreticheskoy anatomii" [Fundamentals of Theoretical Anatomy], Part 1, Saint Petersburg, 1892.

3. Benham, W., "On the Larynx of Certain Whales (Kogia, Balaenoptera and Ziphius)," PROC. ZOOL. SOC. LONDON, Vol 2, 1901.

4. Hein, S., "Contribution to the Anatomy of Monodon monoceros," VERHANDEL. KONINKE AKAD. WET. AMSTERDAMS, Vol 18, 1914.

5. Kukenthal, W., VERGLEICHENDANATOMISCHE UND ENTWICKLUNGGESCHICHTLICHE UNTERSUCHUNGEN AN WALTIEREN, Vol 1, No 11, Jena, 1893.

APPROVED FOR RELEASE: 2007/02/08: CIA-RDP82-00850R000300060001-1

APPROVED FOR RELEASE: 2007/02/08: CIA-RDP82-00850R000300060001-1

6. Rawitz, B., "Die Anatomie des Kehlkopfes und der Wase von Phocaena comminis," INT. MONATSSCHR. ANAT. PHYS., Vol 17, No 6, 1900.

7. Watson, M. and A. Young, "On the Anatomy of the Northern Beluga," TRANS. ROY. SOC., Vol 29, 1880.

8. Wymann, J., "Description of a 'White Fish' or 'Winte Whale' (Beluga leucas L.)," NATURAL HISTORY, Vol 7, No 4, 1863.

APPROVED FOR RELEASE: 2007/02/08: CIA-RDP82-00850R000300060001-1

APPROVED FOR RELEASE: 2007/02/08: CIA-RDP82-00850R000300060001-1

UDC 591.485;597.5

THE PROBLEM OF SOUND PERCEPTION IN FISH

Kiev BIONIKA in Russian No 13, 1979 signed to press 14 Jun 79 pp 73-91

[Article by A. Yu. Neproshin, Far Eastern OKTB Dal'tekhrybprom, from the collection "Bionika," Izdatel'stvo Naukova Dumka, 1,000 copies, 100 pages]

[Text] Despite the extensive development of hydroacoustic methods of finding fish and controlling their behavior near the catching mechanisms, problems related to the practice of controlling the behavior of commercial fish have not been solved until now. Experimental papers in this field made it possible to develop special sound-emitting apparatus designed to scare fish from the mouths of purse seines [19]. Moreover, according to the data of the commercial fleet, the effect of this device was lower than expected. The reason is the insufficient number of biological and bioacoustic investigations which permit justification and checking of the possibility of using this method.

Problems on which concentration is concentrated in many literary sources [4, 24 and so on] are very important in realizing methods of practical use of sound to control fish behavior. They include primarily problems of sound perception by animals, the mechanism of separation and processing of the sound signal by the receptor fields and the higher processes of the nervous system and the mechanism of sound location by the sensory organs of fish. One can say in application to lower vertebrates that publications which illuminate these problems do not usually encompass the problem universally (taking the functional and ecological-morphological characteristics of the sound perception mechanisms of fish into account).

The advances which we have in study of the organs of hearing in fish with an air bladder cannot answer some specific but nevertheless important questions considered in this paper. At the same time we do not pose the task of describing the operation of such receptors as the neuromasts of the lateral line of fish, the air bladder system with Weberian apparatus, which has been already outlined in detail in the papers indicated by us, and also in many other publications [23, 27, 28, 31, 32 and so on]. We feel that the functional aspects of this problem, which permit one to investigate the physical model of the hearing complex of fish and its response to a sound stimulus, are of great interest. Taking into account that the sound wave

APPROVED FOR RELEASE: 2007/02/08: CIA-RDP82-00850R000300060001-1

APPROVED FOR RELEASE: 2007/02/08: CIA-RDP82-00850R000300060001-1

in water differs somewhat in its manifestations from sound in air, data from the field of hydroacoustics and bioacoustics are used to study the receptors which make it possible to analyze quantitatively the distance at which sound perception by fish is possible and to denote the frequency range used to separate and process information received over the acoustic channel.

We intentionally did not touch on some problems related to processing acoustic signals, problems of sound localization by fish and so on since this material (due to its specific nature) can be presented independently.

Despite the significant number of publications of problems related to hearing in fishes and information transmission over the hydroacoustic channel, they are all usually narrowly specialized. There is the need to generalize and analyze all concepts, hypotheses and assumptions for developing a unified theory of sound perception by fishes to understand the existing principles.

The given material (both original and the papers of other authors) was analyzed from the viewpoint of hydroacoustics and bioacoustics, physical acoustics, radio electronics and the physiology of hearing. All the given calculations and graphs are presented with regard to their practical use. At the same time some hypotheses related to the mechanism of sound reception are advanced. Some efforts are probably required to refute or confirm them and the author will assume his task fulfilled if these trends evoke interest on the part of electrophysiologists, morphologists and acousticians.

Sound in the aqueous medium. Underwater sound is elastic oscillations of fluid occurring due to the effect of wave disturbances. They can be measured by several physical values but the main ones of them in bioacoustics are pressure p and displacement of fluid particles ξ. Pressure is caused by variation of the particle density of the medium due to the effect of elastic oscillations and can be measured by using a hydrophone. Particle displacement is a vector value which characterizes the direction of motion of the wave front of the sound disturbance.

Distribution of plane acoustic waves in the fluid depends on its acoustic transmission and in some cases can be limited by rigid boundaries: the bottom, surface and the layer of the temperature jump. Acoustic transmission is characterized by wave impedance z, which is the ratio of sound pressure to the extent of particle displacement in the moving sound wave. At a long distance from the emitter, its value is equal to ρc, where ρ is the density of the medium and c is the speed of sound in the given medium [3].

The medium can be "hard" if the wave impedance is high and "soft" if it is low. If the acoustic wave encounters a barrier (the body of a fish with air bladder) in its path, part of its energy is reflected from this obstacle and another part will be converted to heat and to the mechanical energy of the obstacle. Re-emission of the wave at this point is also possible. If the characteristic impedance of the medium and the obstacle coincide ($z_1 = z_2$) and if their densities ($\rho_1 = \rho_2$) and the speed of sound in them ($c_1 = c_2$) are also equal, the acoustic wave passes through this obstacle without hindrance.

The wave emitted by a point sound source is spherical, but it may be regarded as locally plane at long distances from the source. It is assumed that the zone of

APPROVED FOR RELEASE: 2007/02/08: CIA-RDP82-00850R000300060001-1

APPROVED FOR RELEASE: 2007/02/08: CIA-RDP82-00850R000300060001-1

spherical waves is located at distance $l = \lambda/2\pi$ from the sound source, where λ is the acoustic wavelength. This segment has been called the near zone or near field. Spherical waves in the immediate vicinity of the sound source have an important feature--slight excess pressure of the emitter causes extensive motion of the particles of the medium [11].

Conducting bioacoustic investigations is related to measuring the parameters of the acoustic field: sound pressure, a-c velocity and displacement of the particles, i.e., those parameters which are perceived by fish using their receptor fields. These parameters can be calculated by the formulas

$$v(r) = \frac{p(r)}{z}\left(1 + \frac{j\lambda}{2\pi r}\right)$$

is a-c velocity,

$$\xi(r) = \frac{p(r)}{z\omega}\left(1 + \frac{j\lambda}{2\pi r}\right), \text{ т. е. } \xi(r) = \frac{v(r)}{\omega}$$

is particle displacement,

$$\frac{p(r)}{v(r)} = \frac{z}{\left(1 + \frac{j\lambda}{2\pi r}\right)}$$

is the ratio of pressure to a-c velocity.

The values of these parameters will be different as a function of the distance from the sound source at which the measurement is made and what the signal emission frequency is.

The value of pressure wave attenuation in the far zone is determined as $\beta = 0.036f^2$ dB/km [18], while the law of its variation is more complex in the near zone. The fact is that the speed of sound in the immediate vicinity of the emitter has values considerably different from normal values and it may exceed the speed of sound in the near zone, which is explained by the higher response of the medium to acoustic disturbance since the acoustic impedance has considerable variations. Its value is determined by the formula

$$z_{\text{ак}} = \frac{j\rho r\omega}{1 + jkr},$$

where ρ is the density of the medium (it is 1.04 g/cm^3 for sea water), r is the distance from the emitter, cm, $\omega = 2\pi f$ is the angular frequency, f is frequency, Hz, $k = 2\pi/\lambda$ is wave number and c is the speed of sound, cm/s.

The impedance z is a complex value in the near zone. The active and reactive components of the characteristic impedance are low at short distances from the emitter.

APPROVED FOR RELEASE: 2007/02/08: CIA-RDP82-00850R000300060001-1

APPROVED FOR RELEASE: 2007/02/08: CIA-RDP82-00850R000300060001-1

The absolute value of sound pressure is dependent on the characteristic impedance, while oscillations of the latter cause significant variations of pressure in this region. We calculated the sound pressure field using linear theory for the near zone (Figure 1) on the condition that we found pressure equal to 0.1 Pa at the point of measurement at 1 meter from the emitter.

If an emitter which develops other pressures is used in the experiment, a multiple coefficient must be introduced. For example, if the real emitter develops sound pressure of 0.6 Pa, the coefficients of the points of the curve should be multiplied by six.

It is obvious in Figure 1 that a maximum value of sound pressure exceeding the value measured at 1 meter from the emitter is observed due to variations of the parameters of the acoustic field observed in the near zone at some distance from the emitter more than 1 meter, i.e., at the boundary $r = \lambda/2\pi$. It decreases as the distance increases and approaches the level measured at 1 meter on the boundary of the intermediate zone.

In our case the section of space at the beginning of which the principles of variation of the sound field parameters are valid for the near zone and at the end of which they are valid for the far zone, is called the intermediate zone. This segment is limited by dimensions $\lambda/2\pi - 3\lambda/2\pi$.

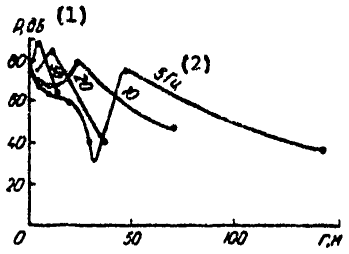

Figure 1. Dependence of Sound Pressure Level on Distance from Emitter (levels are in decibels with respect to $2 \cdot 10^{-5}$ Pa): dark circles--boundary of air zone; light circles--boundary of intermediate zone

Key:
1. Decibels
2. Hz

As frequency increases, the position of the pressure peak shifts to the left along the x axis. There is no rise of the sound pressure level at distances greater than 1 meter for frequency of 500 Hz (or more) when the boundary of the near zone is located at 50 cm from the emitter, while the pressure amplitude beyond this zone decreases according to the principles of the far zone.

It does not follow from the foregoing that additional power appears at the noted points. The fact is that all measurements in bioacoustics are reduced to a distance of 1 meter and, locating the hydrophone at this point, we can have minimum emission

APPROVED FOR RELEASE: 2007/02/08: CIA-RDP82-00850R000300060001-1

APPROVED FOR RELEASE: 2007/02/08: CIA-RDP82-00850R000300060001-1

(although significant sound pressure levels are emitted), while the maximum is located to the right of the point at which the measurement is made.

The indicated relations can be so clearly expressed only for a point emitter in the deep sea upon emission of a harmonic signal. The complex shape of the emitter (which causes the phenomenon of interference), the emission of a wideband signal, the presence of refraction, reverberation and so on conceal this phenomenon, reducing the absolute value of ejections, however they do not occur in a real situation [3]. This phenomenon should be recalled when studying the effect of infrasound (induced by the hull of commercial ships) on shoals of fish.

Graphs of variation of the particle displacement in the near zone upon excitation of acoustic oscillations using an emitter developing pressure of 0.1 Pa at distance of 1 meter are presented in Figure 2. The effective sound pressure of the required frequency at the distance of interest should be determined and then the numerical value of the displacement found from the graph of Figure 2 at the same frequency and same distance should be multiplied by the value of sound pressure to calculate the absolute value of displacement (in the real case) from the graph of pressure wave attenuation (see Figure 1).

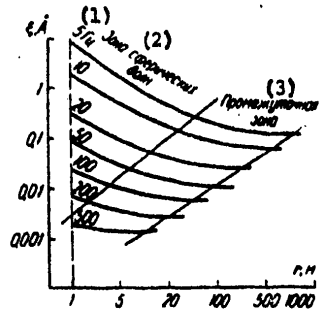

Figure 2. Dependence of Particle Displacement on Distance From Emitter

Key:
1. Hz
2. Zone of spherical waves
3. Intermediate zone

There is the opinion that particle displacement is not dependent on the intensity of the acoustic signal [29], but we feel this is not true. The extent of displacement is $\xi = \frac{p}{2\pi f \rho c}\left[1+\left(\frac{\lambda}{2\pi r}\right)^2\right]^{1/2}$, and its absolute value is directly proportional to sound pressure in the given formula as well as in the formula given by Udo [48]. Thus, the absolute value of displacement may exceed the threshold values perceived by fish even in the near zone. The denominator contains the distance to the sound source and consequently the extent of particle displacement is dependent on distance, which does not correspond to the conclusions of [2].

The organs of sound reception in fish. It was established that all sound receptors in fish are combined into three receptor systems: the inner ear, the inner ear in

APPROVED FOR RELEASE: 2007/02/08: CIA-RDP82-00850R000300060001-1

APPROVED FOR RELEASE: 2007/02/08: CIA-RDP82-00850R000300060001-1

combination with the air bladder and the lateral line since a unified morphological structure is used as the basis--the elementary receptor is a waxy cell [17]. Different species of fish may have the indicated receptor systems in different combinations, which provides reliable contact by them with the medium for several of its parameters.

The inner ear. The sound receptors are located in the lower part of the inner ear (lagenae and sacculus) and the receptors of acceleration and the position of the fish in space are located in the upper part (the semicircular canals with the otolytic organs) [38]. As an organ of hearing, the inner ear is a paired organ located in the anterior part of the head behind the eyes. The sacculus and lagenae (responsible for reception of acoustic oscillations) have regions with waxy receptor cells--maculae. The otolyth is located on them in the layer of the jelly-like mass. It is assumed that when affected by acoustic oscillations, it lags somewhat behind the mechanical oscillations of the system of the auditory apparatus and slides with some delay along the hairs of the receptor field of the maculae--stereocilia and kinocilia, causing them to bend [17]. Bending of the hairs leads to variation of the potential of the cell. If the otolyth is shifted toward the kinocilia, the intracellular potential changes its sign and the cell is depolarized, causing stimulation. If the shift occurs in the opposite direction, the cell is hyperpolarized and inhibition begins.

According to [42], since the characteristic impedance of the water and body of the fish are different, there are no problems relative to the energy reaching the ear. However, it remains unclear in this case how acoustic oscillations are recorded.

Since the properties of the endolymph filling the membranous labyrinth differ in no way (or differ slightly) from the properties of the fish body [20], the receptors of the inner ear do not respond to the pressure wave due to its incompressibility. It is hardly probably in this case that the otolyth is shifted in a viscous fluid due to the effect of pressure waves or displacement, especially at low values of disturbing oscillations.

The presence of a freely floating bladder inside the ear is indicated in some papers (see, for example [47]). It is assumed that it plays the role of the cavity which responds to sound pressure and contributes to displacement of the otolyth along the maculus. However, there is as yet no practical confirmation of this hypothesis.

The air bladder having no relationship to the inner ear. Reports have appeared recently on the transducer function of the air bladder [25, 45]. It is assumed that the pressure amplitude perceived by the air bladder of fish causes vibration of it in time with the exciting frequency. The oscillations induced in the bladder excite the displacement amplitude around it and accordingly in the inner ear of fish, which, as indicated in [25], exceeds the displacement due to the sound source located at 0.5 meter from the fish.

This statement should be regarded critically for the following reasons: 1) it must be assumed that this excess energy of oscillations of the bladder occurs as a result of its resonance properties, but according to available data (see below), the air bladder operates like a wide band, rather than a resonance transducer; 2) the ear is not a receptor of wave displacement (like the lateral line); 3) since

APPROVED FOR RELEASE: 2007/02/08: CIA-RDP82-00850R000300060001-1

APPROVED FOR RELEASE: 2007/02/08: CIA-RDP82-00850R000300060001-1

creation of powerful sound pressure sources (for example, the noise of fishing vessels), the acoustic oscillations from which are propagated for tens of kilometers, is technically possible, one would also expect fish to respond to them at the same distances, which is not observed in reality; and 4) it is pointed out in [32] that removal of individual receptors (the air bladder, otolyth, sagittus, utriculus and the entire labyrinth) causes only a reduction of the sensitivity thresholds at frequency of 150 Hz to various degrees, but it is still difficult to answer the question of the essence of the perceived components of sound due to the complexity of sound perception by different receptors.

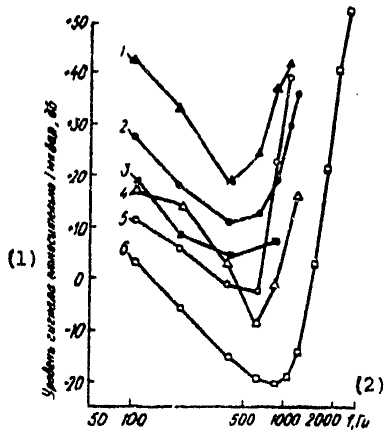

Figure 3. Audiogram of Fish in Which There is No Contact of the Air Bladder to the Inner Ear [42]: 1--Lutinephauls apodus ; 2--Thalassoma bifasciatum; 3--Prianotus scitulus; 4--Holocentrus voxillarious; 5--Haemulon sciurus; 6--Holocentrus ascensionus

Key:
1. Signal level with respect to 1 μbar, dB 2. Hz

The frequency range perceived by fish in which there is no connection of the air bladder to the inner ear is very narrow and occupies the region from 100 to 1,000 Hz with maximum in the frequency range of 300-600 Hz and very rarely reaches frequencies above 2,000 Hz, while their sensitivity to sound varies over a wide range from +20 to -40 dB (with respect to 0.1 Pa), which can apparently be explained by the ecological characteristics of each of the species (Figure 3).

The air bladder combined with the inner ear. Although there is a large diversity of morphological characteristics in the structures of reception of acoustic oscillations in fish in which the air bladder participates, they can be divided into two groups--reception using Weberian's mechanism and using the processes which connect the bladder to the inner ear.

APPROVED FOR RELEASE: 2007/02/08: CIA-RDP82-00850R000300060001-1

APPROVED FOR RELEASE: 2007/02/08: CIA-RDP82-00850R000300060001-1

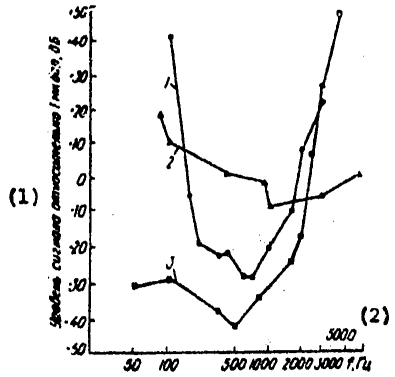

Figure 4. Audiogram of Fish Having Connection of Inner Ear to Air Bladder [42]: 1--Ictarulus nebulosus; 2--Leucaspius delineatus; 3--Ciprinus carpio

Key:
1. Signal level with respect to 1 μbar, dB 2. Hz

The first type of transducer is based on the use of a number of bones which transform the forces occurring during oscillation of the air bladder and transmit them to the rear wall of the unpaired sinus and thus provides contact with the transverse channel of the labyrinth and the lagena [23, 41]. These oscillations are transmitted to the otolyths in the lagena and saggitus where they also excite the waxy cells of the maculus. This mechanism is typical for carp, mainly freshwater fish.

The second type of connection is provided by the processes connecting the bladder to the chambers of the inner ear. The working principle of this system is similar to the previous one. The indicated mechanism of sound perception exists in some marine fish [16].

The frequency range of hearing in fish with Weberian apparatus is the widest and reaches from the lowest to 5,000-8,000 Hz in some of them, although the maximum sensitivity is observed only in the low frequency range (500-1,000 Hz). As can be seen from the audiogram of Figure 4, the variation in sensitivity is not very wide and fluctuates in the range of (-30) to (-45) dB (with respect to 0 dB = 0.1 Pa). In fish related to the second group, the upper bound of the range of hearing does not exceed 3,000 Hz, while maximum sensitivity is in the same range as for the first group of fish.

One should conclude from analysis of available data on the sensitivity of fish to sounds that the highest sensitivity for almost all investigated species is equal to -40 to -45 dB and is located in the range of 300-1,000 Hz. These parameters coincide with the hearing sensitivity and range of man [40].

APPROVED FOR RELEASE: 2007/02/08: CIA-RDP82-00850R000300060001-1

APPROVED FOR RELEASE: 2007/02/08: CIA-RDP82-00850R000300060001-1

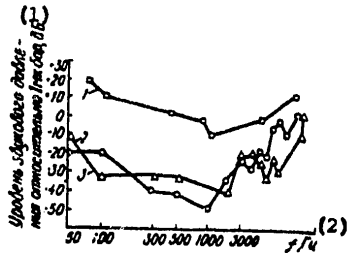

Figure 5. Audiogram of Some Fish Having Wide Frequency Responses [41]: 1--Leucaspius delineatus; 2--Astaynax jordani; 3--Astaynax mexicanus

Key:
1. Sound pressure level with respect to 1 μbar dB
2. Hz

The volume of the air bladder fluctuates over a wide range in different species of fish (from several cubic millimeters in anchovies and others to 200-500 cm^3 in sturgeons) and is dependent on the depth at which the fish is located. As pointed out in [15], one may assume that the shape is spherical when calculating resonance frequencies for small volumes. There is a relationship between the dimensions of some fish and the volumes of their air bladder [8]. Many authors present empirical formulas in their publications to calculate the resonance frequency by the known volume of bladders of fish [35, 36 and so on].

Checking calculations carried out by the formula $f = (6.8/d)k$, where $k = [1 + (10/h)]^{5/6}$, d is the diameter of the bladder, cm, and h is the depth of the fish's location in meters [36], show that the averaged resonance frequency of the sounds emitted by salmon exceed the calculated value by a factor of two. Based on logical prerequisites, the highest q-factor and the maximum sensitivity of hearing should be observed at the resonance frequency of the bladder. These prerequisites have been confirmed in [40], but the presence of a relatively wide frequency response in the resonance range of the bladder in fishes has been pointed out in [45], which is obvious from the audiogram presented in Figure 5. The absence of spectral coincidence of the emitted frequencies and the range of hearing has also been noted by other authors [26].

The lateral line. The acoustic receptor in fish is also the waxy cells of the lateral line--the neuromasts located in the depressions along the line, connecting the mid-part of the gill arch with the notch of the fish's tail [28]. Moreover, there are additional receptor fields with waxy cells on the fish's head. It is assumed that the waxy cell responds to sound, but only to one of its manifestations--the displacement wave.

All the waxy cells of the lateral line have direct contact to the medium and record the slightest motions and microcurrents of the water. The waxy cell is incapable of registering sound pressure due to its morphological and physiological characteristics.

APPROVED FOR RELEASE: 2007/02/08: CIA-RDP82-00850R000300060001-1

APPROVED FOR RELEASE: 2007/02/08: CIA-RDP82-00850R000300060001-1

As indicated previously, the waxy cell performs the functions of sound receptor in the inner ear, being a secondary receptor. There it is connected by a system of auxiliary devices and accessories, by means of which it registers sound pressure.

The waxy cells of the lateral line are oriented in the fish's body such that they permit it to monitor the variation of the displacement wave gradient in three planes independent of the function of the air bladder. The audiograms for the air bladder and lateral line usually do not coincide, but a considerable section of the spectrum (toward the low frequencies) is overlapped during joint work of them, which permits considerable expansion of the range of information used through the acoustic channel [44]. The sensitivity of the waxy cell to the displacement wave has been cited in the literature and its threshold value is equal to 25 A [33]. This value has been found indirectly since there are as yet no devices which permit one to measure the displacement of water particles in this range.

Other types of receptors. As pointed out in [20], the more sensitive mechanical receptors in the tissues of vertebrates are encapsulated formations--so-called Pacinian corpuscles. These types of receptor formations reach their greatest development in the higher vertebrates--birds and mammals. Located along the periphery in mammals, they apparently generate packets of nerve pulses following the frequency of the stimulating oscillations in reponse to the vibrational frequency of the medium and accordingly of the animal's body [4].

The response of the cell and the "discharge" of the potentials occur only at variable values of the applied force, rather than with constant pressure of it. The higher the pressure gradient, the more effective the Pacinian corpuscles generate nerve pulses. These receptors have high sensitivity to mechanical oscillations and may serve, as indicated by Hunt and Macintyre [according to 4], vibration detectors with threshold values of 10-100 μm in the frequency range of 2-300 Hz.

Along with location of the indicated receptors in the surface layers of the skin, they can be found in the most unexpected parts of the body, being located near the sanguiferous vessels and other organs. The sensitivity of these inner Pacinian corpuscles is much higher (up to one micron) compared to surface location. Moreover, their sensitivity to frequencies in the range of 200-400 Hz is enhanced.

If one assumes that they are also found in some fish, then being located in the immediate vicinity of the air bladder, they may play a significant role in perception of the pressure wave in those fish which have no connection of the air bladder to the inner ear (salmon and so on). Oscillations of the bladder excited by an acoustic signal acting Pacinian corpuscles will cause excitation of them.

There is as yet no data on the air bladder's capability to register pressure waves. The presence of some structures similar to strain gauges or other mechanisms or receptors similar in function is required for this.

It was noted in [13] that the specialized receptors of the lateral line--Lorenzini's ampulla--may also perceive sound oscillations like mechanical receptors. However, they are present only in a limited number of fishes--"strongly electric" fish and some sharks. The possible receptors of fish responsible for reception of pressure waves and displacement waves and their functional relationships are presented in Figure 6.

APPROVED FOR RELEASE: 2007/02/08: CIA-RDP82-00850R000300060001-1

APPROVED FOR RELEASE: 2007/02/08: CIA-RDP82-00850R000300060001-1

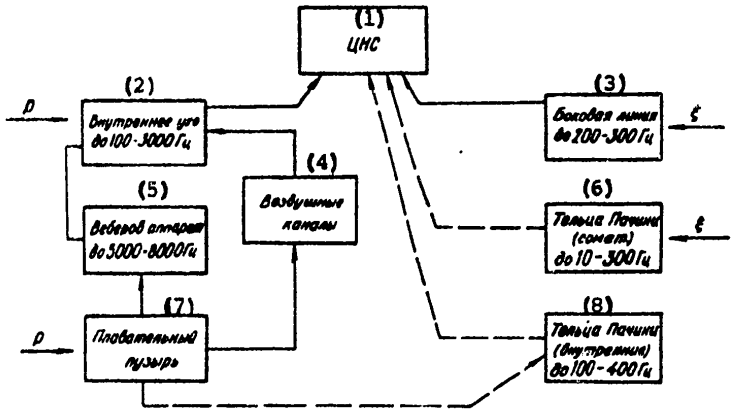

Figure 6. Possible Receptor Systems of Fish Participating in Registry of Acoustic Oscillations

Key:

1. Central nervous system
2. Inner ear up to 100-3,000 Hz
3. Lateral line up to 200-300 Hz
4. Air Channels
5. Weberian apparatus up to 5,000-8,000 Hz
6. Pacinian corpuscles (up to 10-300 Hz)
7. Air bladder
8. Pacinian corpuscles (inner) up to 100-400 Hz

Conformity of the range of hearing and sounds emitted by fish. A large number of diverse sounds from fish inhabiting different ecological conditions has now been recorded. These sounds should be divided into specialized and unspecialized. Using the former, exchange of interspecies information is possible and their main function includes helping specimens to find or avoid each other. The sounds of the second group correspond to physiological processes occurring in the fish organism. Although they are not related to specialized sounds, they may carry information about the presence of food (the crunch of feed being ground, sounds of closing of the jaws, clucking sounds which accompany swallowing of food by large fish and so on), construction of the nest (by the noise of pebbles being rolled) and so on.

Some investigators note that although fish are capable of producing sounds, their acoustic signals do not play such an important role as in other vertebrates and point out in this case the disproportion in development of organs of sound formation and hearing (the latter are more highly differentiated) [43].

To compare the size of the information channel by the width of the spectrum, we considered sounds of 38 species of commercial fish and those with limited commercial importance (Figure 7). The following conclusions can be made from the given graphs: all the specialized sounds of fish are located within the frequency zone to which

APPROVED FOR RELEASE: 2007/02/08: CIA-RDP82-00850R000300060001-1

APPROVED FOR RELEASE: 2007/02/08: CIA-RDP82-00850R000300060001-1

the organs of sound reception are most sensitive, i.e., the signal is within the evolution of advantageous interaction between participants, each of which attempts to increase the efficiency of exchange of the amount of information [37]; unspecialized sounds (accompanying sounds) may occupy the frequency spectrum beyond the hearing range; the range of acoustic signals in fish with air bladder is shifted to the low-frequency region; the additional harmonics and formants in the sound spectrum may occupy a range up to 16-20 kHz but probably do not participate in the process of hearing; we assume (by analogy of human hearing) that different pitch of fish sounds is transmitted in this manner.

Practically all the sounds emitted by fish are in the range of hearing of fish (50-2,500 Hz) and occupy the higher frequency range (up to 5,000 Hz) only in some fish (tuna and sardines). With regard to the lower frequency region of the spectrum, some authors [14] and we recorded sounds in the range of 5-20 Hz in salmon [7], but no careful investigations were conducted on determination of infrasounds in fish.

All sounds emitted by fish can be divided by their nature into groups as a function of their phonetic sounding.

1. Cracks and noise--wideband sound signals of acoustic origin--are sounds accompanying the activity of fish [9]. They can be observed in fish constructing spawning nests in solid soil (salmon) and making jumps on the water surface (salmon and tuna).

2. Sounds similar to grunting and croaking comprise a large group. They usually occur when air is expelled from the air bladder in open-bladder fish (salmon and herring) or when air is pumped into sections of the bladder (in fish with two-chamber bladder). These are harmonic oscillations of the most diverse length (from 1-2 seconds for "grunts" to 10-30 ms for "croaks"). In this case they may consist of a pulse sequence in which there may be the most diverse harmonic components of the spectrum.

3. Whistles. They are usually of a high-frequency nature and the presence of frequency deviation is inherent to them, which leads to different variations of their sounding. The presence of frequency modulation imparts a multifaceted pitch to this type of sounds. They can be similar to chirping, whistling and meowing. The source of their excitation is the passages of the stomach, air bladder and so on which create vibrations when air is pumped through them. By their nature these are acoustic oscillations of oscillating spheres. The mechanism of their sound formation is related closely to the function of the air bladder and stomach [10].

4. Squeaks consist of a series of short pulses (1-10 ms). The total length of a squeaking sound may vary over a wide range from 0.1 to 1.0 second and their characteristic feature is a nonuniform period of repetition of individual pulses during a single such sound. The organ of sound formation of squeaks in salmon is the lips.

5. Clicks are short pulsed sounds lasting up to 30-40 ms and are observed both in the form of single pulses and in the form of infrequent series. The air bladder undoubtedly plays an important role in their sound formation. However, taking the absence of a harmonic component in this spectrum and the wideband nature of them into account, it should be agreed that the air bladder is obviously not their only source.

APPROVED FOR RELEASE: 2007/02/08: CIA-RDP82-00850R000300060001-1

APPROVED FOR RELEASE: 2007/02/08: CIA-RDP82-00850R000300060001-1

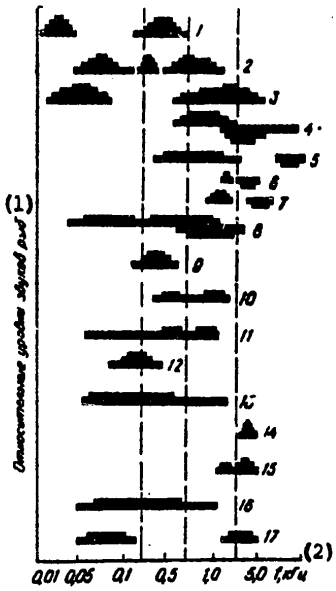

Figure 7. Comparative Analysis of Amplitude-Spectral Characteristics of Sounds Emitted by Some Pelagic and Bottom Fish (gradations by level every 6 dB): 1--sockeye red salmon; 2--humpback salmon; 3--coho salmon; 4--rudd; 5--herring; 6--half-beaks; 7--mackerel; 8--smelt; 9--silvery hake; 10--horse mackerel; 11--yellow karanks; 12--jackfish; 13--haddock; 14--yellowfin tuna; 15--sardine; 16--anchovy; 17--triggerfish

Key:
1. Relative levels of fish sounds
2. kHz

6. Infrasonic oscillations may occur when the abdominal muscles of fish act on the air bladder. Their range may extend from units of a hertz to the beginning of the sound range.

7. Sounds similar to sawing and which are a series of pulses repeated at a specific period occur with participation of the air bladder.

8. Drumming sounds (high- and low-frequency) are usually related to specialized sounds. A constant pulse repetition rate, insignificant fluctuations of the length of individual pulses for each species of fish, stable pulse recurrence frequency and firm relationship to the diurnal and seasonal activity of fish are typical for them.

There is a difference in spectral composition and pulse length between low- and high-frequency sounds of salmon (Figure 8). Their repetition rate coincides. High-frequency sounds are short wideband pulses and the low-frequency sounds

APPROVED FOR RELEASE: 2007/02/08: CIA-RDP82-00850R000300060001-1

APPROVED FOR RELEASE: 2007/02/08: CIA-RDP82-00850R000300060001-1

Figure 8. Sonogram of High- (a) and Low-Frequency (b) Sounds of Salmon

consist of two components. The first part of this signal does not differ in any way from a high-frequency knock and has the same spectral composition and the second part contains the low-frequency component of 20-180 Hz and is a vibration whose level attenuates exponentially. It is assumed that the process of exciting low-frequency sounds is closely related to the work of the muscular structures which induce high-frequency oscillations in the bladder. Connection of the air bladder as a resonator of low-frequency oscillations obviously does not always occur.

The enumerated sounds of fish can be represented in this sturcture in the form of 1) a series of low-frequency pulses with filling of the quasi-sine wave frequency below 600 Hz; the length of a single pulse may reach 100 ms and this type of sound is observed in paired fish and some shoal species; 2) a series of high-frequency pulses 1-15 ms in length and with filling frequency of 1,000-2,500 Hz (paired fishes); 3) transient pulse signals with wide filling spectrum (up to 6-12 kHz), energy distribution in the spectrum is nonuniform and the length of individual pulses fluctuates in the range of 10-40 ms (salmon and other bottom fishes); and 4) noisy signals consisting of a large number of spontaneously emitted sounds lasting up to 40 ms; the levels of these signals reach a maximum value in the high-frequency region of the spectrum, but does not exceed 10 dB above background noise in smooth seas (herring, some tuna and mackerel).

The sound pressure levels and pulse length for sounds of different types in some species of fish are reduced to a table.

The process of discrimination and recognition of signals. Let us consider the process of recognition of acoustic signals by fish. We are talking about recognition of acoustic information on the noisy background of the sea. The term "information" is understood as a combination of sounds acting on the object (fish), among which may also be sounds transmitted (emitted) by specimens of a given species and having signal significance.

In the general case the process of perception of these sounds among higher vertebrates and identification of them may appear as follows. Sound enters the processing system through the animal's receptor fields, where individual frequency components of the signal and its formants (overtones) are separated. "Discharges" of the nerve pulses are formed in the receptors, which then enter the TsNS [Central nervous system] At the same time information about the intensity of sound (in its individual sections of the spectrum) and the length of sounding enters the TsNS with it.

APPROVED FOR RELEASE: 2007/02/08: CIA-RDP82-00850R000300060001-1

APPROVED FOR RELEASE: 2007/02/08: CIA-RDP82-00850R000300060001-1

Physical Characteristics of Sounds of Some Pacific Ocean Fish

(1) № п/п	(2) Вид	(3) Фонетическая характеристика	(4) Длительность звука, мс	(5) Основная частота, Гц	(6) Абсолютное звуковое давление относительно $2 \cdot 10^{-5}$ Па	(7) Верхняя регистрируемая частота в спектре, Гц
1	(8) Красная, чавыча, кижуч, горбуша	(9) Высокочастотный стук	1—5	(10) до 2000	94	2500
2	» всех лососей (11)	Низкочастотный стук (12)	40—80	40—500	до 100	3000
3	То же (13)	«Кри-кроу» (14)	20—300	300—1000	75	4000
4	»	Урчание (15)	до 1000	300—3000	76	5000
5	»	Щелчки (16)	1—40	1000—2000	50—65	до 12000
6	»	Скрип (17)	300—600	до 1500	50	3000
7	»	Свист (18)	до 500	до 6000	50	—
8	»	Инфразвуковые (19) колебания	100—2000	1—60	?	—
9	(20) Голец, кижуч, стальноголов. лосось	Пиление (21)	40—60	до 500	35	500
10	У всех лососей (11)	Всплески (22)	—	до 12000—15000	до 105	—
11	(23) Калуга (24)	Свист (18)	20—150	2000—6000	40	до 20000
12	Косатка-скрипун	Зуммер (25)	500	1000—1500	50	3000
13	Красноперка (26)	Стуки (27)	10—20	600—2000	58	3000
		То же (27)	10—20	1000—5000	54	8000
14	Сельдь (28)	Щелчки (29)	10—20	200—1400	63	3000
		То же	5—20	—	60	8000
15	Корюшка (30)	Щелчки (29)	30—40	20—800	40	5500
		Стуки	60	1500—2000	40	—
16	Полурыл (31)	Щелчки Н4	20—30	1200—1300	54	—
		То же В4	10—20	—	54	2500—3000
17	Скумбрия (32)	Щелчки В4	20—40	—	—	5000
		Скрип (17)	500	800—1500	55	1700
18	Пикша (33)	Ворчание (34)	—	—	—	—
19	Японский ерш (35)	Серии ударов (36)	—	—	114	—
20	Сахалинский подкаменщик (37)	Урчание (15)	—	—	88	—
21	Японский петух (38)	Бубнящие звуки (39)	200	—	—	—
		Удары (40)	40	250—300	—	—
22	Сардина (41)	Чирикание (42)	—	50—1200	40	—

Key:

1. Number of items
2. Species
3. Phonetic characteristic
4. Length of sound, ms
5. Main frequency, Hz
6. Absolute sound pressure relative to $2 \cdot 10^{-5}$ Pa
7. Upper recorded frequency in spectrum, Hz
8. Sockeye red salmon, king-salmon, coho salmon and humpback salmon
9. High-frequency knock
10. Up to 11
11. All salmon
12. Low-frequency knock
13. All salmon
14. "Cree-Croy"
15. Grunting
16. Clicks
17. Squeaks
18. Whistle
19. Infrasonic oscillations

[Key continued on following page]

APPROVED FOR RELEASE: 2007/02/08: CIA-RDP82-00850R000300060001-1

APPROVED FOR RELEASE: 2007/02/08: CIA-RDP82-00850R000300060001-1

[Key continued from preceding page]

20. Common loach, coho salmon, steelhead salmon and common salmon
21. Sawing
22. Splashes
23. Amur sturgeon
24. Pseudobagrus
25. Buzzer
26. Rudd
27. Knocks
28. Herring
29. Clicks
30. Smelt
31. Half-beak
32. Mackerel
33. Haddock
34. Croaking
35. Japanese perch
36. Series of knocks
37. Sakhalin gurnards
38. Japanese redfin
39. Drumming sounds
40. Knocks
41. Sardines
42. Chirping

The brain gathers the incoming information (arriving through the afferent channels), processes it, issues instructions in response to the incoming signals, sending them to the muscles through the efferent channel system, and also stores the characteristic features of the incoming signal in the memory cells. If this is a signal not bearing specific bioacoustic information (a combat challenge, danger signal, threats and so on), it enters the logic "YES"-"NO" cell (neuron) for issue of instructions for action after probability and correlation analysis [34], comparison by stereotypes stored in the memory block. If this signal does not correspond to the stereotype--the object performs an operation to determine the significance of the signal and in the case of its indifference--a "NO" instruction enters the logic block, to which the organism responds in the appropriate manner [12].

The given simplified process of acoustic signal perception and recognition of them is typical for man with his highly developed brain. Separation of acoustic signals in fish differs to a significant degree from that presented above since fish have no associative thinking. However, actions which indicate the presence of a well-developed system (mechanism) which permit them to detect food objects and similar specimens are inherent to fish. Sound signalling plays a less important role in this case. The same can be said about sounds related to a threat to shoals of fish and to their individual specimens (the sounds of predators or the noise of a fishing vessel when a purse seine or trawl is being paid out).

The process of identification in fish can be represented in the following manner. The information coming through the fish's acoustic channel is registered by one of the types of sound detectors (the inner ear, air bladder or lateral line) and possibly by all of them simultaneously (Figure 9). In this case the complex of sound perception and processing of signals functions as a unified system. It is triggered provided that the level of the stimulating acoustic signal at the point of the fish's location exceeds the threshold of sould perception in the optimum frequency range. This threshold signal will not be identical in the working range since the receptors have different sensitivity in the frequency band. The frequency characteristic has a dip in the low frequency range according to the presented audiograms. This is feasible for several reasons.

First, the spectral noise distribution of the sea itself (Knudsen's spectra) has a significant drop of levels from maximum (60 dB at 10-20 Hz) to minimum (10 dB at

APPROVED FOR RELEASE: 2007/02/08: CIA-RDP82-00850R000300060001-1

APPROVED FOR RELEASE: 2007/02/08: CIA-RDP82-00850R000300060001-1

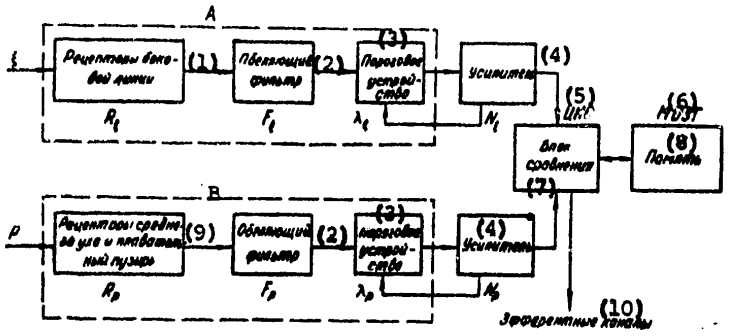

Figure 9. Diagram of Processing Acoustic Information by Fish

Key:

1. Receptors of lateral line
2. White-noise filter
3. Threshold device
4. Amplifier
5. Central nervous system
6. Brain
7. Comparison block
8. Memory
9. Receptors of middle ear and air bladder
10. Efferent channels

6-10 kHz) [46]. In order that the sound-perceiving system of the fish operate continuously in this band, one must assume that the receptors have dynamic range of 50-60 dB (i.e., they are capable of perceiving levels with amplitudes differing approximately by a factor of 1,000).

Second, the signals are recorded by the sound receptors using the threshold devices which respond only to stimuli with a specific suprathreshold level, rather than to absolute values of it [1].

Although the low-frequency range of sea noises where the high levels are observed lag behind the section on which most bioacoustic signals of many fish are located by a significant distance, it is hardly probable that the high levels of low-frequency noise and the signal which slightly exceeds the noise levels in the middle of the frequency band enter the same receptors. Noise masking of the signal would inevitably occur in this case.

Thus, the presence of a system for equalizing the frequency characteristic is assumed in fish, which should provide an optimum conversion factor in the low-frequency region of the spectrum which permits attenuation of low frequencies with high background noise levels and which does not permit attenuation of high frequencies where noise is low, i.e., the conversion factor is $k = 1/N(\omega)$. This is a so-called white-noise filter widely used in technology [5]. These systems considerably simplify further processing of the signal, which is especially important if threshold devices are being used.

The presence of a white-noise filter in fish is indicated by complete agreement of the slope of the audiogram in the low-frequency region to the slope of the noise

APPROVED FOR RELEASE: 2007/02/08: CIA-RDP82-00850R000300060001-1

APPROVED FOR RELEASE: 2007/02/08: CIA-RDP82-00850R000300060001-1

levels of the sea in this plane. It is obvious from the audiogram [31] and sonogram of the sounds of Holocentrus ascensionus [30] that they have energy and spectral conformity. The resulting characteristic of the transceiving biological system will have the form of a horizontal straight line on the segment from low frequencies to the maximum hearing frequency of fish [9]. Its position in the vertical plane (the threshold value of level) will depend on the ecology of the species, but there are data that the levels of emission by marine organisms may vary as a function of variations of the background noise levels, i.e., the signal level always exceeds the background noise level [21].

Thus, any sound exceeding the noise on an arbitrary section of the frequency band (exceeding the response threshold of the acoustic receptors) is registered and perceived as a signal by the fish. The level exceeding noise is of significance to provide reliability, especially if this signal is associated with danger. In this case an increase of the level is a catalyst which accelerates information processing.

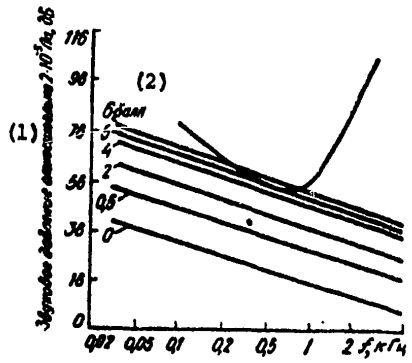

Figure 10. Audiogram [30] and Sonogram [3] Obtained from Nolocentrus ascensionus L.

Key:
1. Sound pressure relative to $2 \cdot 10^{-5}$ Pa dB
2. Units
3. kHz

Information from a sound source in the form of pressure waves p and displacement waves ξ enters the receptors of the acoustic-lateral system of fish. Each of the components is separated independently due to the physical properties of each of the stimuli and the physiological properties of the receptor fields: the lateral line (R_ξ) separates information about the presence of displacement waves and the inner ears in combination with the air bladder distinguishes sound pressure (R_p).

Processing of the signals in the primary receptor field includes 1) perception of the optimum frequencies by the receptor matrices ξ and p; 2) separation of the signal in the optimum frequency band--spectral filtration which permits interpretation of the extent to which the signal can be related to a given species of animal (block A or B); 3) comparison to a previously given threshold of a minimum signal $\lambda_{0\xi}$ or

APPROVED FOR RELEASE: 2007/02/08: CIA-RDP82-00850R000300060001-1

APPROVED FOR RELEASE: 2007/02/08: CIA-RDP82-00850R000300060001-1

λ_{0p} and if the signal exceeds this threshold, triggering of the system for recoding sensory information; and 4) correction of the transfer coefficient of the receptor systems according to the background noise levels, which provides the possibility of separating the signals over a wide frequency band in case they exceed background noise.

Actually, there is no separation of operations; this is a unified process performed by the organism within an exceptionally short time. The primary receptor fields are dynamically flexible. The threshold values of $\lambda_{0\xi}$ and λ_{0p} may vary not only in ontogenesis but also during the course of a shorter time. M. P. Fish notes that marine invertebrates increase the level of emitted signals by 15-20 dB with an increase of the background noise level of the sea by 20 dB during the onset of stormy weather, i.e., the information transmission and receiving system is labile [21].

In response to an adequate stimulus, the receptor fields generate nerve impulse patterns--the response of the receptor cells to a stimulus. The pulses through the system of the nerve channels N_ξ and N_p in which amplification of them is provided enter the central nervous system, where they are compared to an image stored in the memory of the brain (volatile memory acquired during life or nonvolatile (genocode)) and if the response to the stimulus coincides with the image of the memory, instructions are issued through the efferent channels for the organism to carry out the appropriate response.

During passage of the pattern through the nerve pathways, it may be recoded (in the interneurons) and thus a signal completely different from the first signal generated by the waxy cell enters the TsNS. According to this, it remains unclear where identification of acoustic information and comparison of it to a stereotype occurs in fish, since the pulse pattern at first glance does not carry information about the sound spectrum; according to available data, the response of the waxy cell occurs over a wide frequency range, beginning with seismic waves (1-20 Hz) to the maximum hearing frequencies (2-3 kHz) and in this case the signal is separated only by the threshold feature [1]; there are not data on the sensitivity of the individual receptors of the lateral line to specific frequencies or spectral regions, although it would be logical to assume the existence of this type of signal separation mechanism.

The report that receptor cells reponding to perception of signals of specific levels or frequencies of the spectrum have been found in higher vertebrates is hopeful in this regard [12].

The range of audibility of biological signals under natural conditions. The marine medium in which the channel is formed affects the range of information transmission through the sound channel. It is customary to characterize the medium by attenuation coefficient β, which is a value which reflects the effect of the elements of the hydrosphere on the wave process, which finally leads to variation of the initial shape of the spectral composition and level of transmitted signals.

Attenuation in the sea has been investigated and we made use of the known expression for the sound attenuation coefficient for a plane wave, valid at frequencies from 16 Hz to 60 kHz. The following value of $\beta = 0.0091\ f^2$ can be used with sufficient degree of accuracy in the indicated frequency range [22].

APPROVED FOR RELEASE: 2007/02/08: CIA-RDP82-00850R000300060001-1

APPROVED FOR RELEASE: 2007/02/08: CIA-RDP82-00850R000300060001-1

A convenient and precise method of calculating the range of an acoustic signal is the graphical method [3] in which attenuation of the acoustic wave due to divergence of the acoustic beam may also be taken into account under specific conditions.

We previously determined the law of attenuation for low frequencies in the near and intermediate zones (the spherical propagation zone); therefore, the use of a formula which takes into account only absorption in the medium (Figure 11) will be valid beyond its limits. In this case the excess signal over noise in the intermediate zone must be determined by Knudsen's graphs to solve the problem of the range of sound audiability under water. The maximum distance at one or several frequencies must then be determined from Figure 11 with regard to the fact that the signal level at the point of sound reception by the fish should exceed the noise level by not less than 20 dB (S/N = 20 dB).

Let us consider an example. A signal with sound pressure of level of 0.036 Pa, measured in an aquarium at distance of 1 meter, is emitted by fish. The maximum energy is contained in the frequency range of 1,100-1,400 Hz. The real signal is recorded in the sea by an omnidirectional acoustic energy transducer (the air bladder) and the excess signal above noise at the reception point should be S/N = 20 dB in slight seas.

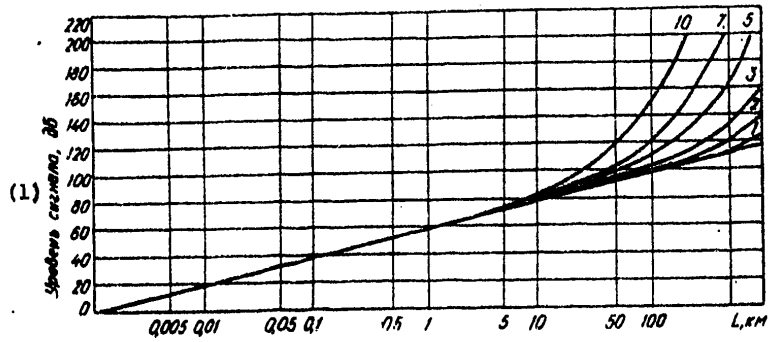

Figure 11. Curves of Sound Attenuation in Far Zone [18]

Key:
1. Signal level, dB

Solution: the spectral noise level at this frequency is $N(\omega)$ = 26 dB (Figure 12). The spectral signal level at this frequency is determined from the same figure. Its absolute value is $S(\omega)$ = 28 dB. The maximum losses on this frequency are

$$H(\omega) = S(\omega) - N(\omega) = 28 - 26 = 2,$$

and sound attenuation (at $\beta = 0.0091\ f^2$ dB/km) is equal to 0.0142 dB/km.

We find the maximum distance at which the signal reaches its own minimum value and is completely lost in noise:

$$r = \frac{H(\omega)}{\beta} = \frac{28-26}{0,0142} \approx 140.$$

APPROVED FOR RELEASE: 2007/02/08: CIA-RDP82-00850R000300060001-1

APPROVED FOR RELEASE: 2007/02/08: CIA-RDP82-00850R000300060001-1

The signal can be perceived by the fish in the range of this distance, but we did not observe the condition S/N = 20 dB in order that the fish respond to this signal. Let us introduce the correction

$$H(\omega) = 28 - 26 - 20 = -18.$$

Thus, we can receive a response to our signal from the fish only in the immediate vicinity of the sound source since its level is considerably below the noise level. It should be assumed that all the motions of the fish in the medium under these conditions will be the result of the effect of any other parameters of the medium or other stimuli which have nothing in common with the sound.

The range of stable reception by other specimens may reach distances of 150-200 meters (with regard to S/N = 20 dB) for high-frequency sounds of salmon with sound pressure level of 1.0 Pa.

The losses do not exceed 8 dB/km in all cases for a plane wave (in the far zone) with regard to reflection from the bottom and surface, attenuation introduced by marine organisms and so on [6]. One of the factors of the medium which may negate the entire acoustic information channel is refraction.

The vitality of fish is related to the presence of plankton, which is the main food base at specific stages of fish development. Consequently, the use of an acoustic communications channel in the presence of sound-scattering and sound-absorbing layers may be sharply limited. Sound absorption by bubbles occurs due to heat dissipation as a result of the resonance oscillations of the bubble [18]. The lowest resonance frequency of bubbles is 1,650 Hz but it may be reduced to 50 Hz during a storm.

The phenomenon of refraction is related to variation of the speed of sound propagation in water. The reason may be various factors, including water temperature, salinity and static pressure. Air bubbles play a no less important role in this case. The compressibility of the water may vary twentyfold and accordingly the speed of sound may be reduced by a factor of 4.5 at depths up to 10 meters, where bubbles with diameter of 1 mm are found.

Temperature, salinity and depth (pressure) also predetermine the direction of motion of the acoustic wave, which is bent toward the region with lower speed of sound propagation.

Heating the surface waters, related to seasonal changes of temperature conditions in the regions of the ocean, causes bending of the acoustic beams. Thus, the beams are bent downward during summer due to an increase of temperature of the surface layer and their path is turned toward the surface in winter.

The beams are bent to the side of pressure water in coastal regions with complex distribution of saline and fresh water.

The thermal barrier in which temperature and density vary sharply has a significant effect on the path of beams. It may be impenetrable to acoustic beams at high gradients of these parameters in shallow water.

APPROVED FOR RELEASE: 2007/02/08: CIA-RDP82-00850R000300060001-1

APPROVED FOR RELEASE: 2007/02/08: CIA-RDP82-00850R000300060001-1

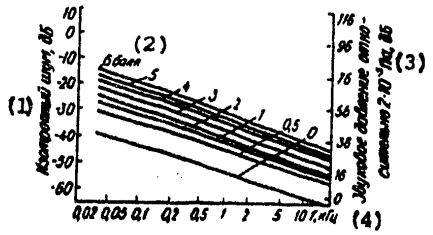

Figure 12. Spectral Characteristics of Ocean Noise as a Function of Its Surface State [47]

Key:
1. Isotropic noise, dB
2. Units
3. Sound pressure relative to $2 \cdot 10^{-5}$ Pa, dB
4. kHz

Conclusions. The purpose of this paper was to give preliminary consideration to some problems of sound perception by fish from the viewpoint of physiology and hydroacoustics, to compare the hearing range to the spectrum of signals emitted by fish and to present a model of perception and separation of these sounds on the noisy background of the medium. One can make the following conclusions from analysis of the materials from the literature and the results of experimental investigation:

science has now accumulated a sufficient amount of information on the auditory capabilities of fish in order to determine the boundaries of auditory perception which can be used to solve problems of controlling fish behavior using acoustic fields;

the main sounds (primarily specialized) emitted by fish are located within frequencies of the acoustic band; signals accompanying the activity of fish may occupy a frequency spectrum of considerably greater width;

the presence of encapsulated receptors (Pacinian corpuscles), with which the mechanism of sound perception by bladderfish in which no connection of the air bladder to the inner ear has been established can be explained, may be assumed in the proposed scheme of the functional relationships of the sound-perceiving apparatus of fish;

sound reception in fish in all probability occurs by the threshold feature (which is confirmed by the path of audiograms in the low-frequency range) since this system of sound perception permits separation of the signal on a noisy background of the medium;

the sound pressure in the near zone and the value of particle displacement of the medium have fluctuations in level (see the graphs for determination of the absolute values);

APPROVED FOR RELEASE: 2007/02/08: CIA-RDP82-00850R000300060001-1

APPROVED FOR RELEASE: 2007/02/08: CIA-RDP82-00850R000300060001-1

acoustic signals, even those which slightly exceed the natural noise level of the medium, can be heard by a fish at a considerable distance.

BIBLIOGRAPHY

1. Astashenko, A. A., "Simulation of Signal Detection in Modern Psychophysical Theories," in "Sensornyye i sensomotornyye protsessy" [Sensory and Sensory Motor Processes], Moscow, Pedagogika, 1972.

2. Volovova, L. A., "Sixty-Third Meeting of IKES on Problems of Fish Management Investigation of Acoustic and Electric Fields," RYB. KHOZ-VO: EKSPRESS-INFORMATSIYA, Nos 5/6, 1976.

3. Giyyes, L. and P. Sabate, "Osnovy akustiki morya" [Fundamentals of Marine Acoustics], Leningrad, Gidrometeoizdat, 1976.

4. Dolyatovskiy, V. A., "Information Processes in the Auditory Analyzer," in "Sovremennyye problemy neyrokibernetiki" [Modern Problems of Neurocybernetics], Leningrad, Nauka, 1972.

5. Dymova, A. I. and L. Ye. Varakin, "Obnaruzheniye signalov" [Signal Detection], Moscow, M-vo svyazi SSSR, 1968.

6. Levastu, T. and I. Khella, "Promyslovaya okeanografiya" [Commercial Oceanography], Leningrad, Gidrometeoizdat, 1974.

7. Neproshin, A. Yu., "Some Physical Characteristics of the Sounds of Pacific Ocean Salmon," ZOOL. ZHURN., Vol 1, No 7, 1972.

8. Neproshin, A. Yu., "Identification of the Species and Size Composition of Salmon by Their Sounds," VOPR. IKHTIOLOGII, Vol 13, No 6, 1973.

9. Neproshin, A. Yu., "The Acoustic Behavior of Salmon," VOPR. IKHTIOLOGII, Vol 14, No 1, 1974.

10. Neproshin, A. Yu. and N. I. Kulikova, "The Sound-Formation Organs of Salmon," VOPR. IKHTIOLOGII, Vol 15, No 3, 1974.

11. Parvulesku, A., "Signal Propagation and Signal Processing," in "Morskaya bioakustika" [Marine Bioacoustics], Leningrad, Sudostroyeniye, 1969.

12. Pribram, K., "Yaziki mozga" [The Languages of the Brain], Moscow, Progress, 1975.

13. Protasov, V. R., "Bioakustika ryb" [The Bioacoustics of Fish], Moscow, Nauka, 1965.

14. Protasov, V. R., L. G. Rudakovskiy, V. M. Krumin', V. I. Tsvetkov and V. R. Vasil'yev, "Low-Frequency Oscillations in the Living and Orientation of Fish," PROBL. AVTOMAT. UPR., No 1, 1969.

APPROVED FOR RELEASE: 2007/02/08: CIA-RDP82-00850R000300060001-1

APPROVED FOR RELEASE: 2007/02/08: CIA-RDP82-00850R000300060001-1

15. Romanenko, Ye. V., "Fizicheskiye osnovy bioakustiki" [Physical Fundamentals of Bioacoustics], Moscow, Nauka, 1974.

16. Svetovidov, A. N., "The Characteristics of the Structure of the Air Bladder of Herring," DOKL. AN SSSR, Vol 24, No 3, 1955.

17. S J., "Kodirovaniye sensornoy informatsii" [Encoding of Sensory Information], Moscow, Mir, 1975.

18. Stashkevich, A. P., "Akustika morya" [Marine Acoustics], Leningrad, Sudostroyeniye, 1966.

19. Truskanov, M. D., "Using Acoustic Fields in Fishing For the Far Eastern Mackeral," RYB. KHOZ-VO, No 1, 1973.

20. "Fiziologiya sensornykh sistem" [The Physiology of Sensory Systems], Leningrad, Nauka, 1975.

21. Fish, M. P., "Biological Sources of Continuous Ambient Sea Noise," in "Morskaya bioakustika" [Marine Bioacoustics], Leningrad, Sudostroyeniye, 1969.

22. Horton, J. W., "Osnovy gidrolokatsii" [The Fundamentals of Sonar], Leningrad, Sudostroyeniye, 1961.

23. Alexander, R. N., "The Structure of the Weberian Apparatus in the Ciprini," PROC. ZOOL. SOC., Vol 139, 1962.

24. Bekesy, G., Experiments in Hearing, New York, McGraw-Hill, 1960.

25. Charmen, C. D. and A. D. Hawkins, "A Field Study of Hearing in the Cod Gadus morhua L.," J. COMP. PHYSIOL., No 85, 1973.

26. Cohen, M. J. and H. E. Winn, "Electrophysiological Observation in the Fish Porichtys notatus," J. EXP. ZOOL., Vol 165, No 3, 1973.

27. Dijkgraaf, S., "Untersuchungen ueber die Funktionen des Ohrlabirints bei Meersfischen," PHYSIOL. COMP. OECOLOG., Vol 2, No 81, 1950.

28. Dijkgraaf, S., "The Function and Significance of the Lateralline Organs," biol. rev., No 38, 1963.

29. Enger, P. S., "Sound Reception in Telost Fishes in Relation to the Sound Source Distance, FAO FISH. REPORTS, No 62, 1969.

30. Fish, M. P. and W. H. Mobray, Sounds of Western North Atlantic Fishes, Baltimore, The Johns Hopkins University Press, 1970.

31. Firucava, T. and Ishii, "Neurophysiological Studies on Hearing in Goldfish," J. NEUROPHYSIOL., No 30, 1967.

32. Hama, K., "Study on the Fine Structure of the Sacular Macula of the Goldfish," Z. ZELLFORISH., No 94, 1969.

APPROVED FOR RELEASE: 2007/02/08: CIA-RDP82-00850R000300060001-1

APPROVED FOR RELEASE: 2007/02/08: CIA-RDP82-00850R000300060001-1

33. Harris, G. and W. A. Bergeijk, "Evidence That the Lateral Line Organ Responds to Near-field Displacements of Sound Sources in Water, JASA, Vol 34, No 12, 1962.

34. Held, R., "Action Contingent Development of Vision in Neonatal Animals," in Experience and Capacity, New York, Acad. Sci., 1968.

35. Haslett, B. and H. E. Winn, Sound Production Mechanism of the Nassau Grouper Ephinophalus striatus, Copeia, 1962.

36. Kellogg, W. N., "Sounds of Sea Snimals," Album FPX 125 (Sci. Ser.), Folkways Records and Service Corp., 1955.

37. Marler, P., "Animal Communication Signals," SCIENCE, Vol 157, No 3790, 1967.

38. Moulton, J. M., "Acoustic Behavior of Fishes," in Acoustic Behavior of Animals, Amsterdam, Elsevier, 1963.

39. Offutt, G. G., "Structures for the Detection of Acoustic Stimuli in the Atlantic Coldfish Gadus morhua," JASA, Vol 56, No 2, 1974.

40. Poggendorf, D., "Die absoluten Horhswellen des Zwergwelles (Amiurus nebulosus) und Beitrage zur Physik des Weberschen Apparates der Ostariophisen," Z. VERGL. FYSIOL., No 34, 1955.

41. Popper, A. N., "Pure-tons Auditory Thresholds for the Carp, Cirpins carpio," J. ACOUST. AMER., Vol 52, No 6, 1972.

42. Popper, A. N. and R. R. Fay, "Sound Detection and Processing by Teleost Fishes: A Critical Review," JASA, Vol 53, No 56, 1973.

43. Schneider, N., "Morphology and Physiology of Sound-Producing Mechanisms in Teleost Fishes," MAR. BIOACOUST., Vol 2, 1966.

44. Tavolga, W. N. and J. Wodinski, "Auditory Capacities in Fishes: Pure Tone Threshold in Nine Species of Marine Teleost," BULL. AMER. MUS. NATUR. HIST., No 126, 1963.

45. Tavolga, W. N., "Psychophysical and Hearing in Fish," NATUR. HIST., Vol 73, No 3, 1964.

46. Buercle, Udo, "An Audiogram of the Atlantic Cod Gadus morhua L., "J. FISH. RES. BOARD, Canada, Vol 24, No 11, 1967.

47. Wenz, G. M., Acoustic Ambient Noise in the Ocean-Spectra and Sources," JASA, Vol 34, No 2, 1962.

48. Wever, E. G., "Cochlear Stimulation and Lempert's Mobilization Theory," ARCH. OTOLARINGOL., Vol 90, No 63, 1969.

APPROVED FOR RELEASE: 2007/02/08: CIA-RDP82-00850R000300060001-1

APPROVED FOR RELEASE: 2007/02/08: CIA-RDP82-00850R000300060001-1

UDC 681.332.63

POSSIBILITY OF CREATING ANALOG PROBABILITY OF A MODEL OF THE SEA

Kiev BIONIKA in Russian No 13, 1979 signed to press 14 Jun 79 pp 91-95

[Article by I. V. Popov, AzNIIRKh, Rostov-na-Donu, from the collection "Bionika," Izdatel'stvo Naukova Dumka, 1,000 copies, 100 pages].

[Text] Practical problems of efficient use of the natural resources of the inland reservoirs of the country, specifically of the Sea of Azov, require quantitative analysis and forecasting of a complex of related parameters of a biological and abiotic nature. It becomes necessary in this regard to model this system on a strict methodological basis. However, the complexity of the system is such that construction of a full mathematical model of it in final analytical form is very problematical.

Each point of space determined on the sea basin can be described in general form by the combination of n parameters which characterize the state of the aqueous medium and the hydrobionts. It is known that each of these parameters is a transient stochastic process $\eta_i(t) = f_i(t) + \zeta_i(t)$ with periodic trend $f_i(t)$. Moreover, it is known that all these parameters are functionally or statistically related to each other [4]. Thus, each point of the basin can be described by an n-dimensional random vector with dependent components $\{\eta_i(t)\}$.

In the general case this vector is also dependent on spatial coordinates $\{\eta_i(x_i, y_i, z_i, t)\}$. A large part of the parameters of the system under consideration is also continuous time and space functions. This means that one can talk about a continuous field of some parameter and about the combination of continuous fields related to each other which describe the state of the sea. Like any continuous field, they can be quantified by time and space on the basis of known theorems of calculation. In other words, one can talk about the discrete representation of continuous fields of the parameters of the sea. To characterize the state of the sea in the statistical sense, one must know the combination of statistical characteristics $\{W_i\}$ of the named random vectors, including the relationships between them and their components. Thus, the problem of analyzing the state of the sea reduces to one of analyzing the statistical characteristics of random vectors and their relationships, while the problem of forecasting includes determination of those characteristics at a given time interval in the future. Moreover, one can talk about the problem of predicting the instantaneous values of the parameters under investigation on the basis of using known methods of predicting stochastic processes which rely on the prehistory of the known model [2].

APPROVED FOR RELEASE: 2007/02/08: CIA-RDP82-00850R000300060001-1

APPROVED FOR RELEASE: 2007/02/08: CIA-RDP82-00850R000300060001-1

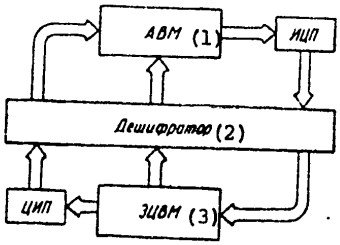

Figure 1. Block Diagram of Hybrid Computer System Which Includes an Analog Probability Model of the Sea: ITsP--pulse-digital converter; TsIP--digital-pulse converter

Key:
1. Analog computer
2. Decoder
3. Digital computer

On the whole the problem of modelling the sea in this postulation reduces to modelling a system of bound random fields adequate to a real object in the statistical sense, with subsequent investigation of their statistical dynamics to predict the possible changes of its state and optimization of its conditions according to a given criterion.

Synthesis of this model on a digital computer is considerably complicated by the need for simultaneous generation of n random sequences of numbers with given statistical characteristics (including the trend) and the need for complete statistical analysis of these flows and control of them with output for optimization of the model. The technical capabilities of the digital computer do not permit complete solution of these problems. Therefore, the best solution, we feel, is separation of the simulation functions, analysis and control between the digital and analog part in a hybrid computer system (GVS) (Figure 1) since the model of the sea itself was realized on an analog physical basis and all the remaining functions were realized on a universal digital computer.

The form of displaying the information in the analog probability model (AVM) is pulse type to provide noise stability of the system and the possibility of separating the digital and analog parts over a considerable distance. Moreover, this form permits considerable simplification of the communications channels between the digital computer and the AVM and consequently permit one to provide the required reliability of the system as a whole. The main informative parameter of the pulse flows is the length of the intervals between pulses. The decoder is designed to select the address of the base components of the AVM and the communications components for subsequent connection of them to the digital computer.

The structure of the AVM (Figure 2) is a homogeneous network in whose assemblies the base components connected to each other by the communications components are located. The base component consists of a primary source of fluctuating oscillations, a nonlinear converter and adder. The communications component is a nonlinear converter in general form and in the special case it is a linear component which provides receipt of a given weight of communications. All the base and communications

APPROVED FOR RELEASE: 2007/02/08: CIA-RDP82-00850R000300060001-1

APPROVED FOR RELEASE: 2007/02/08: CIA-RDP82-00850R000300060001-1

components of the network are identical and are rearranged by using the digital computer. The number of components in the network and the spacing of the array are determined on the basis of the requirements for obtaining representative information about the field of some parameter [1, 3]. The complete model of the reservoir consists of a set of interconnected identical arrays, each of which is a model of the field of one parameter. The operating principle of the analog part of the system is based on reproduction of a multidimensional random process with given statistical characteristics of the models and with given relationships between them. The initial statistical characteristics of the base components, the weight of the communications components and the boundary conditions are established on the basis of empirical data on the object of investigation and the requirements of the postulated problem. Analysis of the state of the system with variations of the inertial and boundary conditions, with different configurations of the network and values of the communications weights is accomplished by direct measurement of the observed fluctuation signals in the array assemblies. With regard to the established time scale, this analysis is a prediction of the future state of the system at a given interval.

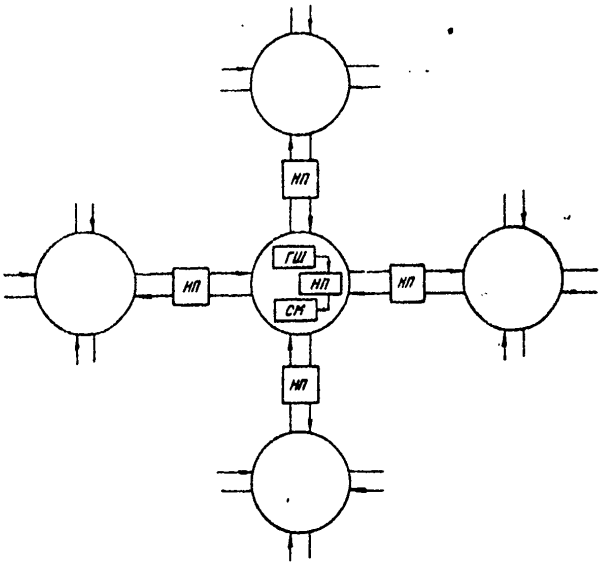

Figure 2. Block Diagram of Probability Network of Analog Part of GVS: GSh--primary sources of fluctuating electric oscillations (noise generators); NP--nonlinear converters; SM--adders

Concerning the principle problems of realizing these models, we note that nature long ago solved this problem and in a very efficient manner. We have in mind primarily the neuron networks of living systems. Numerous investigations both in the Soviet Union and abroad show that the neuron networks combine all functions of the model of complex systems by accomplishing adaptive functions of analysis, checking and control of the natural state and the external medium simultaneously by means of actuating components. It is interesting that the internal language of interneuron

APPROVED FOR RELEASE: 2007/02/08: CIA-RDP82-00850R000300060001-1

APPROVED FOR RELEASE: 2007/02/08: CIA-RDP82-00850R000300060001-1

messages is pulsed in nature, while the main informative parameter, as is known, is the length of the intervals between pulses. Nonlinear transformations of the probability pulse flows are accomplished at the level of the synaptic elements [7] and are developed at the level of converging postsynaptic potentials of the neuron membrane [8]. It is therefore natural to use some ideas of neurocybernetics for synthesis of the AVM.

The main trends in development of the AVM can be characterized in the following manner:

1. Development of the general theory of homogeneous stochastic rearranged networks and the theoretical justification of AVM parameters.

2. Realization of the AVM on the basis of standard semiconductor components and on the base of microelectronics.

3. Realization of the AVM on the basis of new physical components.

4. Synthesis of the AVM on a material biological base.

Detailed analysis of the statistical characteristics of the main hydrophysical and hydrochemical parameters and the relationships between them were carried out with respect to the problem of developing the AVM of the Sea of Azov according to paragraph 1. The elements of the theory of stochastic polysynaptic networks, being a prototype of the AVM of a more complex self-adjusting type, were developed. In this case the mathematical apparatus of the theory of random processes, ideas of queueing theory and automaton theory were used. The general principle of matching and self-matching of the probability networks of neuron-like elements was formulated [6].

According to paragraph 2, several versions of the base components were developed on the basis of ordinary semiconductor technology (the modular version) and on integrated circuits. The communications component was developed.

According to paragraph 3, an attempt was made to use the electronics of nanowatt outputs on the basis of organic semiconductor crystals of the anthracene type. It was possible to develop a semifunctional element which specifically has noise properties and the property of memory [5]. This permits one to synthesize the adaptive base components for the AVM.

A cycle of biophysical investigations was carried out at cellular and subcellular levels in the stochastic stimulation mode by pulsed flows with known statistics (paragraph 4). The data in combination with materials on cultivation of nerve tissue [9, 10] permit positive analysis of this trend and to recognize it as one of the most promising, although the most difficult to realize.

The second and third trends are the most real and most economically effective for the AVM from the technical viewpoint.

In conclusion, one should note the universality of models of this type, determined by the possibility of using them for modelling different reservoirs, with respect

APPROVED FOR RELEASE: 2007/02/08: CIA-RDP82-00850R000300060001-1

APPROVED FOR RELEASE: 2007/02/08: CIA-RDP82-00850R000300060001-1

to which there is initial statistical information. This quality obviously follows directly from the possibility of rearranging the base components of the model and the relationships between them.

BIBLIOGRAPHY

11. Belyayev, V. I. and I. Ye. Timchenko, "Disposition of Measurements and Accuracy of Field Restoration During Automated Gathering and Processing of Hydrophysical Information," in "Avtomatizatsiya nauchnykh issledovaniy morey i okeanov" [Automation of Scientific Investigations of the Seas and Oceans], Sevastopol', MGI AN USSR, 1969.

2. Box, J. and H. Jenkins, "Analiz vremennykh ryadov: Prognoz i upravleniye" [Analysis of Time Series: Prediction and Control], Moscow, Mir, 1974.

3. Dubenko, G. I., "Optimum Arrangement of Sensors When Estimating the Values of a Homogeneous Random Field in the Presence of Additive Noise," AVTOMATIKA I TELEMEKHANIKA, No 7, 1970.

4. Dubinina, V. G., A. M. Berezovskiy and I. V. Popov, "The Stochastic Model of the Complex of Biohydrological Characteristics of the Azov Basin," TR. VNIRO, No 39, 1972.

5. Litvinenko, V. Yu. and A. N. Makhotenko, "An Electroluminescent Diode," Inventor's Certificate 550772 (USSR), published in BYULLETYEN' IZOBRETENIY, No 10, 1977.

6. Ob'mukha, G. I. and I. V. Popov, "Possible Principles of Matching of Neuron Structures," NEYROBIONIKA, No 6, 1973.

7. Popov, I. V., "Stochastic Processes in the Synapse of the Nerve Cell," BIONIKA I MATEMATICHESKOYE MODELIROVANIYE V BIOLOGII, No 1, 1966.

8. Popov, I. V., "The Possibility of Using Queueing Theory to Analyze the Simplest Polysynaptic Structures," BIOL. I MED. KIBERNETIKA I BIONIKA, No 5, 1971.

9. Shtark, M. B., L. V. Voskresenskaya, A. S. Ratushnyak, S. N. Olenev and I. V. Popov, "Investigating the Pulse Activity of the Neurons of the Hippocampus in Vitro," DOKL. AN SSSR, Vol 202, No 3, 1972.

10. Shtark, M. B., I. V. Popov, A. S. Ratushnyak, L. V. Voskresenskaya, V. I. Stratiyevskiy and L. B. Aleksandrovskaya, "The Electrical Characteristics of Membranes of the Central Neurons in Vitro," in "Sbornik trudov IV Mezhdunarodnogo biofizicheskogo kongressa" [Collection of Papers of the Fourth International Biophysical Congress], Moscow, 1972.

END

APPROVED FOR RELEASE: 2007/02/08: CIA-RDP82-00850R000300060001-1